

SIMPLIFIED LIMIT LOAD APPROXIMATIONS AND THEIR BOUNDS

By

© Sakib Lutful Mahmood

A Thesis Submitted to the School of Graduate Studies

In Partial Fulfillment of the Requirements

for the Degree of

Doctor of Philosophy

Faculty of Engineering & Applied Science

Memorial University of Newfoundland

St. John's, NL, Canada

October 2015

Abstract

From a design point of view, a robust simplified limit load solution is the one which is consistently lower bound, yet provides a better estimate compared to the classical lower bound limit load. The robustness is determined by its proximity to the exact limit load. There are several limit load multipliers such as multiplier m_μ'' (Seshadri and Indermohan, 2004), multiplier m'' (Simha and Adibi-Asl, 2012), two bar multiplier (Seshadri and Adibi-Asl, 2007), and multiplier m_α^T (Seshadri and Hossain, 2009) which provides reasonable estimates of limit loads. However their nature of bounds has not been examined. In this thesis limit load bounds for these multipliers have been investigated. Finally, the nature of bounds of all the limit load multipliers in the literature are summarized, where bounds are either already established or will be addressed in this thesis.

The lower bound estimate of the multiplier m_μ'' relies on the exact distribution of plastic flow parameter. It is found that for an approximate distribution of flow parameter, m_μ'' is either upper bound or its bounds are not obvious. Since the exact distribution of plastic flow parameter is only available from the limit state stress distribution, the multiplier m_μ'' could not be established as a lower bound based on the linear elastic analysis.

Simha and Adibi-Asl (2012) proposed an inequality relation ($m'' < m_\mu''$) for lower bound m'' . It is concluded that the inequality ($m'' < m_\mu''$) could not guarantee a lower bound m'' , when m_μ'' is estimated from an approximate distribution of plastic flow parameter.

In order to investigate limit load bounds of the two bar solution, reference two bar multiplier (which gives bounding limit load over the other two bar configurations) is first identified by performing general two bar analysis. Since a mechanical component or structure can be represented by a suitable multi bar model, a general multi bar analysis is then performed. It is found that the reference two bar multiplier bounds the limit load solution of multi bar models. A correction factor has also been introduced to the reference two bar solution in order to eliminate any possibility of overestimation of limit loads using reference two bar multiplier. Hence the

proposed estimate of reference two bar solution provides lower bound limit load. However limit load estimation using this multiplier at times could be conservative (although offers much better accuracy than classical lower bound) compared to the exact limit load.

The m_α^T multiplier which offers better accuracy than the two bar multiplier is also established as a lower bound by investigating exact solution trajectory, utilizing the constraint map construction. Also, it is found that the m_α^T multiplier bounds the limit load solution of multi bar models, which confirms the lower bound nature of the m_α^T multiplier. A guideline is proposed to obtain sufficiently accurate lower bound limit load based on a single linear elastic analysis.

In terms of elastic modulus adjustment procedure (EMAP), classical lower bound limit load multiplier is susceptible to oscillations with iterations, when sharp modulus adjustments are performed thereby raising convergence issues. On the other hand, more gentle element modulus adjustments turn out to be computationally expensive. In this thesis, the m_α -tangent multiplier is used in conjunction with the elastic modulus adjustment procedure for limit load determination. The lower boundedness of the m_α -tangent multiplier for any iteration is ensured by incorporating reference volume and peak stress corrections. By the virtue of the faster convergence feature, the m_α^T -multiplier permits gentler modulus adjustments, and at the same time estimates sufficiently accurate lower bound limit load within a relatively small number of elastic iterations. This minimizes the convergence difficulties usually encountered in EMAP.

Simplified techniques on the basis of linear elastic finite element analysis (FEA) assumes elastic-perfectly-plastic material model. However, due to strain hardening, a component or a structure can store supplementary strain energy and carry additional load. In this thesis, an iterative elastic modulus adjustment scheme is developed for strain hardening material model, utilizing the “strain energy density” theory. The proposed algorithm is then programmed into repeated linear elastic FEA and implemented to a number of practical components. Moreover, the procedure for elastic modulus adjustment to achieve limit state and elastic-plastic state are explained in parallel, to demonstrate their similarity and diversity.

Acknowledgements

I would like to express my heartiest and sincerest gratitude to my supervisors, Dr. C. Daley and Dr. R. Seshadri for their intellectual guidance, tireless support, constructive suggestions, inspiration, and close supervision throughout the entire period of my doctoral program.

I would like to thank Dr. B. Colbourne for his valuable help and support as a member of my supervisory committee.

I would like to thank Dr. A. S. J. Swamidas, Dr. K. Munaswamy, Dr. S. Adluri and Dr. S. A. Usmani, AMEC Foster Wheeler, for their valuable comments and suggestions. I am thankful to Dr. R. Kizhatil, BWXT Canada; Dr. L. Pan, BWXT Canada; Dr. R. Adibi-asl, AMEC Foster Wheeler; and Dr. W.D. Reinhardt, Candu Energy, for valuable technical discussions. I am also thankful to Dr. L.M. Lye the associate Dean of Graduate Studies for his support. Thanks to Ms. Colleen Mahoney and Ms. Moya Crocker, office of the associate Dean, for their above and beyond administrative assistance during the course of my program.

Special thanks to Dr. R. Seshadri who had always been available for help, both as a supervisor and also as a well-wisher.

I would like to extend my acknowledgements to Mahmud Sharif Sazidy, Taufiqur Rahman and other friends for their valuable help and support. Last but not the least; I owe my deepest thanks to my wife Fazilatunnessa Mahmood, my daughter Shadida Mahmood, my son Shakir Mahmood, my siblings and my beloved parents for their tireless encouragement and supports.

Table of Contents

Abstract.....	ii
Acknowledgements	iv
Table of Contents	v
List of Tables	xi
List of Figures.....	xii
List of Abbreviations and Symbols	xiv
Chapter 1: Introduction	1
1.1 General Background	1
1.2 Lower Bound Limit Load	3
1.3 Need for Simplified Approximations.....	4
1.4 Objectives of Research	5
1.5 Scope of Research.....	7
1.6 Organization of the Thesis	8
Chapter 2: Theoretical Background	11
2.1 Introduction.....	11
2.2 Bounding Theorems in Plasticity.....	12
2.2.1 Lower Bound Theorem.....	12
2.2.2 Upper Bound Theorem	13
2.3 Extended Variational Theorems of Limit Load Analysis	14
2.4 Reference Stress Concept	20
2.5 Reference Volume Concept	24

2.6 Linear Elastic Analysis Approach for Limit Load Approximation	25
2.7 Closure	27
Chapter 3: Simplified Limit Load Multipliers and their Bounds	28
3.1 Introduction.....	28
3.2 Classical Lower Bound - Multiplier m_L	30
3.3 Upper Bound Solution - Multiplier m^0	31
3.4 Concept of the Constraint Map.....	34
3.4.1 Construction of the Constraint Map.....	34
3.4.2 The Exact Multiplier, m	36
3.5 Mura's Extended Lower Bound - Multiplier m'	37
3.6 Variational Limit Load Multiplier m''_μ	38
3.6.1 Approximate Distribution of Plastic Flow Parameter	39
3.6.2 Limit Load Bounds for Multiplier m''_μ	41
3.6.3 Analytical Examples.....	42
3.6.3.1 Rectangular Beam Analysis.....	43
3.6.3.2 Thin Circular Pipe Analysis.....	44
3.7 Limit Load Bounds for Multiplier m''	45
3.8 Robust Limit Load Approximations	47
3.9 Discussion and Conclusion.....	50
Chapter 4: Lower Bound Estimate of the Two Bar Multiplier	51
4.1 Introduction.....	51
4.2 The Two Bar Structure.....	53
4.3 Plastic Collapse of Components and Structures	53
4.4 General Two-Bar Analysis	55

4.5 Identification of the Reference Two Bar Model.....	57
4.6 Relating Mechanical Component to Reference Two Bar Model.....	59
4.7 Reference TBM - An Estimate Beyond Mura's Lower Bound	60
4.8 Bounding Nature of Reference TBM - Multi Bar Structures	60
4.8.1 Three Bar Model.....	61
4.8.2 Four Bar Model	63
4.8.3 General Multi Bar Model	65
4.8.4 Limit Load Bounds for Reference TBM	68
4.9 Discussion and Conclusion.....	70
Chapter 5: Lower Bound Estimate of the m_α^T-Multiplier	71
5.1 Introduction.....	71
5.2 The m_α -Tangent Method.....	72
5.3 Reference TBM vs m_α^T formulation.....	74
5.4 Illustrative Example - Reference Volume and Peak Stress Correction	76
5.5 The m_α^T -multiplier - A Lower Bound Estimate.....	78
5.6 Exact Solution Locus - 3D Grillage Analysis Example.....	79
5.7 Bounding Nature of m_α^T -Multiplier - Multi Bar Analysis	82
5.8 Evaluation of the Multiplier m_α^T	84
5.8.1 Multiplier m_α^T : $\zeta \leq 1 + \sqrt{2}$	84
5.8.2 Multiplier m_α^T : $\zeta > 1 + \sqrt{2}$	85
5.9 Combining EMAP with the m_α -tangent method.....	86

5.9.1 Implicit Reference Volume and Peak Stress Correction in EMAP	87
5.9.2 Proposed EMAP Algorithm and Its Features	89
5.10 Discussion and Conclusion	92
Chapter 6: Robust Limit Loads Based on Single Linear Elastic Analysis	94
6.1 Introduction.....	94
6.2 Guideline for Lower Bound m_{TBM} Multiplier Based on Single Linear Elastic FEA.....	96
6.2.1 Multiplier m_{TBM} : $\zeta \leq 1 + \sqrt{2}$	99
6.2.2 Multiplier m_{TBM} : $\zeta > 1 + \sqrt{2}$	99
6.3 Guideline for Lower Bound m_a^T Multiplier Based on Single Linear Elastic FEA	101
6.3.1 Multiplier m_a^T : $\zeta \leq 1 + \sqrt{2}$ (<i>well-designed components with gentle geometric transitions</i>).....	102
6.3.2 Multiplier m_a^T : $\zeta > 1 + \sqrt{2}$ (<i>components with stress concentrations</i>)	103
6.3.3 Multiplier m_a^T : $\zeta > 1 + \sqrt{2}$ (<i>local plastic action along with stress concentrations</i>)..	103
6.4 Analytical Examples	104
6.5 Numerical Examples.....	105
6.5.1 Thick Walled Cylinder	106
6.5.2 Torispherical head	107
6.5.3 Reinforced Axisymmetric Nozzle	108
6.5.4 Plate with a Hole	110
6.5.5 Compact Tension (CT) Specimen	112
6.5.6 Large Grillage.....	114
6.6 Discussion and Conclusion	115

Chapter 7: EMAP for Strain Hardening Material Model	116
7.1 Introduction.....	116
7.2 EMAP Categories	117
7.2.1 Full EMAP.....	117
7.2.2 Partial EMAP.....	119
7.3 Strain Hardening Material Model	120
7.4 Proposed Partial EMAP for Strain Hardening Model.....	121
7.4.1 Partial EMAP for Bilinear Hardening Material Model	121
7.4.2 Partial EMAP for Ramberg–Osgood Material Model.....	125
7.5 Finite Element Implementation.....	127
7.6 Numerical Examples	129
7.6.1 Plate with a Hole	129
7.6.2 Stiffened Plate Subjected to Transverse Loading.....	134
7.7 Applications	136
7.8 Discussion and Conclusion	137
Chapter 8: Conclusions and Future Research	138
8.1 Summary and Conclusions	138
8.2 Original Contributions	141
8.3 Recommendations for Future Research.....	144
References.....	146

APPENDICES	150
Appendix A: Derivation of Limit Load Solution for Several Beam Configurations.....	150
A.1 Rectangular Beam.....	150
A.2 Solid Circular Beam	154
A.3 Thin Circular Pipe	155
Appendix B: Detail Derivation of the m_α -Method.....	158
Appendix C: Modeling of Components with Cracks for Simplified Limit Load Analysis	162

List of Tables

Table 3.1 Limit load multipliers for a rectangular beam	43
Table 3.2 Limit load multipliers for a thin circular pipe.....	44
Table 3.3 Summary of limit load bounds for several multipliers.....	49
Table 4.1 $\frac{m^0}{m}$ ratio for the multi bar model	66
Table 4.2 Limit load multipliers for fixed end beam	68
Table 6.1 Guideline for lower bound limit load multiplier based on single linear elastic FEA	100
Table 6.2 Limit load multipliers for several beam configurations.....	104
Table 6.3 Limit load multipliers for thick walled cylinder	106
Table 6.4 Limit load multipliers for torispherical head	107
Table 6.5 Limit load multipliers for reinforced axisymmetric cylindrical nozzle	109
Table 6.6 Limit load multipliers for plate with a hole	111
Table 6.7 Limit load multipliers for compact tension specimen.....	113
Table 6.8 Limit load multipliers for large grillage.....	114

List of Figures

Figure 2.1 Two bar model.....	21
Figure 2.2 Reference stress variation in a two bar structure.....	23
Figure 2.3 Kinematically active and inactive volume.....	25
Figure 3.1 Constraint map showing relative magnitudes of different multipliers (θ in radian) ..	35
Figure 3.2 Schematic of the stress-strain relationship [15].....	39
Figure 3.3 Variation of m''_{μ} with q	42
Figure 3.4 Variation of m''_{μ} with q for a rectangular beam.....	43
Figure 3.5 Variation of m''_{μ} with q for a thin circular pipe.....	44
Figure 4.1 Relating an indeterminate beam to a two-bar structure.....	54
Figure 4.2 Two-bar trajectories for different values of 'n'.....	58
Figure 4.3 Multi bar model.....	65
Figure 4.4 Fixed end beam geometry.....	67
Figure 4.5 The constraint map showing multi bar solutions.....	68
Figure 5.1 Approximation of reference volume and peak stress correction.....	75
Figure 5.2 Blunting of peak stresses.....	77
Figure 5.3 Bounds for m_{α}^T on the constraint map.....	79
Figure 5.4 Grillage model (dimensions in mm).....	80
Figure 5.5 Results for grillage model.....	82
Figure 5.6 Relative magnitude of m_{α}^T solution over multi bar solutions.....	84
Figure 5.7 Variation of m^0 (m_2^0) during EMAP Iterations.....	88
Figure 5.8 EMAP flow diagram for estimating limit load (m^0 from Eq(3.9), which is m_2^0).....	90

Figure 6.1 Limit load bounds.....	97
Figure 6.2 Error in the m_{TBM} multiplier estimate in comparison to the m_{α}^T multiplier	97
Figure 6.3 Reference TBM error estimation from constraint map	98
Figure 6.4 Finite element model of the thick walled cylinder	106
Figure 6.5 Axisymmetric finite element model of the torispherical head	107
Figure 6.6 Finite element model of the reinforced axisymmetric nozzle	108
Figure 6.7 Finite element model of the plate with a hole	110
Figure 6.8 Finite element model of compact tension specimen.....	113
Figure 7.1 Schematic of the ESED method	118
Figure 7.2 Schematic of the strain hardening material model	122
Figure 7.3 Partial EMAP flow diagram	128
Figure 7.4 Plate with a hole	130
Figure 7.5 Load-deflection curve for plate with a hole.....	131
Figure 7.6 Variation of stress with iterations.....	132
Figure 7.7 Variation of strain with iterations.....	132
Figure 7.8 Normalized stress-strain plot	133
Figure 7.9 Comparison of load-deflection behavior	133
Figure 7.10 Single stiffened plate (dimensions in mm).....	134
Figure 7.11 Comparison of load-deflection behavior	135

List of Abbreviations and Symbols

e	Percent error estimate
e_{max}	Maximum percent error estimate
E_o	Initial Elastic modulus
E_s	Secant modulus
$f(s_{ij}), f(s_{ij}^0)$	von Mises yield function
i	linear elastic iteration number
k	Yield strength of a material in pure shear
m	Exact limit load multiplier / limit load multiplier based on inelastic FEA (m_{NFEA})
m_{NFEA}	Limit load multiplier based on inelastic FEA
m_L	Classical lower bound limit load multiplier
m'	Mura's extended lower bound multiplier
m_U	Classical upper bound limit load multiplier
m^0	Upper bound limit load multiplier
$m^0(V_R)$	Kinematically active reference volume based upper bound multiplier
m_α	Limit load multiplier Alpha
m_α^T	Limit load multiplier m_α -tangent
m_{TBM}	Reference two bar multiplier
m''_μ	Variational limit load multiplier
m''	Limit load multiplier m''
N	Number of elements in V_T
$P, P_{Applied}$	Arbitrary applied traction
P_{Limit}	Exact limit load

q	Elastic modulus adjustment parameter
s_{ij}^0	statically admissible deviatoric stress field corresponding to the plastic collapse state
\tilde{s}_{ij}^0	statically admissible deviatoric stress field corresponding to the applied traction P
V, V_T	Volume, total volume
V_R	Kinematically active reference volume
V_D	Kinematically inactive volume
θ	Angle in radian
ν	Poisson's ratio
σ_{eq}	von Mises equivalent stress
$(\sigma_{eq})_{\max}$	Maximum von Mises equivalent stress
σ_{ref}	Reference stress
$\sigma_{PRIMARY}$	Primary stress
σ_y	Yield strength
ε_{eq}	Equivalent elastic strain
ε_{eq}^p	Elastic-plastic equivalent strain
μ	Plastic flow parameter corresponding to the exact limit state
ζ	Ratio of $\frac{m^0}{m_L}$

Subscript

eq equivalent

ref reference

i linear elastic iteration number

Superscript

0 quantities associated with a statically admissible stress state

Abbreviation

ASME American Society of Mechanical Engineers

FEA Finite Element Analysis

NFEA Inelastic FEA

TBM Two Bar Model

EMAP Elastic Modulus Adjustment Procedure

NSSC Notch Stress Strain Conversion

FFS Fitness-for-Service

Chapter 1: Introduction

1.1 General Background

The primary objective in designing a mechanical component or structure is to ensure its ability to perform the intended function at minimum capital and operational cost. Therefore it is important to design components by taking into account all failure modes that the component could experience. It is also necessary to periodically assess the “integrity” of mechanical components, and structures in operation thereby establishing an estimate of the remaining life of critical components.

Among the various modes that may govern the failure of a component, plastic collapse is one of the most important, since it would lead to gross plastic deformation. Load which causes cross-sectional plasticity in structures resulting in uncontained plastic flow is termed as limit load. Limit load analysis provides a measure of the reserve strength that exists in mechanical and structural components. As well, knowledge of the limit load is necessary for obtaining the reference stress [2], which is used extensively in the United Kingdom [33] [34] in integrity assessment and fracture evaluations.

Conventionally, limit loads are determined either analytically or by using the numerical methods. Analytical methods are mostly used in conjunction with lower and upper bound theorems in plasticity, and application of these methods is generally limited to simple geometric configurations. Numerical methods such as inelastic finite element analysis, on the other hand, are applicable to a wide range of practical components and structures. The most frequently used numerical approach to obtain a limit load is to perform a nonlinear elastic-plastic finite element

analysis with no strain hardening. However inelastic FEA has some limitations. The difficulties arise mainly from the need to carry out analyses in an iterative and incremental form. Since this method always operates at the convergence limit, it tends to be relatively inefficient, i.e. many steps are required to obtain a good estimate of the limit load. Moreover the enormous computational time required for the analysis is expensive and produces a large amount of output data that has to be interpreted properly in order to make practical sense. For complex shakedown analysis, inelastic analysis remains an expensive choice, especially for combined loading.

An independent verification of a detailed nonlinear FEA results is also essential in order to avoid having erroneous results due to numerical errors.

As per the ASME design-by-analysis approach ([1] [11]), primary stresses are to be kept below their corresponding allowable values in order to avoid plastic collapse. However, for complex geometric configurations primary stress classification from a linear elastic stress distribution is not always straightforward.

Structural integrity assessment in an operating plant is practiced at three levels. Level 1 assessment procedures provide conservative screening criteria that can be used with a minimum quantity of inspection data or information about the component. Level 2 is intended for use by facilities or plant engineers, although some owner-operator organizations consider it more suitable for a central engineering evaluation. Level 3 assessments require sophisticated analysis by experts, where advanced computational procedures are often carried out. Level 2 Fitness-for-Service evaluations are often made in an engineering plant environment with the availability of

limited resources and often demands time critical solutions. In this situation implementation of a simplified methodology makes much sense in order to evaluate remaining strength of an in-service component. Clearly an inelastic solution is not an option for this kind of situation.

The above considerations create the need for the development of alternate lower bound limit load approximation techniques. Simplified limit load approximations have been employed for limit load estimation on the basis of linear elastic finite element analysis (FEA). However from a design point of view, a robust limit load solution is required, which is a lower bound, yet provides a better estimate of limit load compared to the classical lower bound limit load. Therefore developing better approximation techniques, examining the bounding nature of several simplified approximations and their systematic implementation are the main aim of this thesis.

It should be pointed here that throughout the thesis the terms ‘limit load bounds’ and ‘bounding nature’ of a limit load solution are used interchangeably, which specifies whether a limit load multiplier is consistently lower bound, consistently upper bound or its bound is not clear.

1.2 Lower Bound Limit Load

Structures can withstand loads beyond the elastic limit of structural materials, and with plastic design, advantage can be taken of the reserve strength that exists beyond the initial yielding. For statically indeterminate structures especially those with large indeterminacy, the reserve strength can be significant. Therefore knowledge of limit loads of components and structures becomes useful to a designer, since it enables the determination of the reserve strength and also addresses the mode of failure associated with load-controlled effects.

Lower bound limit loads are especially relevant from a design point of view since they provide a guaranteed margin of safety against load controlled plastic failure modes, or the related primary stress limits contained in the design codes ([1] [11]). Lower bound limit load guarantees that the stress distribution throughout the component or structure is in equilibrium internally, balances the external loads and at the same time does not violate the yield condition.

1.3 Need for Simplified Approximations

Simplified limit load approximations can be employed as an alternative limit load estimation method on the basis of linear elastic finite element analysis (FEA). This approach utilizes the “bounding theorems in plasticity”, in conjunction with the linear elastic analysis.

The simplified methods rely on statically admissible stress and kinematically admissible strain rate fields obtained from linear elastic FEA. For real-world geometries, it is convenient to estimate the limit load utilizing statically admissible stress and kinematically admissible strain fields. Simplified methods can be based on iterative finite element elastic analyses that involves modification to the element elastic modulus in successive iterations. Also it is possible to compute limit load by utilizing a single linear elastic stress field (no iterations). No matter what the approach is, the objective is to obtain an economic limit load solution which is neither overestimated nor overly conservative. Since the ultimate goal is to achieve an economic but safe estimate of limit load, it is important to understand the bounding nature of several simplified approximation techniques and their systematic implementation.

Even beyond limit state, membrane action and post-yield strain hardening effect enable the structure to withstand increased loads prior to ultimate collapse. Therefore, designers are also interested in the development of simplified formulations that can account for strain hardening and in-plane membrane action, in order to capture the post yield behavior of a component or structure.

Simplified approximation techniques are ideally suited for performing a preliminary analysis, design or qualification of components so that the safety margin of a component or structure can be assessed. These methods can also be used for identifying critical locations; as well as estimating the inelastic effects. Simplified methods are sometimes the only recourse to an independent verification of the results of a detailed nonlinear analysis of a complex geometric configuration.

1.4 Objectives of Research

The primary set of objectives of the proposed research work is as follows:

1. Examine the limit load bounds of several simplified limit load approximations, for which bounds have not been established and suggest guideline for a lower bound estimate. There are several limit load multipliers such as multiplier m''_{μ} [13], multiplier m'' [14], two bar multiplier [10], and multiplier m_{α}^T [12] which provide reasonable estimates of limit loads. However their bounds have not been examined. In this thesis limit load bounds for these multipliers have been investigated. Finally, limit load bounds of all the limit load multipliers in the literature are summarized, where bounds are either already established or will be addressed in this thesis.

2. Develop an elastic modulus adjustment scheme for elastic-perfectly-plastic material model, which reduces the convergence difficulties usually encountered in EMAP for complex component configurations. The m_α -tangent multiplier is used in conjunction with the elastic modulus adjustment procedure in order to eliminate the convergence difficulties and estimate sufficiently accurate lower bound limit load within a relatively small number of elastic iterations.

3. Provide guidelines for calculating lower bound limit loads based on a single linear elastic analysis. Essential correction factors are introduced to some of the limit load multipliers in order to eliminate the possibility of overestimation/underestimation of limit load.

4. Develop an iterative elastic modulus adjustment scheme for strain hardening material model, utilizing the “strain energy density” theory. The proposed algorithm is then programmed into repeated linear elastic FEA and implemented to a number of practical components. Moreover, the procedure for elastic modulus adjustment to achieve limit state and elastic-plastic state are explained in parallel, to demonstrate their similarity and diversity.

1.5 Scope of Research

From a design point of view, lower bound limit loads provide a guaranteed margin of safety against load controlled plastic failure modes. The improvement of the accuracy of lower bound limit load estimation towards the exact limit load has great engineering value. Estimation of lower bound limit load by using simplified methods is of considerable interest due to its simplicity and cost effectiveness. There are several simplified limit load multipliers in literature which provide reasonable estimates of limit loads. However their bounds have not been established. Examining the bounds of several simplified limit load approximation techniques and suggest guideline for accurate lower bound offers a significant scope of research.

During elastic modulus adjustment procedure (EMAP), lower bound limit load multipliers are susceptible to oscillations with iterations, when sharp modulus adjustments are performed thereby raising convergence issues. On the other hand, a more gentle element modulus adjustments turn out to be computationally expensive. There is a scope of developing an EMAP scheme, which minimizes the convergence difficulties usually encountered and at the same time can estimate sufficiently accurate limit load within a few linear elastic iterations.

Simplified limit load analysis techniques assume elastic-perfectly-plastic material model. Due to strain hardening, a component or a structure can store supplementary strain energy and hence carry additional load. Therefore development of elastic modulus adjustment scheme for strain hardening material model has significant engineering and economic value.

1.6 Organization of the Thesis

This thesis is composed of eight chapters. The first chapter addresses the significance of lower bound limit load approximations and the advantage of using simplified techniques for mechanical component and structure design. The objectives and scope of the proposed research work are also presented in this chapter.

The theoretical aspects pertaining to the research reported in this thesis are explained in Chapter 2. The bounding theorems in plasticity are explained in this chapter. The extended variational theorem proposed by Mura and co-workers [30] is introduced and several limit load multipliers, which set the basis for the current thesis, have been re-derived. The concept of reference stress is discussed and the relationship between reference stress and limit load is highlighted. The concept of reference volume is discussed in an attempt to isolate the regions in the structures that most likely do not participate in plastic collapse.

Chapter 3 discusses the upper and lower bound multipliers, basic construction of the constraint map, exact solution locus as well as robust limit load approximations. This chapter also deals with the limit load bounds for the multiplier m''_{μ} [13] and multiplier m'' [14]. Finally a list of limit load multipliers available in the literature and their bounds (either established previously or established in this thesis) are summarized in Chapter 3. Basically chapter 3 gives the essence of this thesis and directs to necessary elaborations provided in the subsequent chapters.

Chapter 4 presents the general two bar analysis to achieve the reference two bar multiplier. The generalized two-bar analysis eliminates the equal two bar area assumption previously considered

in the literature [10]. A transformation parameter is obtained from the reference two bar model which scales up Mura's overly conservative lower bound multiplier to a multiplier with improved accuracy. Since a general mechanical component can be represented by a suitable multi bar model in terms of limit load estimation, the bounding nature of reference two bar model over multi bar structures is also discussed in this chapter.

Chapter 5 discusses theoretical evolution of the m_α -tangent method [12] and establishes this method as a robust lower bound. Reference volume correction is proposed in order ensure lower bound m_α -tangent solution for practical components and structures. This chapter also provides a systematic guideline for elastic modulus adjustment scheme, which reduces the convergence difficulties usually encountered in EMAP for complex geometric configurations. This guideline is then implemented to a complex three dimensional complex grillage FE model.

In chapter 6, a correction factor has been introduced to the reference two bar multiplier (developed in Chapter 4), in order to eliminate any possibility of overestimation of limit loads using this multiplier. In addition, a guideline for appropriate incorporation of reference volume and peak stress correction to the m_α^T multiplier (discussed in Chapter 5) is provided in chapter 6. It is essential to incorporate the reference volume and peak stress corrections judiciously on a component basis, in order to achieve reasonable lower bound estimation of m_α^T multiplier based on single linear elastic analysis. These methods are then implemented to a number of practical mechanical components based on a linear elastic analysis.

Chapter 7 presents an elastic modulus adjustment scheme for strain hardening material model. This involves development of EMAP formulation for bilinear hardening and Ramberg–Osgood material model, followed by the development of an algorithm which can be programmed into repeated linear elastic analyses. The procedure for elastic modulus adjustment to achieve limit state and elastic-plastic state are explained in parallel, to demonstrate their similarity and diversity.

Chapter 8 summarizes and concludes the findings of the present research work. The chapter also presents the original contributions to this thesis along with some guidelines for future work.

Appendix A documents the derivation of analytical limit load solution for several beam configurations.

Appendix B documents the detailed derivation of the m_α -method. This includes some unique algebraic manipulations which have not been documented in any previous works.

Appendix C discusses the modeling strategy of components with cracks, for the purpose of limit load estimation based on a linear elastic analysis.

Chapter 2: Theoretical Background

2.1 Introduction

The theoretical aspects relevant to the simplified limit load approximations are presented here. Simplified methods are originally based on established classical theorems which enable determination of lower bounds and upper bounds for the collapse load. The true collapse load is always larger than or equal to the lower bound collapse load and is always smaller than, or equal to the upper bound collapse load. The collapse load is thus bracketed between the upper and lower bounds.

Alternate formulations for lower and upper bound theorems that were based on extended variational concepts were first proposed by Mura and coworkers [5] [30]. By making use of “statically admissible” stress distributions and “kinematically admissible” strain distributions, and invoking the notion of integral mean of yield, pseudoelastic distributions of stress that exceeded yield were utilized for determining the upper and lower bound limit loads.

The classical bounding theorems and variational concepts of plasticity can be utilized in conjunction with contemporary computational tools in order to achieve robust and rapid limit load estimates. In this thesis, the bounding nature of simplified limit load approximations (which are based on the classical and variational theorems) are studied in terms of iterative linear elastic analysis as well as single linear elastic analysis. A review of the theoretical aspects relevant to the development of this thesis is presented here.

2.2 Bounding Theorems in Plasticity

The main objective of the limit load analysis is to estimate the load at the impending plastic limit state of a body. However, for complicated problems it may be difficult to find the exact limit load. Therefore, based on the extremum principles of limit load analysis, the bounding theorem is employed to estimate the limit load directly, without considering the entire loading history. There are two approaches for establishing approximate values: the equilibrium approach for lower bound estimates, and the geometry approach for upper bound estimates. In the classical limit load analysis, material nonlinearity is included by assuming perfectly plastic material model, while the geometric nonlinearity is not taken into account.

2.2.1 Lower Bound Theorem

A stress field defined throughout a continuum is called statically admissible for the given loads if in addition to satisfying the yield conditions, it represents a state of equilibrium under the given loads. Such a stress field is safe if at each point of the field, the state of stress is represented by a point inside the yield surface.

The statement of the classical lower bound theorem is as follows [3]:

“If any stress distribution throughout the structure can be found, which is everywhere in equilibrium internally and balances the external loads and at the same time does not violate the yield condition, those loads will be carried safely by the structure”

Therefore, the load estimated by the lower bound theorem will be less than, or at most equal to, the exact limit load and can be used for designing mechanical components and structures. In the

lower bound theorem, the equilibrium equations (statically admissible stress field) and yield condition are satisfied without considering the mode of deformation of the structure.

2.2.2 Upper Bound Theorem

A strain rate field defined throughout a continuum is called kinematically admissible for the given conditions of support, if it is derived from a velocity field which is compatible with the conditions of support and certain continuity conditions. Such a strain field is unsafe for given loads, if the total rate of energy dissipated is less than the rate at which the given loads do work on the generating velocities.

The upper bound theorem states that [3]:

“If an estimate of the plastic collapse load of a structure is made by equating the internal rate of dissipation of energy to the rate at which the external forces do work in any postulated mechanism of deformation of body, the estimate will be either high or correct”.

In processes such as metal forming and metal cutting, it is necessary to determine the load that is capable of performing the given operation. Determination of limit loads using the upper bound theorem ensures that the limit load estimates obtained can cause “plastic flow” in the component.

2.3 Extended Variational Theorems of Limit Load Analysis

Mura's variational formulation circumvents the requirement for a statically admissible stress field not to lie outside the yield surface in a lower bound analysis, and in an upper bound analysis the stress associated with a kinematically admissible strain-rate field in calculating the plastic dissipation should lie on the yield surface. In the variational approach proposed by Mura et al. [30] [5], such a requirement was eliminated and replaced by the concept of "integral mean of yield". They showed that the safety factor 'm' (the limit load multiplier) can be obtained from the following functional, F . i.e.

$$F = m - \int_V \mu \left[\frac{1}{2} \delta s_{ij} \delta s_{ij} + (\delta \phi)^2 \right] dV - \int_V \delta \mu [f(s_{ij}^0) + (\phi^0)^2] dV \quad (2.1)$$

In the above equation, ϕ^0 and s_{ij}^0 refers to quantities associated with a statically admissible stress state. The quantities s_{ij} , m , μ and ϕ correspond to a state of impending plastic flow for which the von-Mises yield criterion is given by,

$$f(s_{ij}) = \frac{1}{2} s_{ij} s_{ij} - k^2 \quad (2.2)$$

where 'k' is the yield limit in shear and $k^2 = \frac{\sigma_y^2}{3}$.

The "integral mean of yield" [5], can be expressed as:

$$\int_V \mu^0 [f(s_{ij}^0) + (\phi^0)^2] dV = 0 \quad (2.3)$$

where

$$\mu^0 \geq 0$$

s_{ij}^0 is a statically admissible deviatoric stress tensor close to an impending plastic collapse state and hence corresponds to an applied traction $m^0 P$. μ^0 is a flow parameter and ϕ^0 is a point

function that takes on a value of zero at yield, and remains positive below yield. If \tilde{s}_{ij}^0 is a statically admissible stress distribution corresponding to an applied traction P , then $m^0 \tilde{s}_{ij}^0$ would correspond to $m^0 P$. It is therefore clear that

$$s_{ij}^0 = m^0 \tilde{s}_{ij}^0 \quad (2.4)$$

Mura and co-workers [5] have also shown that m^0 , μ^0 and φ^0 can be determined from the following functional,

$$F = m^0 - \int_V \mu^0 [f(s_{ij}^0) + (\varphi^0)^2] dV \quad (2.5)$$

Since $\mu^0 = \mu + \delta\mu$, Eq.(2.3) can be written as:

$$- \int_V \delta\mu [f(s_{ij}^0) + (\varphi^0)^2] dV = \int_V \mu [f(s_{ij}^0) + (\varphi^0)^2] dV \quad (2.6)$$

Now Eq.(2.6) can be substituted into Eq.(2.1) which can be re-written as:

$$F = m - \int_V \mu \left[\frac{1}{2} \delta s_{ij} \delta s_{ij} + (\delta\varphi)^2 \right] dV + \int_V \mu [f(s_{ij}^0) + (\varphi^0)^2] dV \quad (2.7)$$

Since the second term on the right hand side of the Eq.(2.7) is always a positive quantity, utilizing the concept of ‘‘integral mean of yield’’ (from Eq.(2.3)) in Eq.(2.5), the functional given in Eq.(2.7) and Eq.(2.5) can be related by an inequality as:

$$m^0 \leq m + \int_V \mu [f(s_{ij}^0) + (\varphi^0)^2] dV \quad (2.8)$$

The above inequality in Eq.(2.8) holds if the expression is written in the following form:

$$m^0 \leq m + \max [f(s_{ij}^0) + (\varphi^0)^2] \int_V \mu dV \quad (2.9)$$

Mura et al. [5] scaled the virtual velocity field such that the work done on the structure is unity and presented an expression for the exact multiplier as:

$$m = 2k^2 \int_V \mu dV$$

$$\Rightarrow \int_V \mu dV = \frac{m}{2k^2}$$
(2.10)

Substituting Eq.(2.10) into Eq.(2.9), the expression can be re-written as:

$$m' = \frac{m^0}{1 + \frac{\max[(f(s_{ij}^0) + (\varphi^0)^2)]}{2k^2}} \leq m$$
(2.11)

Conversely, multiplying the second term of the inequality (shown in Eq.(2.8)) by 'm' and dividing by the expression for it from Eq.(2.10), Eq.(2.8) can be re-written as [13]:

$$m''_{\mu} = \frac{m^0}{1 + \frac{\int_V \mu [f(s_{ij}^0) + (\varphi^0)^2] dV}{2k^2 \int_V \mu dV}} \leq m$$
(2.12)

As mentioned above, m^0 , μ^0 and φ^0 can be determined by rendering the functional given in Eq.(2.5) stationary, leading to the following set of equations:

$$\frac{\partial F}{\partial m^0} = 0; \quad \frac{\partial F}{\partial \mu^0} = 0; \quad \frac{\partial F}{\partial \varphi^0} = 0$$
(2.13)

The von-Mises equivalence for statically admissible stress state can be expressed as:

$$f(s_{ij}^0) = \frac{1}{2} s_{ij}^0 s_{ij}^0 - k^2$$
(2.14)

and

$$\frac{1}{2} \tilde{s}_{ij}^0 \tilde{s}_{ij}^0 = \frac{(\sigma^0)^2}{3}$$
(2.15)

Quantities associated with a statically admissible stress state and the quantities correspond to a state of impending plastic flow can be related as:

$$\begin{aligned}
 s_{ij}^0 &= s_{ij} + \delta s_{ij} \\
 \sigma^0 &= \sigma + \delta \sigma \\
 m^0 &= m + \delta m \\
 \varphi^0 &= \varphi + \delta \varphi \\
 \mu^0 &= \mu + \delta \mu
 \end{aligned}
 \tag{2.16}$$

Where the superscript ‘‘0’’ refers to quantities associated with a statically admissible stress state.

The quantities s_{ij} , σ , m , μ and ϕ correspond to a state of impending plastic flow.

Now combining Eq.(2.4), Eq.(2.15) and Eq.(2.14), then substituting into Eq.(2.5),

$$F = m^0 - \int_V \mu^0 \left[\frac{(m^0)^2 (\sigma^0)^2}{3} - \frac{\sigma_y^2}{3} + (\varphi^0)^2 \right] dV
 \tag{2.17}$$

Applying Eq.(2.13) in conjunction with Eq.(2.17), we can get Eq.(2.18), Eq.(2.19), and Eq.(2.20) respectively. i.e.

$$\begin{aligned}
 \frac{\partial F}{\partial m^0} &= 1 - \int_V \mu^0 \left[\frac{2(m^0)(\sigma^0)^2}{3} \right] dV = 0 \\
 \Rightarrow m^0 &= \frac{1}{\int_V \mu^0 \left[\frac{2(\sigma^0)^2}{3} \right] dV}
 \end{aligned}
 \tag{2.18}$$

$$\begin{aligned} \frac{\partial F}{\partial \mu^0} &= - \int_V \left[\frac{(m^0)^2 (\sigma^0)^2}{3} - \frac{\sigma_y^2}{3} + (\phi^0)^2 \right] dV = 0 \\ \Rightarrow m^0 &= \left[\frac{\int_V \left[\frac{\sigma_y^2}{3} - (\phi^0)^2 \right] dV}{\int_V \left[\frac{(\sigma^0)^2}{3} \right] dV} \right]^{\frac{1}{2}} \end{aligned} \quad (2.19)$$

$$\begin{aligned} \frac{\partial F}{\partial \phi^0} &= 2\phi^0 = 0 \\ \Rightarrow \phi^0 &= 0 \end{aligned} \quad (2.20)$$

Letting $\phi^0 = 0$, Seshadri and Mangalaramanan [6] proposed an expression for the upper bound multiplier m^0 from Eq.(2.19) as:

$$m^0 = \frac{\sigma_y}{\left[\frac{\int_V (\sigma^0)^2 dV}{\sqrt{V}} \right]} \quad (2.21)$$

Eq.(2.21) implies that the calculation of m^0 is based on the total volume assuming the parameter μ^0 is constant throughout the structure.

Pan and Seshadri [7] derived an expression for m^0 directly from the ‘‘integral mean of yield’’ that allows for a variation of the flow parameter, μ^0 . The expression for ‘‘integral mean of yield’’ given in Eq.(2.3) can be re-written as (combining Eq.(2.4), Eq.(2.15) and Eq.(2.14)):

$$\int_V \mu^0 \left[\frac{(m^0)^2 (\sigma^0)^2}{3} - \frac{\sigma_y^2}{3} + (\phi^0)^2 \right] dV = 0 \quad (2.22)$$

Letting $\varphi^0 = 0$, Pan and Seshadri [7] proposed an expression for the upper bound multiplier m^0 (named as m_2^0) from Eq.(2.22) as:

$$m_2^0 = \frac{\sigma_y}{\sqrt{\frac{\int_V \mu^0 (\sigma^0)^2 dV}{\int_V \mu^0 dV}}} \quad (2.23)$$

For the initial linear elastic analysis, $m_2^0 = m^0$. Compared to m^0 , the multiplier m_2^0 converge more rapidly to the exact value with successive elastic FEA iterations as discussed in the later part of this thesis.

In terms of linear elastic analysis, statically admissible stress state σ^0 is considered as the von Mises equivalent elastic stress field σ_{eq} . Therefore from this point onward, the statically admissible stress σ^0 will be represented as σ_{eq} throughout the thesis.

Moreover volume ‘V’ in the above expressions implies the total volume of the structure in a finite element discretization scheme. If plastic collapse occurs over a localized region of the structure, m^0 will be significantly overestimated. To overcome this problem, Seshadri and Mangalaramanan [6] introduced the concept of reference volume to identify the kinematically active volume. From this point onward throughout the thesis, the total volume of the structure will be represented as V_T and the reference volume will be represented as V_R .

2.4 Reference Stress Concept

On the basis of energy dissipation considerations, “reference stress” is the stress level at which the average energy dissipation rate in uniaxial tensile test can be equated to the dissipation rate in a component or a structure made of that material under a system of loads [28]. Calladine and Drucker [28] proposed the “theorem of nesting surfaces” and obtained an expression for “reference stress”. The reference stress obtained could be used for approximate estimation of limit load, although such estimate is upper bound in nature.

The dissipation rate in a component or a structure under a system of loads can be equated to the average dissipation rate at the "reference stress state,"

$$\text{i.e.} \quad \sigma_{ref} \epsilon_{ref} V = \int_V \sigma_{eq} \epsilon_{eq} dV \quad (2.24)$$

Using equivalent stresses and strains to represent the three-dimensional stress-states, and stipulating that steady state creep is of the form $\epsilon = B \sigma^n$,

$$\sigma_{ref}^{n+1} V = \int_V \sigma_{eq}^{n+1} dV \quad (2.25)$$

from which the reference stress can be obtained as:

$$\sigma_{ref} = \left[\frac{1}{V} \int_V \sigma_{eq}^{n+1} dV \right]^{\frac{1}{n+1}} \quad (2.26)$$

Calladine and Drucker [29] stated that this functional is strictly monotonically increasing with the exponent n . It is bounded below by the result of $n=1$ (elastic) and above by the limiting functional as $n \rightarrow \infty$ (perfectly plastic).

For a two bar structure shown in **Figure 2.1**, the following analytical example is developed in this thesis in order to clarify the above concept:

The two-bar model is under the load P ; therefore the bars are subjected to axial loading only.

Stresses in bar 1 and 2 can be expressed as (considering isotropic material property), i.e.

$$\sigma_1 = \frac{1/L_1}{A_1/L_1 + A_2/L_2} P$$

$$\sigma_2 = \frac{1/L_2}{A_1/L_1 + A_2/L_2} P$$
(2.27)

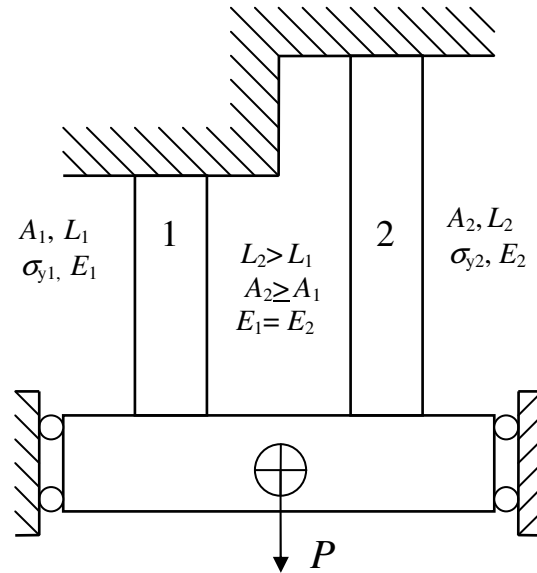


Figure 2.1 Two bar model

Therefore the expression for reference stress for a two bar structure can be written as,

$$\sigma_{ref} = \frac{1}{V^{n+1}} \left[\sigma_1^{n+1} V_1 + \sigma_2^{n+1} V_2 \right]^{\frac{1}{n+1}}$$
(2.28)

Substituting the above equation by the two bar stress terms,

$$\sigma_{ref} = \frac{P}{V^{\frac{1}{n+1}} \left(\frac{A_1}{L_1} + \frac{A_2}{L_2} \right)} \left(\frac{V_1}{L_1^{n+1}} \right)^{\frac{1}{n+1}} \left[1 + \frac{\left(\frac{V_2}{L_2^{n+1}} \right)^{\frac{1}{n+1}}}{\left(\frac{V_1}{L_1^{n+1}} \right)^{\frac{1}{n+1}}} \right] \quad (2.29)$$

For $n=1$ (elastic):

$$\sigma_{ref} = \frac{P}{V^{\frac{1}{2}} \left(\frac{A_1}{L_1} + \frac{A_2}{L_2} \right)} \left[\frac{V_1}{L_1^2} + \frac{V_2}{L_2^2} \right]^{\frac{1}{2}} \quad (2.30)$$

For $n \rightarrow \infty$ (perfectly-plastic):

Expanding Eq.(2.29) in series and neglecting the higher order terms,

$$\sigma_{ref} = \frac{P}{\left(\frac{A_1}{L_1} + \frac{A_2}{L_2} \right) L_1} \quad (2.31)$$

Figure 2.2 shows the reference stress variation with exponent n for a particular set of two bar parameters. The reference stress is monotonically increasing with exponent n and for any value of n it satisfies Eq.(2.32).

$$\sigma_{ref \mid n=1} \leq \sigma_{ref \mid n} \leq \lim_{n \rightarrow \infty} (\sigma_{ref}) \quad (2.32)$$

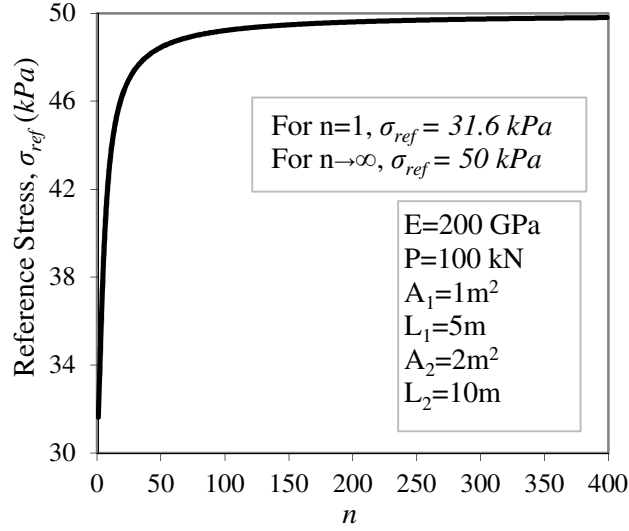


Figure 2.2 Reference stress variation in a two bar structure

With respect to Eq.(2.32), $\sigma_{ref/n}$ is enveloped above by $\sigma_{ref/n=1}$ and below by the limit surface $\lim_{n \rightarrow \infty} (\sigma_{ref})$, which is the yield surface.

For general linear elastic analysis ($n=1$), the reference stress expression (Eq.(2.26)) is used in the form,

$$\sigma_{ref} = \frac{\sqrt{\int_{V_T} (\sigma_{eq})^2 dV}}{\sqrt{V_T}} \quad (2.33)$$

Comparing Eq.(2.33) with Eq.(2.21) implies that the denominator of Eq.(2.21) is essentially the reference stress estimate. The estimation of multiplier m^0 being an upper bound thus makes sense, since the reference stress has been derived on the basis of the energy dissipation consideration.

2.5 Reference Volume Concept

When plastic flow occurs over a localized region of the mechanical component or structure, the remaining regions do not participate in inelastic action and may remain rigid or elastic at the limit state. Therefore only a portion of the total volume carries the external loads at the limit state. The volume that actively participates in plastic action is called kinematically active volume or reference volume and the remaining regions are called kinematically inactive volume or dead volume.

When the primary load is carried by a localized region, it causes significant reduction in load carrying capacity of the total component or structure. Therefore, m^0 will be significantly overestimated if it is calculated based on the total volume V_T .

Consider a component subjected to arbitrary loading condition, as shown in **Figure 2.3**. The component is divided into two regions: (1) reference volume (V_R), which is kinematically active volume; and (2) the dead volume (V_D), which is kinematically inactive volume. If V_T is the total volume of the mechanical component or structure,

$$V_R + V_D = V_T \quad (V_R \leq V_T) \quad (2.34)$$

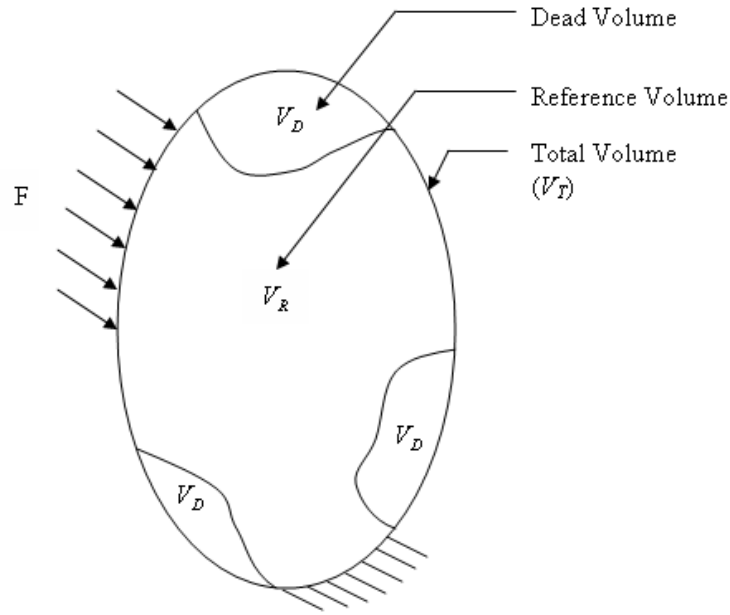


Figure 2.3 Kinematically active and inactive volume

Therefore it is important to incorporate the proper reference volume corrections in the limit load approximation techniques, when they have explicit dependency on the multiplier m^0 .

2.6 Linear Elastic Analysis Approach for Limit Load Approximation

The linear elastic analysis deals with the behavior of solid deformable bodies, which are able to recover their original shape upon the removal of the applied loads. The elastic analysis of a mechanical component or structure essentially involves the determination of the statically admissible and kinematically admissible stress and strain fields, which satisfies the equilibrium, compatibility as well as constitutive relationships.

Analytical linear elastic solutions are limited to simple geometries and loading conditions in terms of calculating limit loads. Therefore, numerical methods are required for the general mechanical component and structure configurations. Elastic Modulus Adjustment Procedure

(EMAP) [6] is an example of a numerical method which involves iterative linear elastic analysis. The aim of EMAP is to generate inelastic-like stress redistribution by modifying the local elastic moduli during iterative linear elastic analysis. An arbitrary load set with the original material elastic modulus is applied in the first iteration of elastic FEA. Subsequently, the elastic modulus of each element is modified in each successive iteration by following:

$$E^{i+1} = \left(\frac{\sigma_{ref}^i}{\sigma_{eq}^i} \right)^q E^i \quad (2.35)$$

where q is the elastic modulus adjustment parameter, and the superscript “ i ” is the iteration number ($i=1$ for the initial elastic analysis).

Eq.(2.35) describes how the elastic modulus at a location is updated from the i^{th} to the $(i+1)^{th}$ elastic iteration. In order to simulate the plastic incompressibility condition, Poisson’s ratio is usually chosen close to 0.5. Therefore by specifying spatial variations in the elastic modulus, numerous sets of statically admissible and kinematically admissible stress and strain distributions are generated, and limit loads for practical components can be obtained.

Simplified limit load approximations can also be made based on a typical single linear elastic analysis. In this approach, an arbitrary load set with the original material elastic modulus is applied on the FE model and a linear elastic analysis is performed. The upper and lower bound limit load solution are then obtained from the statically admissible and kinematically admissible stress and strain distribution. These two solutions are then systematically combined together in order to achieve a lower bound limit load solution with acceptable accuracy. It should be mentioned here that single linear elastic run is nothing but the first iteration of EMAP.

2.7 Closure

Statically admissible and kinematically admissible stress and strain distributions can be obtained by performing a single linear elastic analysis or a series of linear elastic FEA in conjunction with systematic elastic modulus adjustments. Robust concepts of extended variational theorems in plasticity, reference stress, load control and lower bound limit load theorem can be conveniently coupled with the linear elastic analysis for obtaining limit load estimates. The extended lower bound theorem of Mura et al. introduces new ideas such as integral mean of yield. Researchers have investigated this method further and proposed improved limit load estimates. However their bounds have not been investigated. Improved limit load approximations based on Mura's variational formulation and their nature of bounds are discussed in the next chapter.

Chapter 3: Simplified Limit Load Multipliers and their Bounds

3.1 Introduction

Limit load multiplier scales the applied loads proportionally to the level where the structure reaches its limit state. Consider a component or structure made of an elastic–perfectly-plastic material that is in equilibrium with the applied surface traction $P_{Applied}$. It is assumed that the surface traction is applied as proportional loading. When the load ‘ $mP_{Applied}$ ’ is applied, the body will be in a state of impending limit state. The exact limit load multiplier (m) or the safety factor can then be expressed as:

$$m = \frac{P_{Limit}}{P_{Applied}} = \frac{\sigma_y}{\sigma_{PRIMARY}} \quad (3.1)$$

Here $\sigma_{PRIMARY}$ is the primary stress, which ensures equilibrium with externally applied loads.

In traditional limit load analysis, the applied load is incremented in steps until a non-convergence occurs due to the lack of equilibrium condition. The corresponding load is considered as the limit load. On contrary, simplified methods attempt to estimate primary stress (which maintains equilibrium with the externally applied loads) from the linear elastic stress distribution. With respect to Eq. (3.1), the primary stress is proportional to the applied load and the limit load is proportional to the yield strength of a material. It should be noted here that for a simplified limit load multiplier, the denominator of its expression represents an estimate of primary stress when it is re-arranged according to Eq. (3.1).

Lower bound estimates of the limit load multiplier can provide margin of safety against load controlled plastic failure modes. As per the ASME Code guideline [11], yield limit is taken as 1.5 times the allowable strength (which is typically yield strength/1.5) under the design loading condition. Also a factor of safety of 1.5 is to be applied to the calculated limit load multiplier (m) as per the code requirement.

Several estimates of the limit load multipliers can be obtained on the basis of linear elastic analysis. This chapter discusses the upper and lower bound multipliers and the construction of the constraint map. Several limit load multipliers which have explicit dependency on the upper bound multiplier m^0 and lower bound multiplier m_L , their bounds can be established utilizing the constraint map.

This chapter also deals with the limit load bounds for the multiplier m''_{μ} (Seshadri and Indermohan [13]) and m'' (Simha and Adibi-asl [14]). An expression for the multiplier m''_{μ} is proposed in a form which enables parametric examination of its estimate based on the possible approximations of the plastic flow parameter distribution.

Subsequently a list of limit load multipliers available in the literature and their bounds (either established previously or addressed in this thesis) are summarized in this chapter. Basically this chapter gives the essence of the thesis and directs to necessary elaborations provided in the later chapters.

3.2 Classical Lower Bound - Multiplier m_L

The lower bound multiplier, m_L , can be directly obtained by invoking the lower-bound theorem of plasticity. Assume that some stress distribution throughout the component or structure can be found, which is everywhere in equilibrium internally, balances the external loads and at the same time does not violate the yield condition. Then the corresponding applied loads will be less than, or at most equal to, the exact limit load; and will be carried safely by a sufficiently ductile material.

The estimated stress distribution does not violate the yield condition if the material yield strength is considered equal to the maximum equivalent stress $(\sigma_{eq})_{\max}$, anywhere in the structure. If σ_y is the yield strength of the elastic-plastic material, then the classical lower-bound multiplier (m_L) can be expressed as:

$$m_L = \frac{\sigma_y}{(\sigma_{eq})_{\max}} \quad (3.2)$$

Proof of the lower bound theorem can be found in the books by Calladine [3] and Lubliner [4].

3.3 Upper Bound Solution - Multiplier m^0

As discussed in Chapter 2, Seshadri and Mangalaramanan [6] proposed an expression for the upper bound multiplier m^0 , by assuming that the flow parameter μ^0 for any statically admissible stress state will be a constant throughout the structure. The expression given in Eq.(2.21) can be re-written as:

$$m^0 = \frac{\sigma_y}{\left[\frac{\sqrt{\int_{V_T} (\sigma_{eq})^2 dV}}{\sqrt{V_T}} \right]} = \frac{\sigma_y}{\sigma_{ref}} \quad (3.3)$$

The denominator of Eq.(3.3) refers to the "reference stress" (σ_{ref}). In chapter 2, σ_{ref} has been derived on the basis of energy dissipation considerations, therefore m^0 would correspond to an upper bound limit load.

Pan and Seshadri [7] proposed an improved expression for evaluating m^0 (named as m_2^0), based on the "integral mean of yield" criterion (detail derivation is provided in Chapter 2). It is based on the idea that m^0 is a distributed parameter that characterizes the degree of plastic flow at a given location and can be expressed as (see Eq.(2.23)):

$$m_2^0 = \frac{\sigma_y}{\left[\frac{\int_{V_T} \mu^0 (\sigma_{eq})^2 dV}{\int_{V_T} \mu^0 dV} \right]} \quad (3.4)$$

With respect to Eq.(3.4) the super-scripted variable μ^0 is a flow parameter distribution, associated with any statically admissible stress state.

On the basis of deformation theory of plasticity, the flow rule can be expressed as:

$$\varepsilon'_{ij} = \mu \sigma'_{ij} \quad (3.5)$$

The above expression relates the stress and strain deviators using a scalar parameter μ , known as actual plastic flow parameter. Therefore the distribution of actual flow parameter (μ) can be defined as [7]:

$$\mu = \frac{3 \bar{\varepsilon}}{2 \bar{\sigma}} = \frac{3}{2} \frac{1}{E_S} \quad (3.6)$$

where $\bar{\sigma} = \sqrt{\frac{3}{2} \sigma'_{ij} \sigma'_{ij}}$ is the effective stress and $\bar{\varepsilon} = \sqrt{\frac{2}{3} \varepsilon'_{ij} \varepsilon'_{ij}}$ is the effective strain and E_S is the secant modulus of an element.

Now that the super-scripted variable μ^0 associated with any statically admissible stress state, it is also a function of the secant modulus of every element in a given elastic FEA scheme, i.e.,

$$\mu^0 = \frac{C}{E_S} \quad (3.7)$$

where C is a constant whose value depends on the specific geometric configuration and loading pattern. As the stress distribution approaches the limit-type distribution, the distribution of the plastic flow parameter μ^0 will get closer to the distribution of actual flow parameter μ .

i.e.,

$$m_2^0 = \frac{\sigma_y}{\sqrt{\frac{\int_{V_T} \frac{1}{E_S} (\sigma_{eq})^2 dV}{\int_{V_T} \frac{1}{E_S} dV}}} \quad (3.8)$$

In terms of linear elastic stress distribution, E_s is assumed as the ratio of equivalent stress and equivalent strain. Therefore the above expression can be written as:

$$\text{i.e.,} \quad m_2^0 = \frac{\sigma_y}{\sqrt{\frac{\int_{V_T} \sigma_{eq} \varepsilon_{eq} dV}{\int_{V_T} \frac{\varepsilon_{eq}}{\sigma_{eq}} dV}}} \quad (3.9)$$

For the initial linear elastic analysis, $m_2^0 = m^0$, therefore the upper bound multiplier is denoted simply as m^0 when single linear elastic analysis is employed.

3.4 Concept of the Constraint Map

The constraint map [8] is a plot where the classical lower bound multiplier (m_L) and the upper bound multiplier (m^0) are set to be the extreme bounds, in order to identify the exact solution region for any component or structure. The constraint map also represents a primary stress state, which corresponds to the limit state.

3.4.1 Construction of the Constraint Map

When the exact solution (m) is assumed to be coincide with the lower bound multiplier (m_L), then

$$\text{i.e.,} \quad m = m_L \quad (3.10)$$

Eq.(3.10) can be rewritten in the following form,

$$\frac{m^0}{m} = \frac{m^0}{m_L} \quad (3.11)$$

Defining $R^0 = \frac{m^0}{m}$ and $\zeta = \frac{m^0}{m_L}$, the above equation can be expressed as:

$$R^0 = \zeta \quad (3.12)$$

Conversely, when the exact solution (m) is assumed to be coincide with the upper bound multiplier (m^0), then

$$m = m^0 \quad (3.13)$$

Eq.(3.13) can be rewritten in the following form,

$$R^0 = 1 \quad (3.14)$$

The constraint map is a plot of R^0 versus ζ , where Eq.(3.12) represents the line with a slope of $\tan \theta = \left(\frac{dR^0}{d\zeta}\right) = 1$ and Eq.(3.14) represents the horizontal axis $\left(\tan \theta = \left(\frac{dR^0}{d\zeta}\right) = 0\right)$, as shown in **Figure 3.1**. The exact multiplier for a mechanical component or a structure lies between $R^0 = 1$ and $R^0 = \zeta$ line.

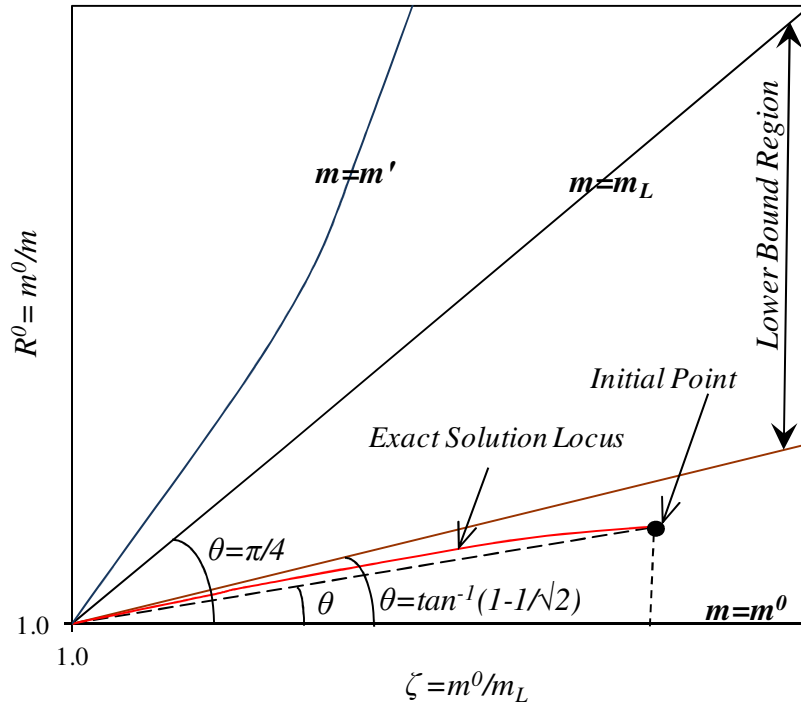


Figure 3.1 Constraint map showing relative magnitudes of different multipliers (θ in radian)

The origin of the constraint map ($R^0=1$, $\zeta=1$) represents a primary stress state, which also corresponds to a limit state. For a particular component or structure, ζ signifies the degree of stress concentration or “kinematic redundancy” in its linear elastic stress distribution, due to the presence of varying proportion of secondary and peak stresses.

3.4.2 The Exact Multiplier, m

As discussed above, the constraint map enables identification of a region where the exact solution (as shown in **Figure 3.1**) for any mechanical component and structure is located. The general expression of exact limit load multiplier, m (which is not known a priori) can now be expressed as:

$$R^0 = \frac{m^0}{m} = 1 + (\zeta - 1)\tan\theta \quad (3.15)$$

In the above equation, $\zeta = \frac{m^0}{m_L}$. In this expression $\tan\theta$ could be any value between $0 \leq \tan\theta \leq 1$.

In **Figure 3.1** ' m ' is represented by 'initial point'. A detail description of exact solution locus is given in Section 5.6.

For a component or structure, m^0 and m_L are available from the linear elastic stress distribution, leaving $\tan\theta$ being the only unknown towards the evaluation of the exact multiplier.

Setting $\tan\theta=1$ in Eq.(3.15) leads to the equation $m=m_L$, and specifying $\tan\theta=0$ results in the equation, $m=m^0$. Specifying an appropriate value of $\tan\theta$ which is less than 1 but greater than 0, could narrow down the region where exact solution could be located. Once an appropriate value of $\tan\theta$ could be specified for Eq.(3.15), it will give more accurate lower bound limit load solution compared to the classical lower bound m_L , for any practical mechanical component or structure.

In this thesis it is established that the exact multiplier ' m ' for a component or a structure lies between the lines having slope of $\tan\theta = \left(1 - \frac{1}{\sqrt{2}}\right)$ and $\tan\theta=0$. A detailed description is provided in Chapter 5.

3.5 Mura's Extended Lower Bound - Multiplier m'

As discussed in Chapter 2, Mura's extended variational principle [30] [5] leads to a lower bound multiplier (m') and can be expressed as (see Eq.(2.11)):

$$m' = \frac{m^0}{1 + \frac{\max \left[\frac{(m^0)^2 (\sigma_{eq})^2}{3} - \frac{\sigma_y^2}{3} + (\varphi^0)^2 \right]}{\frac{2}{3} \sigma_y^2}} \leq m \quad (3.16)$$

Specifying $\varphi^0 = 0$ Eq.(3.16) can be expressed as:

$$m' = \frac{2m^0}{1 + \frac{\sigma_y^2}{(\sigma_{eq})_{\max}^2}} \leq m \quad (3.17)$$

Using uniaxial equivalents for multiaxial stress states, Eq.(3.17) can be written in a form that is suitable for an FEA scheme [6], i.e.,

$$m' = \frac{2m^0}{1 + \left(\frac{m^0}{m_L} \right)^2} \quad (3.18)$$

The expression of m' by normalizing with the exact multiplier m can be represented as,

$$R' = \frac{2R^0}{1 + \zeta^2} \quad (3.19)$$

where $R' = \frac{m'}{m}$, $\zeta = \frac{m^0}{m_L}$ and $R^0 = \frac{m^0}{m}$

In the constraint map, $R'=1$ trajectory ($m=m'$ trajectory) can be represented by plotting the relationship given in Eq.(3.20) as shown in **Figure 3.1**.

$$R^0 = \frac{m^0}{m'} = \frac{1 + \zeta^2}{2} \quad (3.20)$$

In order to obtain the slope of the tangent line for the curve at any ζ location, differentiate Eq.(3.20) with respect to ζ . The slope of the tangent line at limit state ($m^0 = m_L = m' = m$) can be obtained as,

$$\left(\frac{dR^0}{d\zeta} \right)_{\zeta=1} = 1 \quad (3.21)$$

This is the slope of the $R^0 = \zeta$ line (Eq.(3.12)) as discussed earlier. Therefore $R^0 = \zeta$ line is tangent to the curve defined by Eq.(3.20), at limit state. Hence the trajectory of classical lower bound multiplier always lies below the Mura's lower bound trajectory with the exception at limit state (at limit state $m_L = m'$), as shown in **Figure 3.1**. This proves that for any value of ζ , $m' < m_L$, except $\zeta=1$.

3.6 Variational Limit Load Multiplier m''_{μ}

Letting $\varphi^0 = 0$, in Eq.(2.12) Seshadri and Indermohan [13] derived the multiplier m''_{μ} as:

$$m''_{\mu} = \frac{m^0}{1 + G_{\mu}} \leq m$$

where

$$G_{\mu} = \frac{3}{2\sigma_y^2} \frac{\int_{V_T} \mu f(s_{ij}^0) dV}{\int_{V_T} \mu dV} \quad (3.22)$$

Here m is the exact limit load multiplier.

As shown in Chapter 2, the von Mises yield function $f(s_{ij}^0)$ for any element can be expressed as:

$$f(s_{ij}^0) = \frac{1}{3} \left[(m^0 \sigma_{eq})^2 - \sigma_y^2 \right] \quad (3.23)$$

The exact distribution of plastic flow parameter μ can only be determined from the limit state stress distribution. In order to achieve an approximate distribution of μ from a linear elastic stress distribution, following approximation is proposed.

3.6.1 Approximate Distribution of Plastic Flow Parameter

The secant modulus (also known as effective modulus of elasticity in inelastic state) E_s of various elements in a finite element discretization scheme was specified by Pan and Seshadri [7] (as discussed in Section 3.3), in order to simulate the distributed effect of the plastic flow parameter. The general expression for the distribution of plastic flow parameter across elements proposed by Pan and Seshadri can be represented as (shown in **Figure 3.2**):

$$\mu = \frac{3}{2} \frac{1}{E_s} \quad (3.24)$$

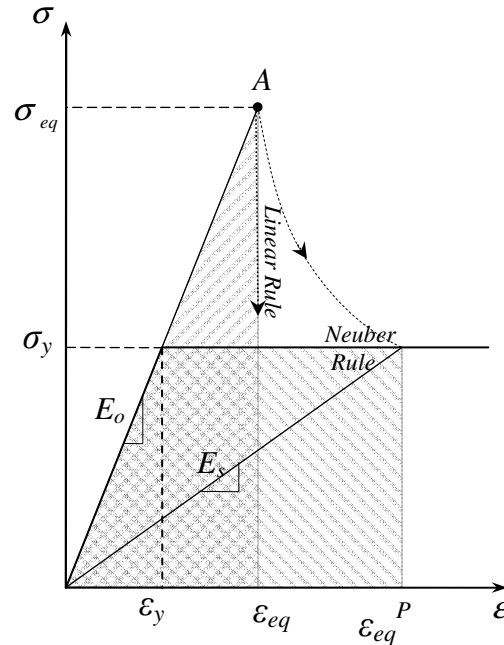


Figure 3.2 Schematic of the stress-strain relationship [15]

With respect to **Figure 3.2**, E_o is the linear elastic modulus and E_s is the Secant Modulus of an element.

A general relation between the linear elastic modulus (elastic state) and the Secant Modulus (inelastic state) can be expressed as [15]:

$$E_s = \left(\frac{\sigma_y}{\sigma_{eq}} \right)^q E_o \quad (3.25)$$

Now, substituting Eq.(3.24) by E_s , the general expression for the flow parameter distribution is proposed as follows:

$$\mu = \frac{3}{2} \frac{1}{\left(\frac{\sigma_y}{\sigma_{eq}} \right)^q E_o} \quad (3.26)$$

As illustrated in **Figure 3.2**, in order to bring point A (which represents the equivalent stress and strain calculated from elastic solution) to the yield surface level, q would be dependent on the local constraint (the constraint in each part of a component or structure). Depending on the value of ' q ', several approximations of μ (based on Eq.(3.26)) could be made. The accurate value of q ($q=q_{exact}$) will vary for different geometric configurations and is not known a priori.

Notch stress strain conversion (NSSC) rules [15] are widely used to estimate nonlinear and history-dependent stress-strain behavior of the notch components or structures. NSSC rules provide an approximate formula to relate local elastic-plastic stress and strain at the notch root to those predicted elastically. In Eq.(3.26), $q=1$ refers to the linear NSSC rule, which assumes that the strains for pseudo elastic and inelastic states are same (shown in **Figure 3.2**). This rule gives a better estimation for plane strain compared with the plane stress condition [17]. On the other

hand, $q=2$ refers to the Neuber rule [16] (shown in **Figure 3.2**), which assumes that the redistribution of elastic stress to inelastic state occurs along the Neuber's hyperbola. Studies revealed that $q \geq 2$ generally overestimate the local inelastic strain and stress [18][19]. Therefore $q \geq 2$ usually gives higher assurance of lower bound limit load.

As per equivalent strain energy density (ESED) rule [20], $q = \ln\left(\frac{2\sigma_y^2}{\sigma_{eq}^2 + \sigma_y^2}\right) / \ln\left(\frac{\sigma_y}{\sigma_{eq}}\right)$ can also be used in Eq.(3.26). In this approach, the value of 'q' varies in element basis.

3.6.2 Limit Load Bounds for Multiplier m_μ''

Based on the above discussion, the proposed μ from Eq.(3.26) and $f(s_{ij}^0)$ from Eq.(3.23) can be substituted into Eq.(3.22) and the modified expression for m_μ'' is proposed as shown in Eq.(3.27). This expression enables parametric examination of m_μ'' multiplier estimate based on the possible approximations of the plastic flow parameter distribution, by varying the value of 'q' in Eq.(3.27).

$$m_\mu'' = \frac{m^0}{1 + \frac{1}{2} \frac{\int_{V_r} \left[\frac{3}{2} \frac{1}{\left(\frac{\sigma_y}{\sigma_{eq}}\right)^q} E_o \right] \left[\left(m^0 \frac{\sigma_{eq}}{\sigma_y}\right)^2 - 1 \right] dV}{\int_{V_r} \left[\frac{3}{2} \frac{1}{\left(\frac{\sigma_y}{\sigma_{eq}}\right)^q} E_o \right] dV}} = \frac{m^0}{1 + G_\mu} \quad (3.27)$$

With respect to Eq.(3.27), an approximate flow parameter distribution obtained on the basis of single linear elastic analysis gives an estimate of m_μ'' for which its bounds are not obvious. For example when $q=0$ is specified in Eq.(3.27), G_μ becomes zero, leading to $m_\mu''=m^0$. For any other values of q , the nature of the bounds for the multiplier m_μ'' is not obvious.

It is found that, the multiplier m_μ'' decreases with increasing of q , as shown in **Figure 3.3** (starting from $m_\mu''=m^0$ when $q=0$). Therefore for a particular value of $q=q_{exact}$ the multiplier $m_\mu''=m$. However the value of q_{exact} is not known a priori for a particular component or structure. It should be mentioned here that $q \geq 2$ generally overestimate the local inelastic strain and stress [18][19]. Therefore $q \geq 2$ usually gives higher assurance of lower bound limit load.

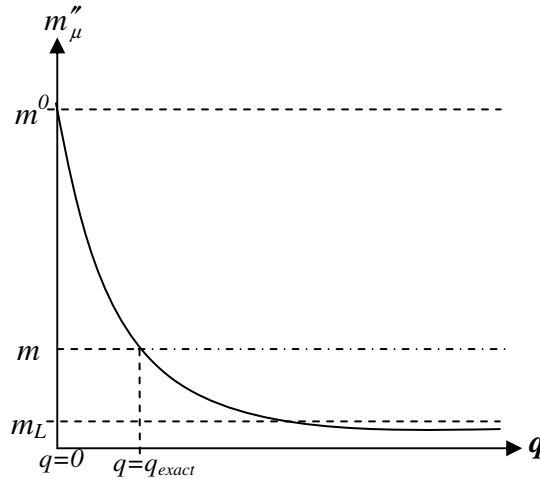


Figure 3.3 Variation of m_μ'' with q

3.6.3 Analytical Examples

The estimates of multiplier m_μ'' is examined using the analytical solution of different beam configurations. Detailed analytical derivations are provided in Appendix A.

3.6.3.1 Rectangular Beam Analysis

Assuming the beam of unit width (w), thickness (t) and yield strength (σ_y) shown in **Figure 3.4**, consider the elastic stress field under bending moment (M), and the axial stress as a function of height from the neutral axis, y . For this configuration, the estimates of limit load multipliers are presented in **Table 3.1**. Detailed derivations are given in Appendix A.1.

Table 3.1 Limit load multipliers for a rectangular beam

m^0	m_L	m	$\frac{m''}{m}$	$\frac{m''_\mu}{m}$ (when $q=1$)	$\frac{m''_\mu}{m}$ (when $q=2$)
$\frac{1}{\sqrt{12}} \frac{\sigma_y t^2}{M}$	$\frac{1}{6} \frac{\sigma_y t^2}{M}$	$\frac{1}{4} \frac{\sigma_y t^2}{M}$	0.8	0.93	0.83

With respect to **Figure 3.4**, m''_μ decreases from m^0 to m_L with increasing q , as shown in a normalized form. For this particular example, exact solution corresponds to $q=0.5$.

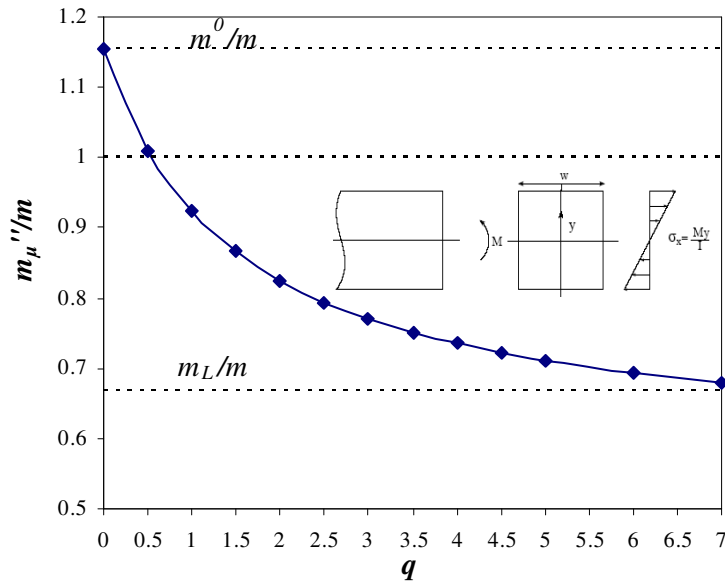


Figure 3.4 Variation of m''_μ with q for a rectangular beam

3.6.3.2 Thin Circular Pipe Analysis

Assuming the pipe radius (r) and yield strength (σ_y) shown in **Figure 3.5**, consider the elastic stress field under bending moment (M), and the axial stress as a function of angular position in the cross-section, θ . For this configuration, the estimates of limit load multipliers are presented in

Table 3.2.

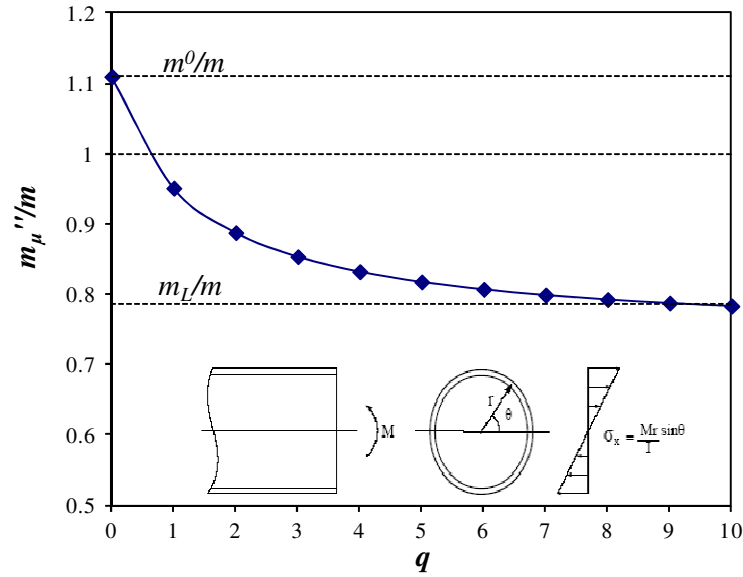


Figure 3.5 Variation of m''_{μ} with q for a thin circular pipe

Table 3.2 Limit load multipliers for a thin circular pipe

m^0	m_L	m	$\frac{m''}{m}$	$\frac{m''_{\mu}}{m}$ (when $q=1$)	$\frac{m''_{\mu}}{m}$ (when $q=2$)
$\frac{\sqrt{2}\sigma_y \pi r^2 t}{M}$	$\frac{\sigma_y \pi r^2 t}{M}$	$\frac{4\sigma_y r^2 t}{M}$	0.82	0.95	0.89

Figure 3.5 shows how m''_{μ} decreases from m^0 to m_L with increasing of q , in a normalized form.

For this particular example, exact solution corresponds to $q=0.7$.

As seen in the above examples, the value of $q=q_{exact}$ is not known a priori for a particular component or structure. This implies that the bounds of m_{μ}'' based on the approximate distribution of μ is not definitive. On contrary, exact distribution of flow parameter is not available based on linear elastic analysis.

3.7 Limit Load Bounds for Multiplier m''

Since the exact distribution of the plastic flow parameter μ is not known (as discussed above), it can be eliminated by applying the Cauchy–Schwartz inequality [8] both in the numerator and denominator of Eq.(3.22). i.e.

$$\int_{V_T} \mu f(s_{ij}^0) dV \leq \sqrt{\int_{V_T} \mu^2 dV} \sqrt{\int_{V_T} (f(s_{ij}^0))^2 dV} \quad (3.28)$$

and

$$\int_{V_T} \mu dV \leq \sqrt{\int_{V_T} \mu^2 dV} \sqrt{\int_{V_T} dV} \quad (3.29)$$

Substituting Eq.(3.28) and Eq.(3.29) into Eq.(3.22), leads to the following expression for G , which replaces G_{μ} .

$$m'' = \frac{m^0}{1+G}$$

where

$$G = \frac{3}{2\sigma_y^2} \sqrt{\frac{\int_{V_T} (f(s_{ij}^0))^2 dV}{V_T}} \Leftrightarrow \frac{1}{2} \sqrt{\frac{\int_{V_T} \left[\left(m^0 \frac{\sigma_{eq}}{\sigma_y} \right)^2 - 1 \right]^2 dV}{V_T}} \quad (3.30)$$

The use of Cauchy–Schwartz inequality above renders the quantity m'' independent of μ but it is not necessarily a lower bound. Comparing Eq.(3.30) and Eq.(3.22), a general expression of lower bound criterion for m'' , can be expressed as:

$$\begin{aligned}
m'' &\leq m''_{\mu} \\
\Rightarrow G &\geq G_{\mu}
\end{aligned}
\tag{3.31}$$

The multiplier m'' is a lower bound provided, $G \geq G_{\mu}$ where G_{μ} has to be evaluated on the basis of the plastic flow parameter distribution at limit state. However the distribution of plastic flow parameter at limit state is not known from a single linear elastic analysis as discussed earlier.

Simha and Adibi-asl [14] approximated a distribution of the flow parameter μ , in order to estimate m''_{μ} and suggested to use this m''_{μ} in Eq.(3.31) for a lower bound check of m'' . Their approximation of μ is shown below. Incidentally their approximation of μ work out to be $q=1$ in Eq.(3.26). Therefore their approximation of μ assumes that the equivalent plastic strain is equal to the equivalent elastic strain (as discussed in section 3.6.1), which could be at times a non-conservative assumption.

$$\mu = \frac{3}{2} \frac{\varepsilon_{eq}}{\sigma_y}
\tag{3.32}$$

Now for the sake of discussion, if m''_{μ} could be achieved based on the exact flow parameter distribution, then there is no need to apply Cauchy–Schwartz inequality [8] on the m''_{μ} formulation at all in order to obtain m'' -multiplier. Conversely, using an approximate value of m''_{μ} in Eq.(3.31) cannot guarantee that m'' -multiplier will be lower bound. Hence the bounds for the multiplier m'' cannot be defined. The estimates of multiplier m'' for several beam configurations are given in **Table 3.1** and **Table 3.2**.

3.8 Robust Limit Load Approximations

From a design point of view, a robust limit load approximation is the one which is consistently lower bound for any practical components or structures. At the same time its magnitude is larger than the classical solution and close to exact limit load solution.

Although the multiplier m' is a lower bound, its estimate is always lower than or equal to the classical lower bound solution. Therefore its estimation does not have any practical significance.

For multiplier m''_{μ} and m'' , their bounds are not obviously lower bound based on linear elastic analysis as investigated in this chapter.

The bounds of limit load multipliers which has explicit dependency on the multiplier m^0 and m_L , can be investigated using the constraint map. The two bar multiplier [10] and multiplier m_{α}^T [12] has explicit dependency on the multiplier m^0 and m_L . These estimates are found to be sufficiently accurate in the literature although their bounds have not been investigated. There is a scope of investigating the bounds of these multipliers.

Seshadri and Adibi-Asl [10] assumed a two-bar configuration of equal cross-sectional area and proposed the two bar multiplier. In chapter 4 this assumption is eliminated by performing a generalized two bar analysis and reference two bar multiplier is re-evaluated. Subsequently reference two bar multiplier is established as a lower bound multiplier. A guideline for lower bound two bar multiplier estimate for practical components and structures is proposed in Chapter 6.

Chapter 5 investigates the limit load bounds for the multiplier m_α^T and establish this multiplier as a lower bound. A guideline for accurate lower bound limit load based on EMAP is proposed in Chapter 5. A guideline for improving the accuracy of lower bound m_α^T multiplier during single linear elastic analysis is proposed in Chapter 6.

A summary of limit load bounds for several limit load multipliers available in the literature (for which bounds are either already established in the literature or will be addressed in the subsequent chapters of this thesis) are presented in **Table 3.3**. The relative magnitudes of some of the following multipliers can also be viewed from the constraint map as shown in **Figure 5.1**.

Table 3.3 Summary of limit load bounds for several multipliers

Limit Load Multiplier	Nature of Bounds	Remarks
Multiplier, m	Exact solution	Usually not known from linear elastic analysis
Multiplier, m^0	Upper bound	$m \leq m^0$ [8]
Multiplier, m_2^0	Upper bound	$m \leq m_2^0 \leq m^0$ [8]
Classical multiplier, m_U	Upper bound	$m \leq m_U \leq m_2^0$ [8]
Classical multiplier, m_L	Lower bound	$m_L \leq m$ [3] [4]
Mura's multiplier, m'	Lower bound	$m' \leq m_L \leq m$ [8]
Suggested estimate of two bar multiplier (m_{TBM}) in this thesis	Lower bound	$m_L \leq m_{TBM} \leq m_\alpha^T \leq m$ m_{TBM} offers much better accuracy than m_L
Suggested estimate of m_α^T multiplier in this thesis	Lower bound	$m_L \leq m_\alpha^T \leq m$ m_α^T is more accurate than m_{TBM}
Multiplier m_α [6]	Lower bound	$m_L \leq m_\alpha \leq m_\alpha^T \leq m$
Multiplier m_μ''	Bounds could not be established	Exact distribution of plastic flow parameter is not available from linear elastic analysis.
Multiplier m''	Bounds could not be established	Exact distribution of plastic flow parameter is not available from linear elastic analysis.

3.9 Discussion and Conclusion

A summary of the simplified limit load approximation techniques which sets the stage for the development of this thesis are discussed. The construction of the constraint map is presented mathematically, which was originally conceptualized by Reinhardt and Seshadri [8] as a constraint plot.

NSSC rules are introduced into the expression of plastic flow parameter distribution proposed by Pan and Seshadri [7]. A general expression of plastic flow parameter distribution is proposed in a form which enables parametric examination of the possible approximations of the plastic flow parameter based on a linear elastic analysis.

Limit load bounds for the multiplier m''_{μ} and m'' have also been investigated. The lower bound estimate of the multiplier m''_{μ} relies on the exact distribution of plastic flow parameter. It is shown that for an approximate distribution of flow parameter, m''_{μ} is either an upper bound or its bounds are not obvious. Simha and Adibi-Asl [14] proposed an inequality relation ($m'' < m''_{\mu}$) for lower bound m'' . It is concluded that the inequality ($m'' < m''_{\mu}$) cannot guarantee a lower bound m'' , when m''_{μ} is estimated from an approximate distribution of plastic flow parameter.

A list of limit load multipliers available in the literature and their bounds are summarized. Limit load bounds for the two bar multiplier and multiplier m_{α}^T as well as their systematic implementation will be addressed in the following chapters of this thesis.

Chapter 4: Lower Bound Estimate of the Two Bar Multiplier

4.1 Introduction

In a mechanical component configuration, load-controlled stresses are statically determinate in that they are induced in order to preserve equilibrium with externally applied forces and moments. Deformation-controlled stresses on the other hand are induced as a result of statically indeterminate actions. When widespread inelastic action occurs, the statically indeterminate stresses undergo redistribution throughout the component and become statically determinate after the onset of yielding.

In the above context the two bar [10] structure is the simplest structure in which stress redistribution phenomena occurs after the onset of yielding. Limit loads for mechanical components and structures can be determined, by invoking the concept of equivalence of “static indeterminacy,” which relates a component configuration to the “reference two-bar structure”. Reference two bar structure is the one which provides the bounding limit load estimate over any two bar configurations.

Seshadri and Adibi-Asl [10] first introduced the concept of equivalence of “static indeterminacy” to relate a mechanical component (in which two or more plastic hinges form during the plastic collapse) to a two-bar structure. The idea was to represent a mechanical component by an equivalent reference two bar structure, in order to achieve a limit load solution for the component. However, the two bar model proposed by Seshadri and Adibi-Asl [10] assumed equal cross-sectional area of the bars. As a result the nature of bounds for the limit load solution

is not obvious. There is a scope for developing a general two bar formulation for variable areas, and identify the reference two bar configuration.

In this chapter, effort has been directed to developing the general two bar solution. General two bar analysis enables identification of the reference two bar model, which bounds other two bar configurations in terms of limit load estimation.

A general mechanical component or structure forms multiple plastic hinges during its plastic collapse mechanism. In this sense it is equivalent to a multi bar structure of similar collapse mechanism. . In this chapter, a general multi bar model is developed and the nature of bounds of the reference two bar multiplier over the general multi bar model is investigated. Based on the investigation, the two bar multiplier is established as a potential lower bound solution.

4.2 The Two Bar Structure

Consider a two-bar structure of length L_1 and L_2 with the cross-sectional area A_1 and A_2 respectively, rigidly attached to a horizontal bar under a tension load of P . The basic equations for the two-bar structure shown in **Figure 4.1(c)** assuming equal cross-sectional area ($A_1=A_2$) are:

$$\begin{aligned} \text{Equilibrium equation:} & \quad \sigma_1 + \sigma_2 = \frac{P}{A} \\ \text{Strain-displacement relationship:} & \quad \varepsilon_1 = \frac{\delta_1}{L_1} \quad \text{and} \quad \varepsilon_2 = \frac{\delta_2}{L_2} \\ \text{Compatibility equation:} & \quad \delta_1 = \delta_2 \\ \text{Constitutive relationship:} & \quad \varepsilon_1 = \frac{\sigma_1}{E_1} \quad \text{and} \quad \varepsilon_2 = \frac{\sigma_2}{E_2} \end{aligned}$$

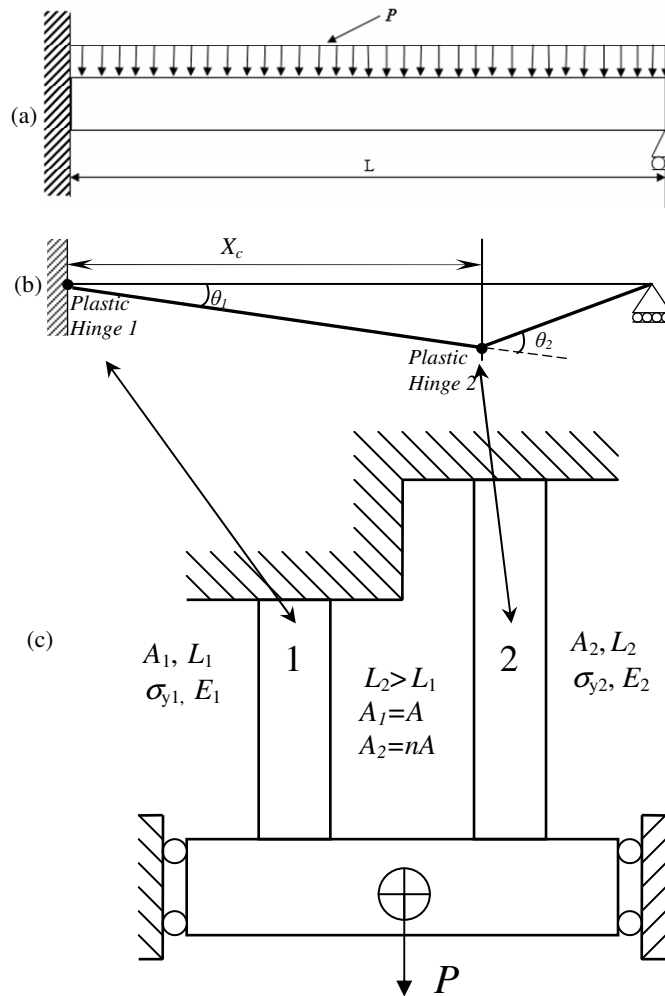
where $(\sigma_1, \varepsilon_1, \delta_1, E_1)$ and $(\sigma_2, \varepsilon_2, \delta_2, E_2)$ are the stress, strain, displacement and elastic modulus for bar1 and bar2 respectively.

4.3 Plastic Collapse of Components and Structures

A component or structure can be visualized to be made up of finite number of sections across the thickness, throughout its length. Every section is a potential plastic hinge location. As the applied load increases, sequential plastic hinges form until local or global plastic flow occurs.

A typical statically indeterminate mechanical component or structure releases static indeterminacies through the sequential formation of plastic hinges eventually resulting in a collapse mechanism. If a plastic collapse mechanism corresponding to two hinges for a beam structure (**Figure 4.1(b)**) where σ_1 and σ_2 are the elastic equivalent stresses ($\sigma_1 \geq \sigma_2$) at the plastic hinge locations of the beam (**Figure 4.1(a)**), then it is sufficient to satisfy equilibrium against the

externally applied surface traction P . As the external load is increased, plastic hinge first forms at the location with stress σ_1 and then at the location with stress σ_2 . When plastic collapse mechanism corresponds to two hinges, it can be represented by a two bar model as shown in **Figure 4.1**. For a multi bar structure, plastic hinge will form in a numerically decreasing order of stress until a local or global collapse mechanism can be identified. In this context, a general mechanical component can be represented by a suitable multi bar model.



(a) Indeterminate beam under uniformly distributed load, (b) Plastic hinge formation and Collapse Mechanism (c) Two bar structure

Figure 4.1 Relating an indeterminate beam to a two-bar structure

Mechanical components which generate multiple hinges can also be represented by a reference two bar structure in terms of achieving lower bound limit load solutions.

By definition, reference two bar structure provides the bounding limit load estimate over all other two bar configurations. Therefore in order to ensure appropriate equivalency, the reference two bar structure needs to be identified by performing a general two bar analysis. In the following section, reference two bar structure has been identified on the basis of general two bar analysis.

4.4 General Two-Bar Analysis

As discussed earlier (in Section 2.4), the geometric configuration of a two bar model is function of length of the bars as well as their cross-sectional areas. Under the applied load P acting on the rigid connection (as shown in **Figure 4.1**); stresses in bar 1 and 2 can be expressed as:

$$\sigma_1 = \frac{1/L_1}{A_1/L_1 + A_2/L_2} P \quad (4.1)$$

$$\sigma_2 = \frac{1/L_2}{A_1/L_1 + A_2/L_2} P$$

For the above two-bar structure, the classical lower bound multiplier can be expressed as,

$$m_L = \frac{\sigma_y}{(\sigma_{eq})_{\max}} = \frac{\sigma_y}{\sigma_1} \quad (4.2)$$

The upper bound m^0 for a homogeneous two bar structure can be obtained as,

$$m^0 = \frac{\sigma_y}{\sigma_{ref}} = \sigma_y \sqrt{\frac{V_1 + V_2}{\sigma_1^2 V_1 + \sigma_2^2 V_2}} \quad (4.3)$$

Here $V_1=A_1L_1$ and $V_2=A_2L_2$.

Substituting Eq.(4.1) into Eq.(4.2) and Eq.(4.3) respectively, when $A_1 = A$ and $A_2 = nA$,

$$m^o = \frac{\sigma_y A}{\sqrt{L_1 L_2} P} \sqrt{(nL_1 + L_2)} \sqrt{(L_1 + nL_2)} \quad (4.4)$$

$$m_L = \frac{\sigma_y A (nL_1 + L_2)}{L_2 P}$$

Hence,

$$\frac{m^o}{m_L} = \sqrt{\frac{L_2}{L_1}} \frac{\sqrt{(L_1 + nL_2)}}{\sqrt{(nL_1 + L_2)}} \quad (4.5)$$

When $n=1$, Eq.(4.5) can be re-written as,

$$\zeta = \frac{m^o}{m_L} = \sqrt{\frac{L_2}{L_1}} \quad (4.6)$$

Yielding initially occurs in the bar with a smaller ratio of yield strength over stress. After the load is increased, the other bar yields and the configuration reaches its limit state. From equilibrium consideration, the exact limit load multiplier for homogeneous two bar structure (m_{TBM}) can be obtained as (when $A_1 = A$ and $A_2 = nA$). i.e,

$$m_{TBM} = P_L / P = \frac{\sigma_y A (1+n)}{P} \quad (4.7)$$

Therefore the ratio of $\frac{m^o}{m_{TBM}}$ can be obtained as,

$$\frac{m^o}{m_{TBM}} = \frac{\sqrt{nL_1 + L_2} \sqrt{L_1 + nL_2}}{\sqrt{L_1} \sqrt{L_2} (1+n)} \quad (4.8)$$

Re-arranging Eq.(4.5) and Eq.(4.8), and substituting them by ζ ,

$$\frac{m^o}{m_L} = \zeta \frac{\sqrt{1+n\zeta^2}}{\sqrt{n+\zeta^2}} \quad (4.9)$$

$$\frac{m^o}{m_{TBM}} = \frac{\sqrt{n+\zeta^2} \sqrt{n+\frac{1}{\zeta^2}}}{1+n} \quad (4.10)$$

Eq.(4.10) can be referred to the family of two bar multiplier.

4.5 Identification of the Reference Two Bar Model

Limit load of a particular two bar structure is unique depending on the length ratio and area ratio of its bars. The constraint map of general two bar configurations can be obtained by plotting Eq.(4.10) against ζ for several values of n . **Figure 4.2** is a similar plot, where Eq.(4.10) has been plotted for $0 \leq n \leq 1$. Each point on a two bar trajectory (in **Figure 4.2**) is a limit load solution for a particular two bar configuration, having a particular length ratio (ζ) and area ratio (n). Based on the plot as shown in **Figure 4.2**, it is evident that, as the value of n decreases, the trajectory tends to approach towards $m=m^o$ trajectory and for $n=0$, the trajectory aligns with the horizontal axis (can also be shown in Eq.(4.10)). Therefore the trajectory for $n=1$, bounds the two bar family (in terms of limit load solution) and hence considered as the reference two bar structure.

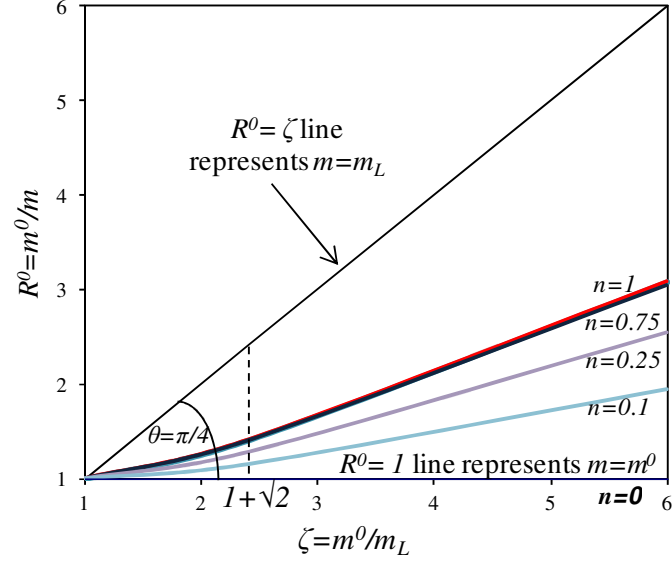


Figure 4.2 Two-bar trajectories for different values of ‘ n ’

Based on the general two bar analysis, Eq. (4.10) can be expressed in the form,

$$\frac{m^0}{m_{TBM}} = \varphi(\zeta, n) = \beta_n f(\zeta) \quad (4.11)$$

where $f(\zeta) = \frac{1 + \zeta^2}{2\zeta}$ and $\beta_n \leq 1$.

$\beta_n = 1$ implies $n = 1$ in Eq.(4.11) (equal cross-sectional area of the bars). Now substituting Eq.(4.11) by Mura’s lower bound expression (Eq.(3.20)), i.e.,

$$\begin{aligned} \frac{m'}{m_{TBM}} &= \frac{m^0}{m_{TBM}} \frac{2}{1 + \zeta^2} \\ \Rightarrow \frac{m'}{m_{TBM}} &= \frac{\beta_n}{\zeta} \\ \Rightarrow m_{TBM} &= \frac{m' \zeta}{\beta_n} \end{aligned} \quad (4.12)$$

Since $\beta_n \leq 1$, therefore it is shown that the reference two bar model ($\beta_n = 1$) provides bounding limit load solution over all the other two bar configurations. This also confirms that the two bar

model of equal cross-sectional area pointed out by Seshadri and Adibi-Asl [10] is indeed the reference two bar structure.

4.6 Relating Mechanical Component to Reference Two Bar Model

As discussed earlier, the general expression for the reference two bar multiplier can be obtained by considering $\beta_n=1$ in Eq.(4.12) (implying equal cross-sectional area of the bars). The expression for reference two bar multiplier is shown below:

$$m_{TBM} = m' \zeta$$

i.e.

$$\Rightarrow m_{TBM} = \frac{m^0}{\left(\frac{1 + \zeta^2}{2\zeta} \right)} \quad (4.13)$$

Limit loads for practical mechanical components and structures can be determined, by using the concept of equivalence of “static indeterminacy,” which relates a component configuration to the “reference two-bar structure”. As an example, the value of $\zeta = \frac{m^0}{m_L}$ for the indeterminate beam (typically obtained from linear elastic FEA) shown in **Figure 4.1(a)** represents the length ratio of the equivalent reference two bar structure.

Based on the linear elastic analysis, m_L and m^0 are known for a mechanical component or structure. Now $\zeta = \frac{m^0}{m_L}$ for the component implies the length ratio of the equivalent reference two bar structure. Therefore once m_L and m^0 are obtained for a mechanical component based on linear elastic analysis (typically by performing a linear elastic finite element analysis), the two bar limit load multiplier (m_{TBM}) estimate for that particular component can be achieved from Eq.(4.13).

4.7 Reference TBM - An Estimate Beyond Mura's Lower Bound

The extended variational form of Mura and coworkers provides a guaranteed lower bound solution, which is however overly conservative compared to the exact limit load. When Mura's lower bound solution is scaled by $\zeta = \frac{m^o}{m_L}$, it points to the reference two bar solution as evident from Eq.(4.13). The quality of the $m'\zeta$ estimate is investigated in Chapter 6 by analyzing a number of mechanical components and structures.

4.8 Bounding Nature of Reference TBM - Multi Bar Structures

The occurrence of a single plastic hinge across the thickness of a component is indicative of a load controlled membrane mode of collapse. This situation can be represented by a one bar model. The presence of a pair of plastic hinges is indicative of a load-controlled membrane plus bending mode of plastic collapse and can be represented by the two bar model. General mechanical components often generate more than two plastic hinges and can be represented by a suitable multi bar model. Multiple numbers of hinge formations can also be expressed in terms of the reference two-bar structure, if it gives bounding limit load estimate over the multi bar models. In this section, general multi bar model has been established and it is shown that the multi bar solutions are bounded by the reference two bar solution.

4.8.1 Three Bar Model

Under the applied load P acting on the rigid connection; stresses in bar 1, 2 and 3 (having same cross-sectional area) can be expressed as (considering isotropic homogeneous material property), i.e.

$$\begin{aligned}\sigma_1 &= \frac{1/L_1}{A_1/L_1 + A_2/L_2 + A_3/L_3} P \\ \sigma_2 &= \frac{1/L_2}{A_1/L_1 + A_2/L_2 + A_3/L_3} P \\ \sigma_3 &= \frac{1/L_3}{A_1/L_1 + A_2/L_2 + A_3/L_3} P\end{aligned}\tag{4.14}$$

For the above three bar structure, the classical lower bound multiplier can be expressed as,

$$m_L = \frac{\sigma_y A (L_2 L_3 + L_1 L_3 + L_1 L_2)}{L_2 L_3 P}\tag{4.15}$$

The upper bound m^0 for a homogeneous three bar structure can be obtained as,

$$m^0 = \frac{\sigma_y A \sqrt{L_2 L_3 + L_1 L_3 + L_1 L_2} \sqrt{L_1 + L_2 + L_3}}{\sqrt{L_1 L_2 L_3} P}\tag{4.16}$$

Hence

$$\zeta = \frac{m^0}{m_L} = \frac{\sqrt{L_1 + L_2 + L_3} \sqrt{L_2 L_3}}{\sqrt{L_2 L_3 + L_1 L_3 + L_1 L_2} \sqrt{L_1}}\tag{4.17}$$

Now considering $L_1=L$, $L_2=\eta L_1$, $L_3=x\eta L_2$. where $L_3>L_2>L_1$.

i.e. $\eta>1$ and $x\eta>1$ or we can say $x>1/\eta$

Therefore,

$$L_1=L, L_2=\eta L, L_3=x\eta^2 L$$

From equilibrium consideration, the exact limit load multiplier for homogeneous three bar structure can be obtained as:

$$m_{Three_bar} = P_L / P = \frac{3\sigma_y A}{P} \quad (4.18)$$

Now Eq.(4.16) and Eq.(4.17) can be written as:

$$\frac{m^0}{m_{Three_bar}} = \frac{1}{3} \sqrt{1 + x\eta + x\eta^2} \sqrt{1 + \frac{1}{x\eta} + \frac{1}{x\eta^2}} \quad (4.19)$$

$$\zeta = \frac{m^o}{m_L} = \frac{\sqrt{1 + x\eta + x\eta^2} \sqrt{1 + \frac{1}{x\eta} + \frac{1}{x\eta^2}}}{1 + \frac{1}{x\eta} + \frac{1}{x\eta^2}} \quad (4.20)$$

Considering the bars are related by the same proportion, we can use $x=1$ in the above equations.

Therefore,

$$\begin{aligned} \frac{m^0}{m_{Three_bar}} &= \frac{1}{3} \sqrt{1 + \eta + \eta^2} \sqrt{1 + \frac{1}{\eta} + \frac{1}{\eta^2}} \\ \Rightarrow \frac{m^0}{m_{Three_bar}} &= \frac{1}{3} \left[\frac{1 + \eta + \eta^2}{\eta} \right] \end{aligned} \quad (4.21)$$

$$\begin{aligned} \zeta = \frac{m^o}{m_L} &= \frac{\sqrt{1 + \eta + \eta^2}}{\sqrt{1 + \frac{1}{\eta} + \frac{1}{\eta^2}}} \\ \Rightarrow \zeta &= \eta \end{aligned} \quad (4.22)$$

Substituting Eq.(4.22) into Eq.(4.21)

$$\frac{m^0}{m_{Three_bar}} = \frac{1}{3} \left[\frac{1 + \zeta + \zeta^2}{\zeta} \right] \quad (4.23)$$

Based on the three bar analysis, the trajectory for the three bar model can be established in the constraint map by plotting Eq.(4.23) against ζ , as shown later in **Figure 4.5**.

4.8.2 Four Bar Model

Under the applied load P acting on the rigid connection; stresses in bar 1, 2, 3 and 4 can be expressed as (considering isotropic homogeneous material property), i.e.

$$\begin{aligned}\sigma_1 &= \frac{1/L_1}{A_1/L_1 + A_2/L_2 + A_3/L_3 + A_4/L_4} P \\ \sigma_2 &= \frac{1/L_2}{A_1/L_1 + A_2/L_2 + A_3/L_3 + A_4/L_4} P \\ \sigma_3 &= \frac{1/L_3}{A_1/L_1 + A_2/L_2 + A_3/L_3 + A_4/L_4} P \\ \sigma_4 &= \frac{1/L_4}{A_1/L_1 + A_2/L_2 + A_3/L_3 + A_4/L_4} P\end{aligned}\tag{4.24}$$

For the above four bar structure, the classical lower bound multiplier can be expressed as,

$$m_L = \frac{\sigma_y A (L_2 L_3 L_4 + L_1 L_3 L_4 + L_1 L_2 L_4 + L_1 L_2 L_3)}{L_2 L_3 L_4 P}\tag{4.25}$$

The upper bound m^0 for a homogeneous four bar structure can be obtained as,

$$m^0 = \frac{\sigma_y A \sqrt{L_2 L_3 L_4 + L_1 L_3 L_4 + L_1 L_2 L_4 + L_1 L_2 L_3} \sqrt{L_1 + L_2 + L_3 + L_4}}{\sqrt{L_1 L_2 L_3 L_4} P}\tag{4.26}$$

Hence

$$\zeta = \frac{m^0}{m_L} = \frac{\sqrt{L_1 + L_2 + L_3 + L_4} \sqrt{L_2 L_3 L_4}}{\sqrt{L_2 L_3 L_4 + L_1 L_3 L_4 + L_1 L_2 L_4 + L_1 L_2 L_3} \sqrt{L_1}}\tag{4.27}$$

Now considering $L_1=L$, $L_2=\eta L_1$, $L_3=x\eta L_2$ and $L_4=y\eta L_3$ where $L_4>L_3>L_2>L_1$.

i.e. $x>1$ and $x\eta>1$ and $y\eta>1$

Therefore,

$$L_1=L, L_2= \eta L, L_3=x\eta^2L, L_4=y\eta^3L \quad (4.28)$$

From equilibrium consideration, the exact limit load multiplier for homogeneous four bar structure can be obtained as:

$$m_{Four_bar} = P_L / P = \frac{4\sigma_y A}{P} \quad (4.29)$$

Now considering the bars are related by the same proportion, we can use $x=y=l$ in the above equations.

Therefore,

$$\begin{aligned} \frac{m^0}{m_{Four_bar}} &= \frac{1}{4} \sqrt{1+\eta+\eta^2+\eta^3} \sqrt{1+\frac{1}{\eta}+\frac{1}{\eta^2}+\frac{1}{\eta^3}} \\ \Rightarrow \frac{m^0}{m_{Four_bar}} &= \frac{1}{4} \left[\frac{1+\eta+\eta^2+\eta^3}{\eta^{\frac{3}{2}}} \right] \end{aligned} \quad (4.30)$$

$$\begin{aligned} \zeta = \frac{m^o}{m_L} &= \frac{\sqrt{1+\eta+\eta^2+\eta^3}}{\sqrt{1+\frac{1}{\eta}+\frac{1}{\eta^2}+\frac{1}{\eta^3}}} \\ \Rightarrow \zeta &= \eta^{\frac{3}{2}} \end{aligned} \quad (4.31)$$

Substituting Eq.(4.31) into Eq.(4.30)

$$\frac{m^0}{m_{Four_bar}} = \frac{1}{4} \left[\frac{1+\zeta^{\frac{2}{3}}+\zeta^{\frac{4}{3}}+\zeta^2}{\zeta} \right] \quad (4.32)$$

Based on the four bar analysis, the trajectory for the four bar model can be established in the constraint map by plotting Eq.(4.32) against ζ , as shown later in **Figure 4.5**.

4.8.3 General Multi Bar Model

Number of plastic hinges formed in a mechanical component can be represented by a suitable multi bar model as shown in **Figure 4.3**. Based on the analysis shown in Section 4.8.1 and 4.8.2, the general expression for a multi bar model can be represented as:

$$\frac{m^o}{m_{n_bar}} = \frac{1 + \zeta^{\frac{2}{n-1}} + \zeta^{\frac{4}{n-1}} + \zeta^{\frac{6}{n-1}} + \zeta^{\frac{8}{n-1}} + \zeta^{\frac{10}{n-1}} \dots + \zeta^2}{n\zeta}$$

where

(4.33)

$$\zeta = \frac{m^o}{m_L} = \eta^{\frac{n-1}{2}}$$

where n is the number of bars in the multi bar model and η is the length ratio between the bars.

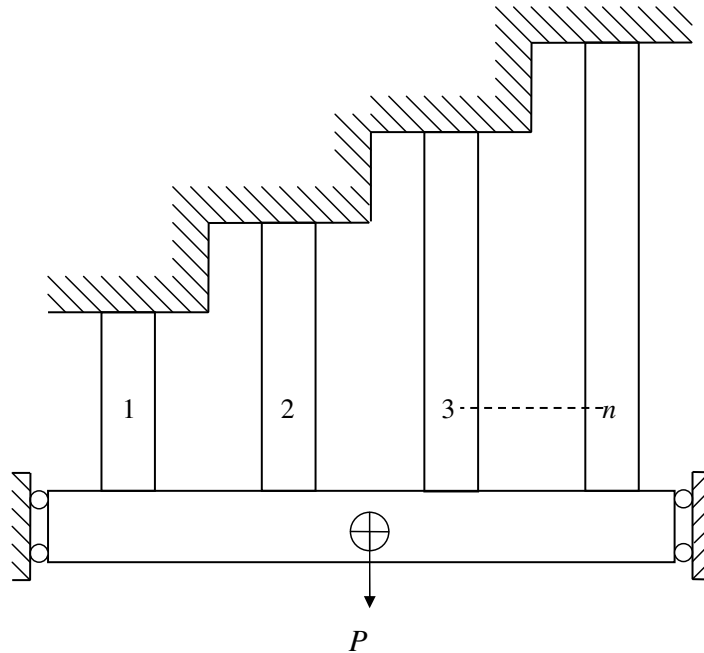


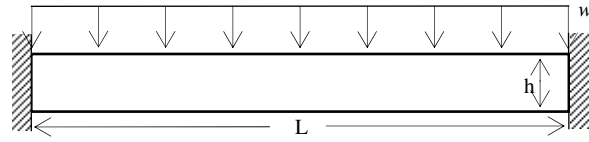
Figure 4.3 Multi bar model

Based on the general multi bar expression presented in Eq.(4.33), multi bar solution for any number of bars are readily available. For example for a five bar structure substituting Eq. (4.33) by $n=5$ will give the five bar solution as shown in **Table 4.1**. Some of the multi bar solutions are tabulated in **Table 4.1**.

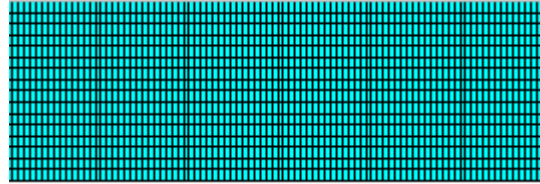
Table 4.1 $\frac{m^0}{m}$ ratio for the multi bar model

Model Description	$\frac{m^0}{m}$ ratio	ζ
'n' bar Model	$\frac{1 + \zeta^{\frac{2}{n-1}} + \zeta^{\frac{4}{n-1}} + \zeta^{\frac{6}{n-1}} + \zeta^{\frac{8}{n-1}} + \zeta^{\frac{10}{n-1}} \dots + \zeta^2}{n\zeta}$	$\eta^{\frac{n-1}{2}}$
Two bar Model ($n=2$)	$\frac{1 + \zeta^2}{2\zeta}$	$\eta^{\frac{1}{2}}$
Three bar Model ($n=3$)	$\frac{1 + \zeta + \zeta^2}{3\zeta}$	η
Four bar Model ($n=4$)	$\frac{1 + \zeta^{\frac{2}{3}} + \zeta^{\frac{4}{3}} + \zeta^2}{4\zeta}$	$\eta^{\frac{3}{2}}$
Five bar Model ($n=5$)	$\frac{1 + \zeta^{\frac{1}{2}} + \zeta + \zeta^{\frac{3}{2}} + \zeta^2}{5\zeta}$	η^2
Six bar Model ($n=6$)	$\frac{1 + \zeta^{\frac{2}{5}} + \zeta^{\frac{4}{5}} + \zeta^{\frac{6}{5}} + \zeta^{\frac{8}{5}} + \zeta^2}{6\zeta}$	$\eta^{\frac{5}{2}}$
Seven bar Model ($n=7$)	$\frac{1 + \zeta^{\frac{1}{3}} + \zeta^{\frac{2}{3}} + \zeta + \zeta^{\frac{4}{3}} + \zeta^{\frac{5}{3}} + \zeta^2}{7\zeta}$	η^3

As a demonstrative example let us consider a fixed-fixed beam as shown in **Figure 4.4**. For this beam, plastic collapse mechanism involves formation of three plastic hinges. Therefore plastic collapse mechanism of a fixed-fixed beam corresponds to an equivalent three bar structure.



(a) Beam geometry



(b) Finite element model segment (plane stress with thickness)

Figure 4.4 Fixed end beam geometry

A fixed end beam with length, $L = 508$ mm; height, $h = 25.4$ mm and width, $w=25.4$ mm is modeled. The modulus of elasticity of the material is 206.85 GPa and yield strength is 206.85 MPa. The beam is subjected to uniformly distributed load of 1 MPa. The model is meshed using PLANE82 elements in ANSYS [21] and width is taken by plane stress with thickness (TK) real constant input. Mesh convergence study is performed to verify the sensitivity of the multipliers with respect to the mesh density. Based on linear elastic analysis m^0 and m_L are evaluated (from from Eq.(3.3) and Eq. (3.2) respectively) and based on inelastic finite element analysis m_{NFEA} is evaluated as shown in **Table 4.2**. Inelastic finite element analysis is performed as per guideline provided in Section 5.6. Analytical limit load solution ($m_{Analytical}$) is also documented. It is evident from **Table 4.2** that a three bar model gives sufficiently accurate limit load solution for a fixed-fixed beam on the basis of single linear elastic analysis. $\frac{m^0}{m_{Analytical}}$ vs $\frac{m^0}{m_L}$ is plotted in the constraint map as a point shown in **Figure 4.5**, which lies close to the three bar trajectory.

Table 4.2 Limit load multipliers for fixed end beam

m^0	m_L	$\zeta = m^0 / m_L$	$m_{Three_bar} = \frac{m^0}{\left[\frac{1 + \zeta + \zeta^2}{3\zeta} \right]}$	m^{NFEA}	$m_{Analytical}$
3.937	0.875	4.498	2.065	2.154	2.069

4.8.4 Limit Load Bounds for Reference TBM

Figure 4.5 shows the constraint map, where several multi bar expressions are plotted against ζ . It is evident that as the number of bars increase, the limit load capacity increases. In this context, reference two bar solution (m_{TBM}) bounds limit load solution of other multi bar models as shown in **Figure 4.5**.

i.e. $m_{TBM} \leq m_{Three_bar} \leq m_{Four_bar} \dots \dots \dots \leq m_{n_bar}$

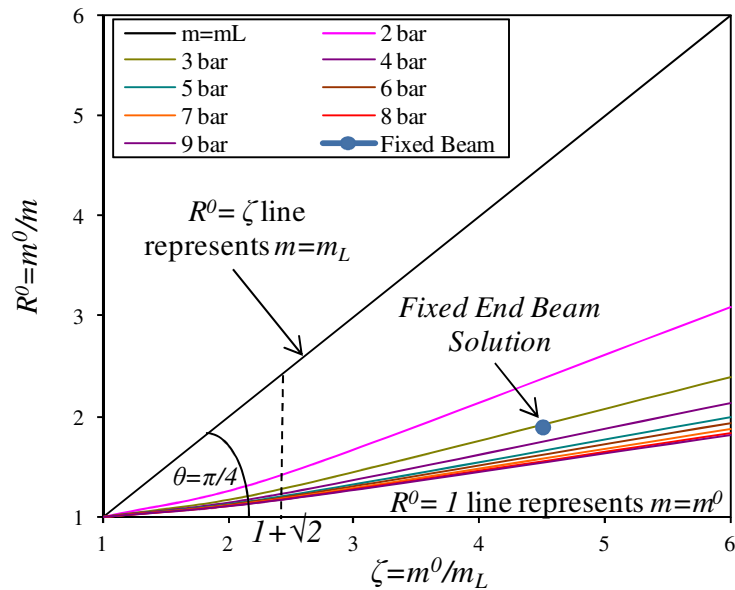


Figure 4.5 The constraint map showing multi bar solutions

Now referring back to the inequality relationship shown in Eq.(2.11), the inequality expression can be re-written as:

$$m' \leq m \quad (4.34)$$

With respect to general two bar solution shown in Eq.(4.12) and general multi bar solutions (shown in **Table 4.1**) it can be concluded that $m' \zeta$ is the bounding limit load solution for multi bar structures. Therefore when the transformation parameter ζ is introduced into Mura's inequality, the quantity still satisfies the inequality for multi bar structures. i.e.

$$m' \zeta \leq m \quad (4.35)$$

In Eq.(4.35) ' m ' signifies the exact limit load solution for any multi bar structures.

General mechanical components can be represented by a suitable multi bar model. Hence general mechanical components forming two or more two plastic hinges can be represented by the reference two bar model and lower bound limit load solution can be anticipated.

4.9 Discussion and Conclusion

The reference two bar model is developed on the basis of the generalized two-bar analysis which eliminates the assumption previously considered in the literature [10]. A transformation parameter has been obtained from the reference two bar model which scales up Mura's overly conservative lower bound multiplier to a multiplier with improved accuracy.

A general mechanical component can be represented by a suitable multi bar model. Since the reference two bar solution (m_{TBM}) bounds the limit load solution of other multi bar models, the multiplier m_{TBM} is a potential lower bound solution.

Although the reference two bar structure is identified on the basis of the general two bar analysis, the shape of a cross-section has not been taken into account. A number of beam cross-sections have been studied in Chapter 6 in order to investigate the shape effect. A guideline for lower bound two bar multiplier is then proposed for practical mechanical components or structures.

Chapter 5: Lower Bound Estimate of the m_α^T -Multiplier

5.1 Introduction

The constraint map identifies the region (as shown in **Figure 3.1**) bounded by the classical lower bound multiplier ($m=m_L$ line) and the upper bound multiplier m^0 ($m=m^0$ line). Exact limit load solution for any practical component or structure is located in this region. It is possible to narrow down the exact solution region further. This can be achieved by specifying an appropriate trajectory in the constraint map, which has a slope (θ) less than the slope of the $m=m_L$ line (as shown in **Figure 3.1**). In this chapter, it is established that a straight line with a slope of $\tan \theta = \left(1 - \frac{1}{\sqrt{2}}\right)$ (as shown in **Figure 3.1**) is such a trajectory and hence the limit load estimates

based on this specified line is a lower bound. The exact multiplier 'm' for any component or structure therefore lies between the lines having slope of $\tan \theta = \left(1 - \frac{1}{\sqrt{2}}\right)$ and $\tan \theta = 0$ shown in

Figure 3.1. The line is tangent to the $m=m_\alpha$ trajectory [8] (as shown in **Figure 5.1**) and known as the $m=m_\alpha^T$ line, originally proposed by Seshadri and Hossain [12]. However its limit load bounds have not been investigated previously.

The classical lower bound multiplier is expected to converge to the exact limit load during the redistribution of stresses based on EMAP. However, the use of classical lower bound multiplier requires a number of linear elastic analyses to converge. Restricting the number of iterations to a single elastic analysis or a few iterative elastic analyses could lead to overly conservative result. In this chapter, the m_α^T multiplier is used in conjunction with the EMAP, in order to minimize the convergence difficulties usually encountered in traditional EMAP and obtain an accurate estimate of lower bound limit load.

5.2 The m_α -Tangent Method

The m_α -tangent method was proposed by Seshadri and Hossain [12] which is an extension of the m_α -method [6]. The following section summarizes the development of the m_α -tangent method.

Mura's extended lower bound multiplier m' is a function of m^0 and m_L , which can be regarded as a surface in a three dimensional space with the two independent variables m^0 and m_L . In reality, m^0 and m_L are derived from the stress distributions in a body, and are therefore strictly not independent. Differentiation of the Mura's extended lower bound formula (Eq.(3.18)) leads to the expression of the m_α multiplier. i.e.

$$\frac{dm'}{d\left(\frac{m^0}{m_L}\right)} = \left(\frac{\partial m'}{\partial m^0}\right) \frac{dm^0}{d\left(\frac{m^0}{m_L}\right)} + \left(\frac{\partial m'}{\partial \frac{1}{m_L}}\right) \frac{d\frac{1}{m_L}}{d\left(\frac{m^0}{m_L}\right)} \quad (5.1)$$

Written in terms of finite differences, the above equation becomes:

$$m' - m_\alpha = 2 \frac{1 - \left(\frac{m^0}{m_L}\right)^2}{\left(1 + \left(\frac{m^0}{m_L}\right)^2\right)^2} (m^0 - m_\alpha) - 4 \frac{(m^0)^3}{m_L \left(1 + \left(\frac{m^0}{m_L}\right)^2\right)^2} \left(\frac{1}{m_L} - \frac{1}{m_\alpha}\right) \quad (5.2)$$

This equation is a polynomial of second degree in m_α . It can be solved for m_α to achieve the following expression:

$$m_\alpha = 2m^0 \frac{2\left(\frac{m^0}{m_L}\right)^2 \pm \sqrt{\frac{m^0}{m_L}\left(\frac{m^0}{m_L}-1\right)^2\left(1+\sqrt{2}-\frac{m^0}{m_L}\right)\left(\frac{m^0}{m_L}-1+\sqrt{2}\right)}}{\left(\left(\frac{m^0}{m_L}\right)^2+2-\sqrt{5}\right)\left(\left(\frac{m^0}{m_L}\right)^2+2+\sqrt{5}\right)} \quad (5.3)$$

The detailed steps of the m_α -multiplier derivation is provided in Appendix B.

Choosing the larger of the two roots above, the expression for m_α , normalized by the exact value of the multiplier m (unknown), can be represented as:

$$R_\alpha = 2R^0 \left[\frac{2\zeta^2 + \sqrt{\zeta(\zeta-1)^2(1+\sqrt{2}-\zeta)(\zeta-1+\sqrt{2})}}{(\zeta^2+2-\sqrt{5})(\zeta^2+2+\sqrt{5})} \right] \quad (5.4)$$

Here, $R_\alpha = \frac{m_\alpha}{m}$, $R^0 = \frac{m^0}{m}$ and $\zeta = \frac{m^0}{m_L}$.

The slope of the tangent line at the origin (1,1) of the $R_\alpha=1$ curve can be obtained by differentiating the above equation with respect to ζ , i.e. $\left(\frac{dR^0}{d\zeta}\right)_{\zeta=1}$. The equation corresponding

to the tangent line can be obtained as:

$$\frac{m^0}{m_\alpha^T} = 1 + (\zeta - 1) \left(1 - \frac{1}{\sqrt{2}}\right) \quad (5.5)$$

Comparing with Eq.(3.15), $\tan \theta = \left(1 - \frac{1}{\sqrt{2}}\right)$ is the slope of the $m=m_\alpha^T$ line as shown in **Figure**

3.1. The expression for the m_α^T -multiplier can be written as:

$$m_\alpha^T = \frac{m^0}{1 + (\zeta - 1) \left(1 - \frac{1}{\sqrt{2}}\right)} \quad (5.6)$$

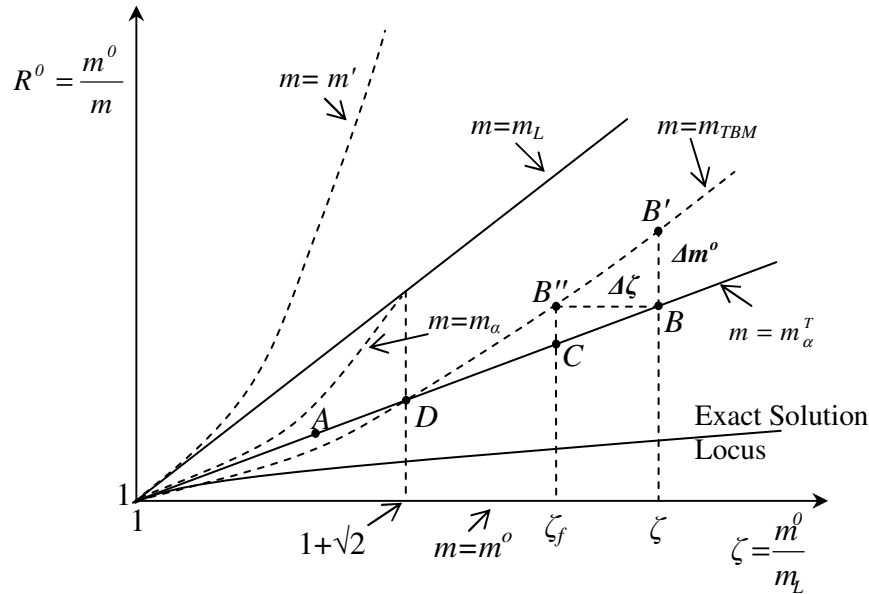
5.3 Reference TBM vs m_α^T formulation

Reference two bar model gives the bounding limit load solution over any multi bar models as discussed in Chapter 4. With respect to **Figure 5.1** it is evident that the $m=m_\alpha^T$ line bounds the two bar trajectory ($m=m_{TBM}$) within the range of $\zeta \leq 1 + \sqrt{2}$. Therefore the m_α^T -multiplier is a lower bound estimate within the range of $\zeta \leq 1 + \sqrt{2}$.

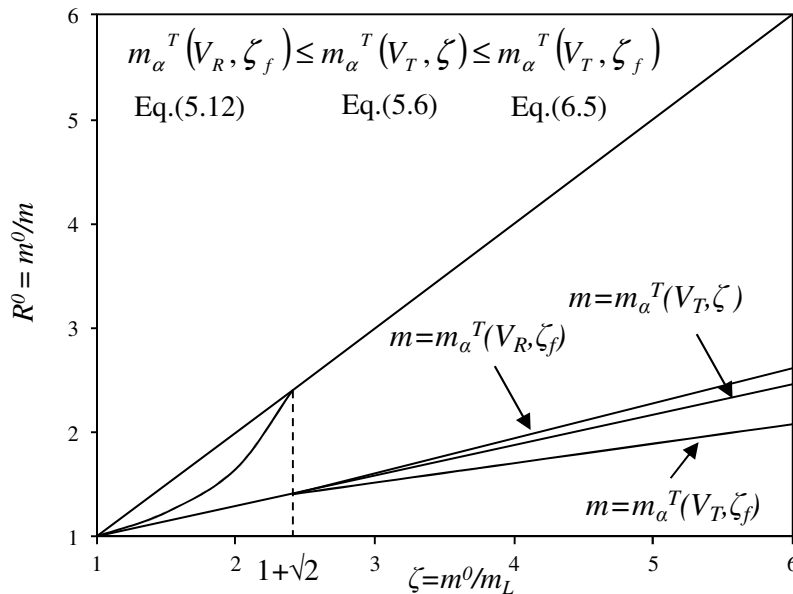
As shown in **Figure 5.1**, the intersection of the $m=m_\alpha^T$ line and the two bar trajectory work out to be $\zeta = 1$ and $1 + \sqrt{2}$. Beyond $\zeta > 1 + \sqrt{2}$, these two trajectories diverge. The divergence of the $m=m_\alpha^T$ line from the two bar trajectory can be postulated as the requirement for reference volume and peak stress corrections. The postulation is based on the intuitive assumption that the reference two bar trajectory represents primary plus secondary plus peak stresses, while the $m=m_\alpha^T$ line represents primary plus secondary stresses. The idea is that for practical components which collapse by formation of two plastic hinge, ζ is usually less than $1 + \sqrt{2}$. Therefore any increase in ζ beyond $1 + \sqrt{2}$, is postulated to be the presence of kinematically inactive volume and/or peak stress. Reference volume and peak stress corrections are required to eliminate the possibility of overestimation/underestimation of limit load using the m_α^T -multiplier.

Peak stress correction is assumed to occur when $\Delta m^0 \approx 0$, and the implied trajectory is horizontal (BB'' in **Figure 5.1**). The vertical drop $B'B$ (when $\Delta\zeta=0$) implies the reference volume correction. The combined effect of reference volume and peak stress correction ($m_\alpha^T(V_R, \zeta_f)$ in **Figure 5.1(b)**) increases the slope of the $m=m_\alpha^T$ line (i.e. $\tan\theta > 1 - 1/\sqrt{2}$) beyond $\zeta > 1 + \sqrt{2}$. Incorporation of peak stress correction ($m_\alpha^T(V_T, \zeta_f)$ in **Figure 5.1(b)**) alone reduces the slope

of the $m=m_\alpha^T$ line (i.e. $\tan\theta < 1-1/\sqrt{2}$) beyond $\zeta > 1+\sqrt{2}$. Incorporation of these corrections into the m_α^T -multiplier formulation is presented in Section 5.8 and an example to demonstrate the concept is illustrated in Section 5.4.



(a) The constraint map showing reference volume correction Δm^o and peak stress correction $\Delta \zeta$



(b) Deviation from $m=m_\alpha^T$ line due to reference volume and peak stress correction

Figure 5.1 Approximation of reference volume and peak stress correction

5.4 Illustrative Example - Reference Volume and Peak Stress Correction

During local collapse, plastic action is confined to a sub-region of the total volume, as discussed in Chapter 2 (Section 2.5). Hence, the magnitude of the multiplier (m^0) would depend on the sub-volume, V_R (reference volume), where

$$V_R = \sum_{k=1}^{\alpha} (\Delta V_k), \text{ and } \alpha < N \quad (5.7)$$

Here N is the total number of elements.

As an illustrative example, cylinder under internal pressure (**Figure 5.2(a)**) is considered using plane strain consideration. The cylinder model is meshed using eight noded isoparametric quadrilateral elements (Plane82) using symmetric boundary condition. An internal axial crack is present on the inner bore of the cylinder. The crack region (**Figure 5.2(a)**) is meshed using eight singular elements around the crack tip. The crack is modeled by applying no constraints along the crack length, thus providing the crack tip node at a certain distance away from the inner radius.

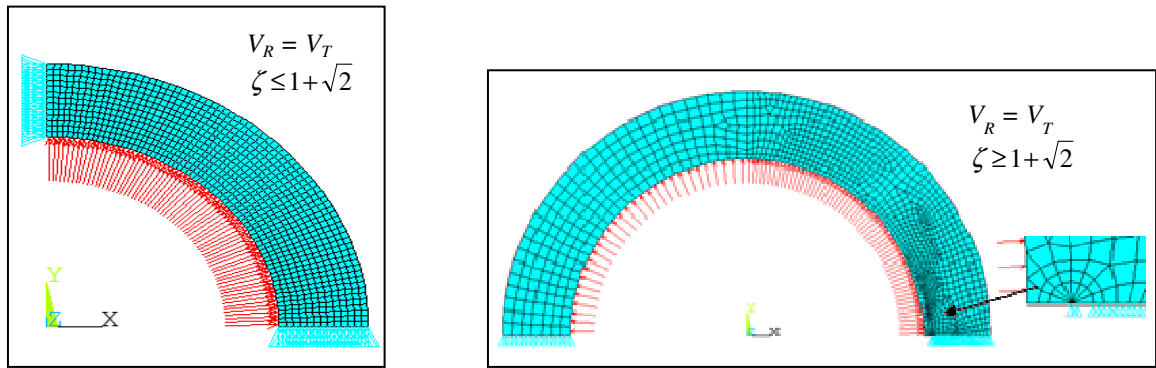
With reference to **Figure 5.2(a)**, $V_R = V_T$ for a cylinder without defect. If a defect is developed in service, the reference volume is still $V_R = V_T$. No reference volume corrections (Δm^0 in **Figure 5.1**) are required due to defect although blunting of peak stress ($\Delta \zeta$ in **Figure 5.1**) is required.

With reference to **Figure 5.2(b)**, when blunting of the crack occurs, the peak stress drops, with only primary and secondary stress remains.

When the primary load is carried by a localized region ($V_R < V_T$), it causes significant reduction in load carrying capacity of the total component or structure. Kinematically inactive volume usually

appears due to concentrated loading. The vertical drop $B'B$ in **Figure 5.1** (when $\Delta\zeta=0$) implies the reference volume correction. If there is ambiguity in deciding whether $V_R < V_T$ while analyzing a component, it is conservative to incorporate the reference volume correction.

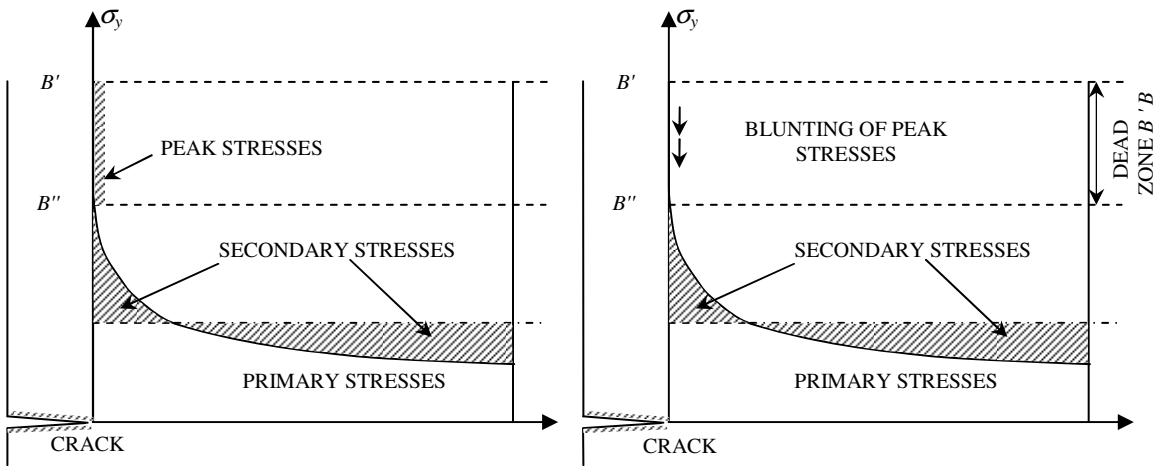
Incorporation of reference volume and peak stress corrections into the m_α^T -multiplier formulation is presented in Section 5.8.



(i) Model without defect

(ii) Model with axial crack

(a) Cylinder Geometry



(b) Structure with crack (refer to **Figure 5.1**)

Figure 5.2 Blunting of peak stresses

5.5 The m_α^T -multiplier - A Lower Bound Estimate

With respect to **Figure 5.3**, stresses are purely primary (limit state), and therefore load-controlled at the origin (1,1). The exact solution locus (shown in **Figure 5.3**) proceeds toward the origin with a continuous reduction in the magnitudes of $\frac{m^0}{m_L}$ and $\frac{m^0}{m}$.

The exact solution locus (limit load estimation based on inelastic FEA or closed-form analytical solutions are considered as exact solution) is not known when elastic analysis based computations are carried out. However, the shape of the exact solution locus/trajectory (on the constraint map) could be inferred as follows:

- (a) the trajectory starts out almost horizontally.
- (b) as ζ approaches 1.0, the trajectory would coincide with the limiting slope of the $m=m_\alpha^T$ line; and
- (c) for $1.0 < \zeta < \zeta_i$, the trajectory blends with the two extremes mentioned above.

The exact solution locus is always below the $m=m_\alpha^T$ line for $\zeta > 1.0$, and satisfies the conditions:

$$\left. \begin{array}{l} \text{i) } R^o \leq (R_\alpha^T = 1) \\ \text{ii) } \frac{dR^o}{d\zeta} \geq 0 \\ \text{iii) } \frac{d^2R^o}{d\zeta^2} \leq 0 \end{array} \right\} \text{ for } \zeta \geq 1.0 \quad (5.8)$$

Therefore, we can expect m_α^T to be a lower bound during iterative linear elastic analysis (EMAP), provided m^0 is modified for reference volume. Basically the first EMAP iteration is nothing but the single linear elastic analysis.

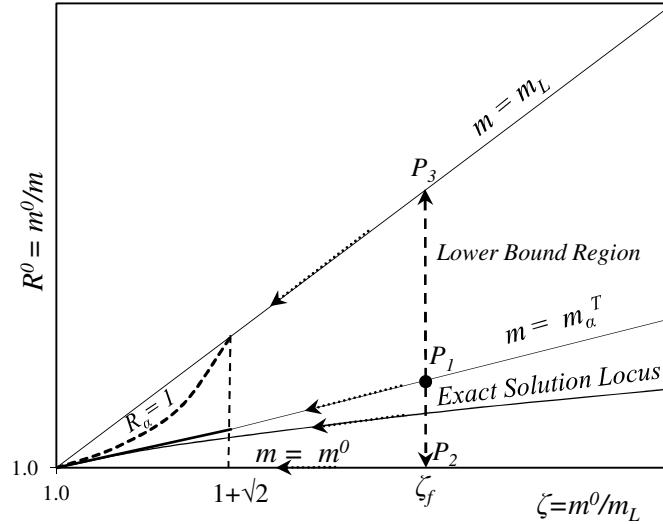


Figure 5.3 Bounds for m_α^T on the constraint map

5.6 Exact Solution Locus - 3D Grillage Analysis Example

In order to confirm the shape of the exact solution locus for practical components as discussed above, a 3D grillage model is modeled and analyzed. The grillage model, as shown in **Figure 5.4**, is a 6756 mm long plate, stiffened in longitudinal and transverse directions. The transverse frame ends, and the two longitudinal ends of the grillage are fixed. The length of transverse members is 2260 mm and the span between the transverse members is 2000 mm. A uniform pressure of 5 MPa is applied as transverse load on the plate bottom. The modulus of elasticity of the material is 207 GPa and yield strength is 315 MPa. Rest of the model dimensions are shown in **Figure 5.4**. Shell181 [21] element is chosen due to its suitability to model thin to moderately thick shell structures.

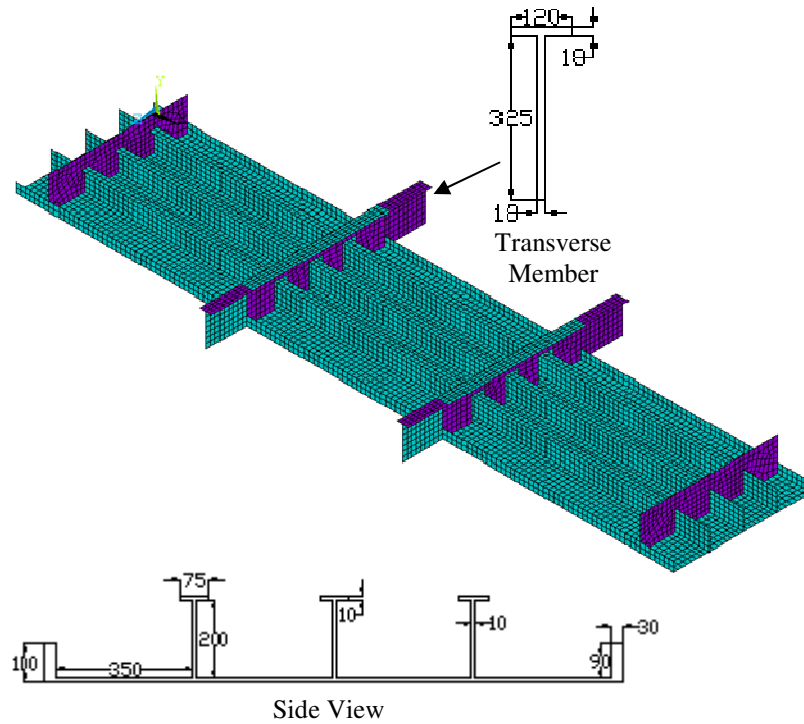
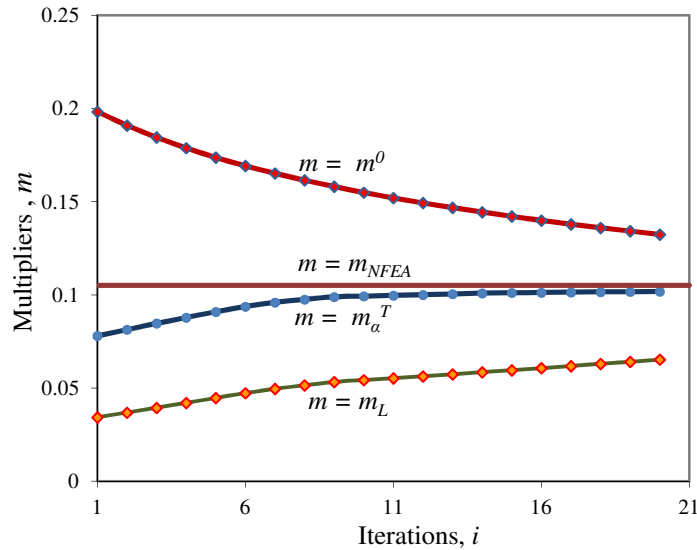


Figure 5.4 Grillage model (dimensions in mm)

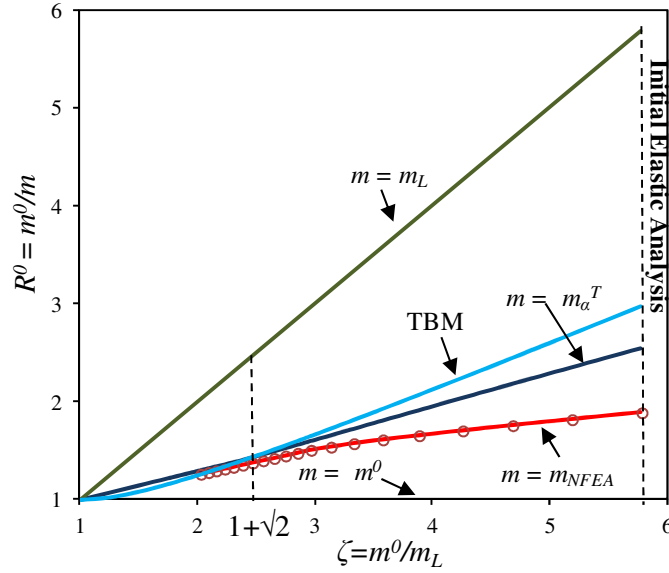
Inelastic finite element analysis is performed using an elastic-perfectly-plastic material model. In order to achieve limit state, load is incremented in steps and a solution for each load step is found successively (until equilibrium and compatibility conditions are satisfied). Within each load step, a large number of sub-steps are used in order to ensure the gradual increase of load applied in that step. The iterative scheme of Newton-Raphson is used for solving simultaneous non-linear equations. Solution enhancement features like bisection (to decide whether or not to reduce the present time step) and automatic load stepping (to estimate the next time-step size) are also used as permitted by the selected iterative scheme. The inelastic finite element analysis gives the value of limit load multiplier $m_{NFEA} = 0.105$.

In order to plot $\frac{m^0}{m_{NFEA}}$ vs $\frac{m^0}{m_L}$ in the constraint map as shown in **Figure 5.5(b)**, iterative elastic analysis is also performed and m^0 (m_2^0) and m_L are achieved as shown in **Figure 5.5(a)**. Iterative linear elastic analysis is performed based on EMAP as discussed in Chapter 2 (Section 2.6) using $q = 0.1$ and algorithm in **Figure 5.8** is followed. It should be noted here that during EMAP, m^0 is evaluated based on Eq(3.9), which is essentially m_2^0 .

With respect to **Figure 5.5(b)** it is evident that the exact solution locus ($m=m_{NFEA}$) for grillage model starts out almost horizontally satisfying the conditions given in Eq.(5.8). This locus lies below the $m = m_\alpha^T$ line as shown in **Figure 5.5(b)**. Therefore for this grillage model the m_α^T multiplier provides lower bound estimate of limit load.



(a) Variation of limit load multipliers with iterations for grillage model



(b) Constraint trajectory map showing exact solution locus for grillage model

Figure 5.5 Results for grillage model

5.7 Bounding Nature of m_α^T -Multiplier - Multi Bar Analysis

A general mechanical component can be represented by a suitable multi bar model where collapse occurs by formation of multiple plastic hinges. In this section, the relative position of several multi bar trajectories and the $m=m_\alpha^T$ line are compared as shown in **Figure 5.6**. Each point on a multi bar trajectory is an exact limit load solution for a particular multi bar configuration. The objective is to plot a vast number of exact limit load solutions of multi bar structures (as derived in section 4.8) in the constraint map and show that the m_α -tangent multiplier solution is lower bound. This gives a higher confidence on the m_α -tangent multiplier as a lower bound solution for practical components and structures.

With respect to **Figure 5.6**, multi bar trajectories are bounded by the $m=m_\alpha^T$ line within the region where $\zeta \leq 1+\sqrt{2}$. Therefore the m_α^T multiplier provides lower bound solution for any multi bar configurations when $\zeta \leq 1+\sqrt{2}$. This implies that for well-designed components or structures (as represented by a suitable multi bar model), the m_α -tangent method is expected to provide lower bound solutions with acceptable accuracy.

Beyond $\zeta > 1+\sqrt{2}$ most of the multi bar trajectories are bounded by the $m=m_\alpha^T$ line within the practical range of $\zeta = \frac{m^0}{m_L}$ as shown in **Figure 5.6**. However the two bar trajectory diverge out from the m_α -tangent line ($m=m_\alpha^T$ line) when $\zeta > 1+\sqrt{2}$. Since in a well-designed component ζ usually does not exceed $1+\sqrt{2}$, the divergence of the $m=m_\alpha^T$ line from the two bar trajectory (when $\zeta > 1+\sqrt{2}$) is considered as the requirement for reference volume and peak stress corrections (discussed in Section 5.3 and 5.4). Reference volume and peak stress corrections are required to eliminate the possibility of overestimation/underestimation of limit load using the m_α^T -multiplier.

Therefore it can be concluded that the exact limit load solution for practical components and structures are located within the region where $0 \leq \tan \theta \leq \left(1 - \frac{1}{\sqrt{2}}\right)$ as shown in **Figure 5.6**.

Hence the m_α^T -multiplier gives reasonable estimate of lower bound limit load, providing the reference volume and peak stress corrections are incorporated appropriately.

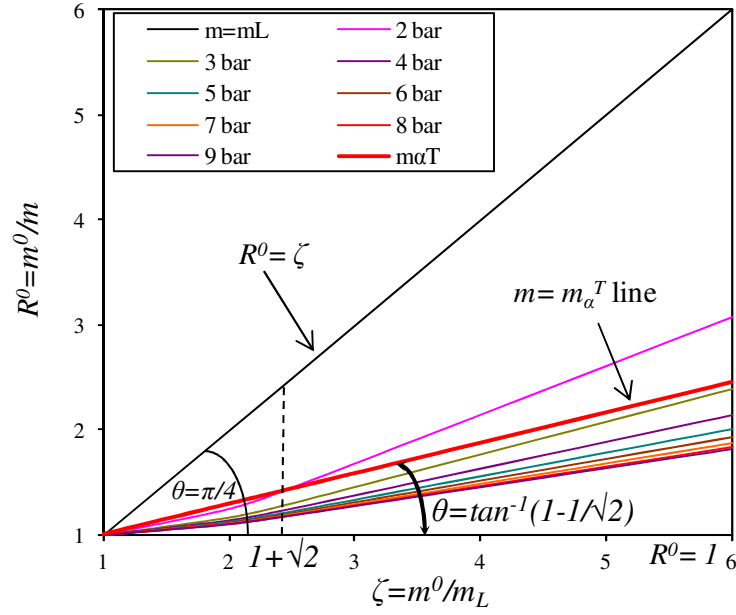


Figure 5.6 Relative magnitude of m_α^T solution over multi bar solutions

5.8 Evaluation of the Multiplier m_α^T

In order to ensure lower bound estimate of the multiplier m_α^T , it is also important to incorporate reference volume and peak stress corrections appropriately. Therefore, the following two cases are considered in the m_α^T formulation:

5.8.1 Multiplier m_α^T : $\zeta \leq 1 + \sqrt{2}$

This case refers to properly sized mechanical/pressure components with gentle geometric transitions. The implication is that the entire volume participates in the plastic action. Therefore, for these structures, ζ lies in between $1 \leq \zeta \leq 1 + \sqrt{2}$ and Eq.(5.6) is directly used to evaluate the multiplier m_α^T . Note that m^0 in Eq.(5.6) has to be calculated based on the total volume (V_T).

5.8.2 Multiplier m_α^T : $\zeta > 1 + \sqrt{2}$

This case applies to components that develop flaws or cracks during service, or to components with sharp notches. Components having some sort of discontinuity or concentrated load over a certain region also fall into this category. These components may possess significant amount of peak stress and/or kinematically inactive volume.

With respect to **Figure 5.1**, $B'B''$ is assumed to be the peak stress relaxation. This relaxation can be viewed as a drop $B'B$ vertically representing the inactive volume (V_D) and the peak stress blunting BB'' . Based on **Figure 5.1**, the multiplier $m^0(V_R)$ can be evaluated by the expression:

$$m^0(V_R) = \left(\frac{R_B^0}{R_{B''}^0} \right) m^0 = \left[\frac{1 + \left(1 - \frac{1}{\sqrt{2}} \right) (\zeta - 1)}{\frac{(1 + \zeta^2)}{2\zeta}} \right] m^0 \quad (5.9)$$

Based on **Figure 5.1**, the peak stress correction [12] can be determined by the expression:

$$\frac{R_B^0}{R_{B''}^0} = \frac{1 + (\zeta - 1) \left(1 - \frac{1}{\sqrt{2}} \right)}{\frac{1 + \zeta_f^2}{2\zeta_f}} = 1 \quad (5.10)$$

The following root of Eq.(5.10) gives the final value of the variable ζ

$$\zeta_f = \left[1 + \left(1 - \frac{1}{\sqrt{2}} \right) (\zeta - 1) \right] + \sqrt{\left[1 + \left(1 - \frac{1}{\sqrt{2}} \right) (\zeta - 1) \right]^2 - 1} \quad (5.11)$$

Using $m^0(V_R)$ and ζ_f from Eq.(5.9) and Eq.(5.11) respectively, the expression for the multiplier m_α^T for the region of $\zeta > 1 + \sqrt{2}$ can be evaluated as:

$$m_\alpha^T(V_R) = \frac{m^0(V_R)}{1 + (1 - \frac{1}{\sqrt{2}})(\zeta_f - 1)} \quad (5.12)$$

The m_α -tangent method presented above provides lower bound estimates for the limit loads. The estimates of the values of the upper bound multiplier m^0 and the classical lower bound multiplier m_L are obtained from the statically admissible and kinematically admissible strain distributions and m_α^T -multiplier is calculated, depending on the value of ζ .

5.9 Combining EMAP with the m_α -tangent method

The rate of convergence of a lower bound limit load multiplier towards the exact solution depends on the elastic modulus adjustment parameter (q) as well as the accuracy of the lower bound multiplier. Smaller modulus adjustment parameter (usually $q \leq 0.5$ [25]) enables smoother multiplier variation with iterations although requires a large number of iterations before convergence is achieved. On contrary, a larger ' q ' value results inconsistent variation in multipliers with iterations [25] and as a result convergence might not be achieved. Since the m_α -*tangent* multiplier is a better estimate of lower bound, it converges to the exact solution faster, even if a smaller ' q ' value is chosen. In this section an algorithm is proposed to calculate accurate estimates of limit loads, by using the m_α -*tangent* multiplier in conjunction with EMAP. The procedure ensures sufficiently accurate limit loads within a reasonable number of iterations. It should be noted here that during EMAP, m^0 is evaluated based on Eq(3.9), which is essentially m_2^0 .

5.9.1 Implicit Reference Volume and Peak Stress Correction in EMAP

During EMAP, infinitesimal changes to the element elastic modulus of the various elements during the second and subsequent linear elastic FEA would result in a corresponding change in the value of multipliers m^0 and m_L . This change in magnitude implies to the implicit reference volume and peak stress correction.

The upper bound multiplier reduces due to element modulus adjustment in subsequent linear elastic iterations as shown in **Figure 5.7** while approaching the final solution. It can be assumed that, in every iteration, m^0 is split into a constant value and a variable portion that vanishes with iterations. Hence,

$$m^0(V_T) = m^0(V_R) + \Delta m \quad (5.13)$$

where $m^0(V_R)$ is the constant part and Δm which vanishes after a certain number of linear elastic iterations. It is observed that the vanishing part represents the zone that is not participating in the plastic action.

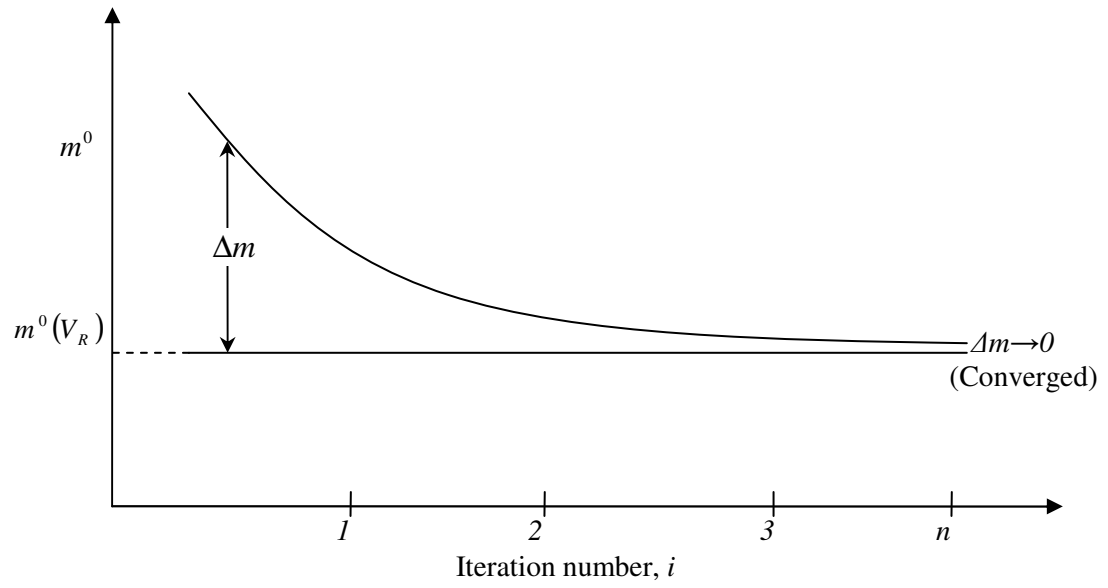


Figure 5.7 Variation of m^0 (m_2^0) during EMAP Iterations

Similarly, classical lower bound multiplier also converges towards the exact limit load solution in subsequent linear elastic iterations due to successive peak stress corrections. In other words, the reference volume and peak stresses are implicitly corrected in subsequent iterations due to modulus adjustments. However, a large number of iterations may be anticipated for the convergence (both for m_2^0 and m_L) to the exact solution, especially for three dimensional FEA models.

5.9.2 Proposed EMAP Algorithm and Its Features

Figure 5.8 shows the proposed EMAP flow diagram for estimating the m_α^T multiplier in successive linear elastic iterations. This algorithm systematically adjusts the elastic modulus of different elements in a finite element discretization scheme. It also utilizes the proposed m_α^T multiplier expression from Eq.(5.12) in case of $\zeta_i > 1 + \sqrt{2}$ in order to ensure lower bound solution in all the iterations. For $\zeta_i \leq 1 + \sqrt{2}$, Eq.(5.6) is used for the m_α^T multiplier evaluation. During EMAP, m^0 is evaluated based on Eq(3.9), which is essentially m_2^0 . Therefore ζ_i is

evaluated as $\zeta_i = \left(\frac{m_2^0}{m_L} \right)_i$.

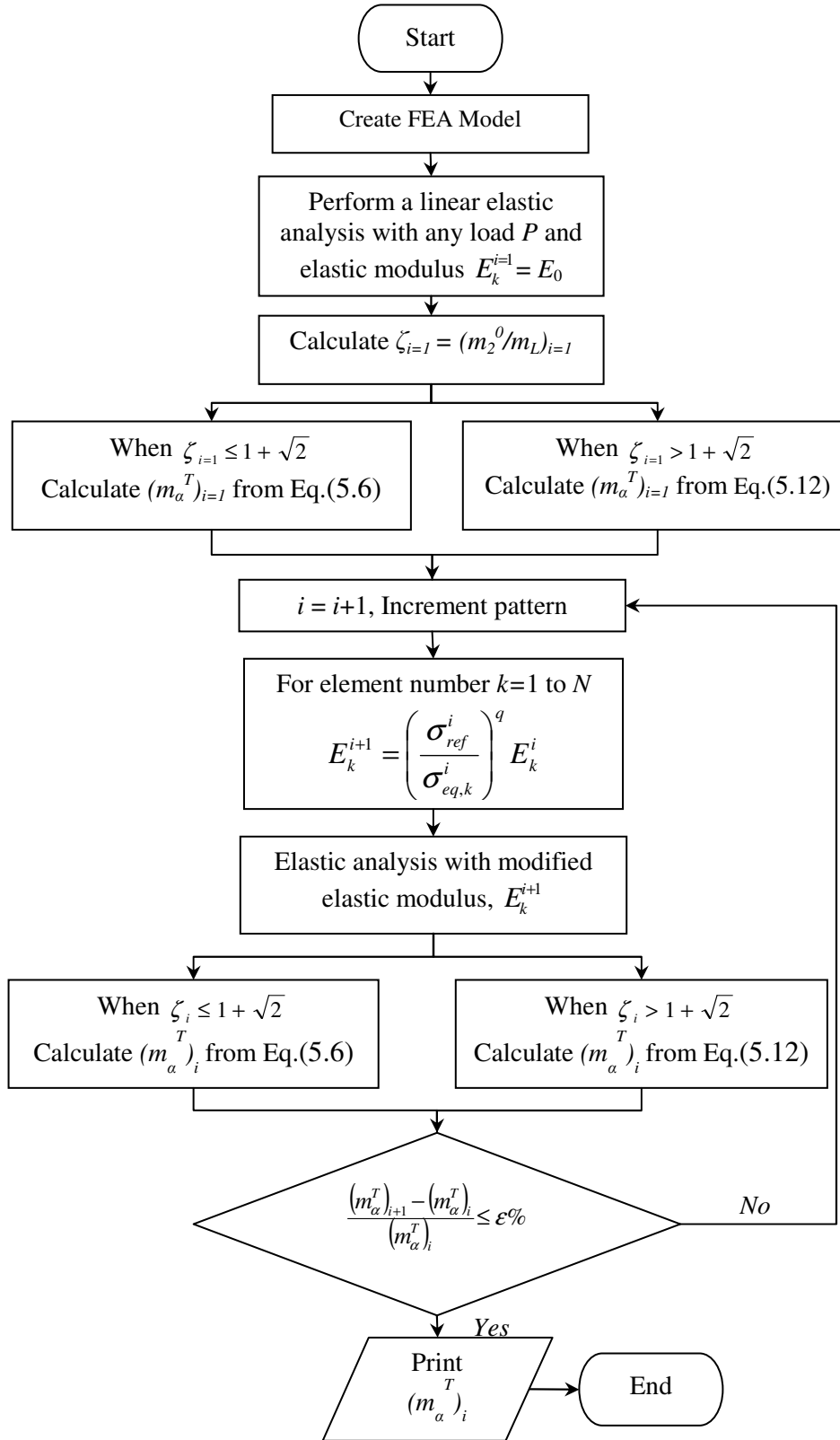


Figure 5.8 EMAP flow diagram for estimating limit load (m^0 from Eq(3.9), which is m_2^0)

The magnitude of a limit load multiplier with iterations, and its rate of convergence towards the exact solution, depends on the elastic modulus adjustment parameter (q). Smaller modulus adjustment parameter enables smoother multiplier variation with iterations. However, the convergence of upper and classical lower bound multipliers require a larger number of iterations to reach convergence when a small ' q ' value is chosen (as shown in **Figure 5.5(a)**). The following features of the proposed algorithm ensure converged lower bound solutions, and eliminate the usually experienced convergence difficulties involved in EMAP:

(a) Convergence is considered to be achieved when the variation of the m_α^T multiplier at a given iteration becomes negligible.

(b) The m_α^T multiplier converges to the limit load corresponding to nonlinear FEA within a number of iterations, even for a very small modulus adjustment parameter (' q ' value). From the 3D grillage model example it is evident that when m_α^T multiplier achieves convergence, the other multipliers (specifically m^0 and m_L) are still far from a converged state (shown in **Figure 5.5(a)**).

(c) The m_α^T multiplier converges from the lower bound side as shown in **Figure 5.5(a)**; hence its value at any iteration is conservative. For well-designed pressure components, it is expected that the m_α^T multiplier from initial elastic analysis will be sufficiently accurate.

(d) The selection of elastic modulus adjustment parameter (q) depends on the kinematic redundancies present in the component. If a particular value of ' q ' is suitable for a component of

certain redundancy, it is expected to work for components with lesser redundancy. In this algorithm, a considerably smaller modulus adjustment parameter is suggested (close to $q = 0.1$) for EMAP in order to ensure proper convergence. In order to simulate the plastic incompressibility condition, Poisson's ratio is chosen to be 0.47.

5.10 Discussion and Conclusion

A comparison to the multi bar models shows that the m_α -tangent multiplier is expected to provide reasonable lower bound estimate of limit load for practical components and structures, providing the reference volume and peak stress corrections are incorporated appropriately. Moreover, by investigating the shape of the exact solution locus on the constraint map it is concluded that the exact solution locus always lies below the $m=m_\alpha^T$ line for $\zeta > 1.0$. This signifies that the m_α^T -multiplier is a lower bound solution during the iterative elastic runs as well.

The proposed algorithm incorporates the reference volume corrections and hence ensures lower bound solutions in all iterations. The algorithm maintains consistent trend of limit load multipliers with iterations even for complex three dimensional geometric models. Moreover it also ensures relatively rapid computation of limit loads by utilizing the faster convergence feature of the m_α^T multiplier.

The initial linear elastic run of EMAP is nothing but the typical linear elastic analysis. The initial linear elastic run provides lower bound limit load estimate and the accuracy of lower bound solution improves during the EMAP iterations. In terms of design qualification, sometimes it is important to estimate lower bound limit load with better accuracy, especially when the analyst

cannot afford any kind of conservatism. In this sense the EMAP iterations can be terminated as soon as the acceptance criteria for design load are satisfied against the m_α^T -multiplier solution.

While performing iterative linear elastic analysis of a component, it is convenient to apply all the corrections into the m_α^T -multiplier formulation as a conservative approach. Since EMAP redistributes the stresses in subsequent analysis, the conservatism is adjusted during iterations. However this conservatism could be an issue when the multiplier needs to be estimated based on single linear elastic analysis (when a quick and inexpensive calculation is required). Therefore a guideline for appropriate incorporation of reference volume and peak stress correction is addressed in chapter 6 which is essential to achieve reasonable estimate of m_α^T multiplier based on single linear elastic analysis.

Chapter 6: Robust Limit Loads Based on Single Linear Elastic Analysis

6.1 Introduction

As per ASME design philosophy ([1] [11]), the primary membrane, primary local membrane and primary bending stress obtained from a linear elastic analysis has to be limited by the corresponding ASME allowable limit for the purpose of design qualification. However if the stress limits are not met, limit analysis can show that the design is qualified. In this context if the limit load can be estimated from the existing linear elastic stress analysis, then it will save the expense to set-up and perform a detailed inelastic analysis. Single linear elastic analysis based techniques are also attractive whenever a quick and inexpensive calculation is required (e.g. Level 2 FFS type assessment).

In terms of limit load estimation, a general mechanical component is equivalent to a suitable multi bar model. Since the reference two bar solution (m_{TBM}) bounds the limit load solution of other multi bar models (discussed in Chapter 4), the multiplier m_{TBM} is a potential lower bound solution. In Chapter 4 reference two bar model has been identified based on the generalized two bar analysis. Generalized two bar configuration implies variable two bar area and length ratio. However the shape of a cross-section has not been taken into account. The shape of a cross-section is essential to consider during bending. Therefore in order to eliminate any possibility of overestimation of limit load using two bar multiplier (m_{TBM}), a correction factor is introduced into the two bar formulation. A guideline is proposed to obtain lower bound two bar multiplier for practical mechanical components and structures based on linear elastic analysis.

As discussed in Chapter 5, it is important to incorporate reference volume and peak stress corrections into the m_α^T multiplier formulation in order to achieve lower bound limit load. While performing iterative linear elastic analysis of a component, it is convenient to apply all the corrections. Since the convergence is eventually achieved in subsequent elastic iterations, therefore the possibility of conservatism due to the above mentioned corrections is adjusted. However in order to achieve robust estimate of m_α^T multiplier based on linear elastic analysis, it is essential to apply these corrections judiciously on a component basis. In this chapter a guideline is proposed to obtain robust m_α^T multiplier based on single linear elastic analysis.

The above mentioned methods are then applied to a number of practical components and structures. Results are compared with the inelastic FEA results and/or available analytical solutions.

6.2 Guideline for Lower Bound m_{TBM} Multiplier Based on Single Linear Elastic FEA

The reference two bar structure is identified on the basis of the general two bar analysis which considers variable bar length and variable area. The shape of the beam cross-section is essential to consider while calculating limit load. With respect to **Table 6.2**, it is evident that the exact limit load of rectangular beam cross-section (having shape factor $S=1.5$) corresponds to the reference two bar limit load solution ($m'\zeta$). The shape factor of rectangular beam section ($S=1.5$) is widely considered in the ASME code [11], which implies that the two bar model is consistent with the ASME code design consideration.

For beam cross-sections having shape factor greater than 1.5 (e.g. solid circular section in **Table 6.2** has a shape factor of 1.70), reference two bar model gives lower bound solution. On contrary beam sections having shape factor less than 1.5, reference two bar limit load could be an overestimation (e.g. thin circular pipe section in **Table 6.2** has a shape factor of 1.27). Therefore in order to eliminate any possibility of overestimation of limit load for general mechanical components using two bar multiplier, a correction factor 'e' has been introduced into the two bar formulation as described below.

As discussed earlier, the $m = m_\alpha^T$ line having a slope of $\tan \theta = \left(1 - \frac{1}{\sqrt{2}}\right)$, provides an improved estimate of lower bound limit load. Since the reference two bar trajectory lies below the m_α -tangent line within the range of $1 \leq \zeta \leq 1 + \sqrt{2}$ (**Figure 6.1**), the reference two bar multiplier could lead to an upper bound estimate within this range. However it can be seen that the maximum possible error in the reference two bar estimation is $e_{max} = 5.83$ percent, which occurs at $\zeta = 1.5$ (**Figure 6.2**). For any other value of ζ within the range of $1 \leq \zeta \leq 1 + \sqrt{2}$, the error will be less.

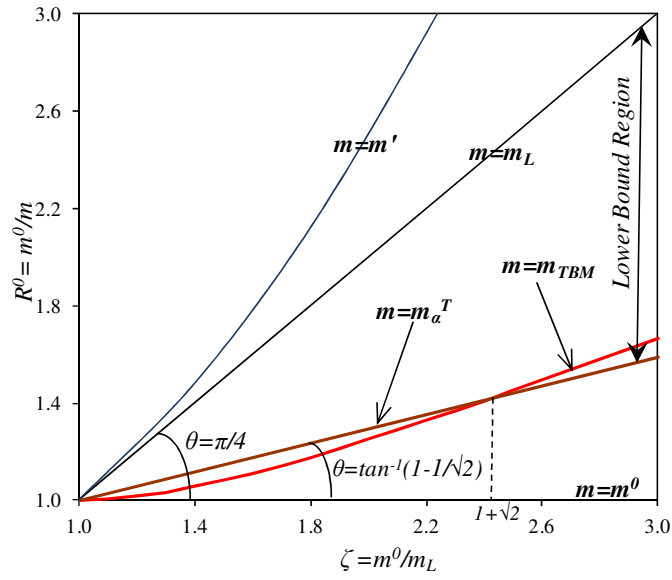


Figure 6.1 Limit load bounds

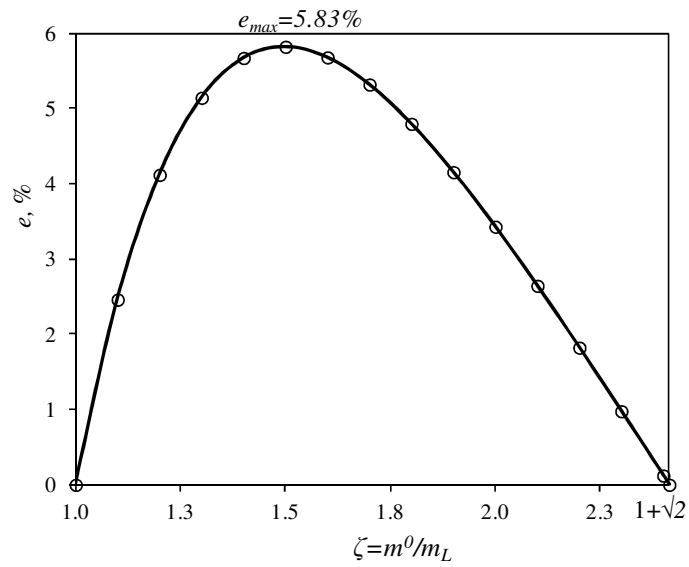


Figure 6.2 Error in the m_{TBM} multiplier estimate in comparison to the m_{α}^T multiplier

The error estimation shown in **Figure 6.2** is calculated as follows:

With respect to Figure 6.3, at a particular ζ location, $(R^0)_b$ will be greater than or equal to $(R^0)_a$, where 'b' and 'a' are points located on the $m=m_\alpha^T$ line and reference TBM ($m=m_{TBM}$) trajectory respectively (for the range $1 \leq \zeta \leq 1+\sqrt{2}$). Therefore the error estimate ($e\%$) for the reference two bar multiplier within this range can be expressed as:

$$(R^0)_a = \frac{1+\zeta^2}{2\zeta} \quad (6.1)$$

$$(R^0)_b = 1 + (\zeta - 1) \left(1 - \frac{1}{\sqrt{2}} \right) \quad (6.2)$$

$$\Delta R^0 = (R^0)_b - (R^0)_a \quad (6.3)$$

$$e = \frac{\Delta R^0}{(R^0)_a} \times 100$$

$$\Rightarrow e = \frac{\left[1 + (\zeta - 1) \left(1 - \frac{1}{\sqrt{2}} \right) \right] - \left[\frac{1 + \zeta^2}{2\zeta} \right]}{\left[\frac{1 + \zeta^2}{2\zeta} \right]} \times 100 \quad (6.4)$$

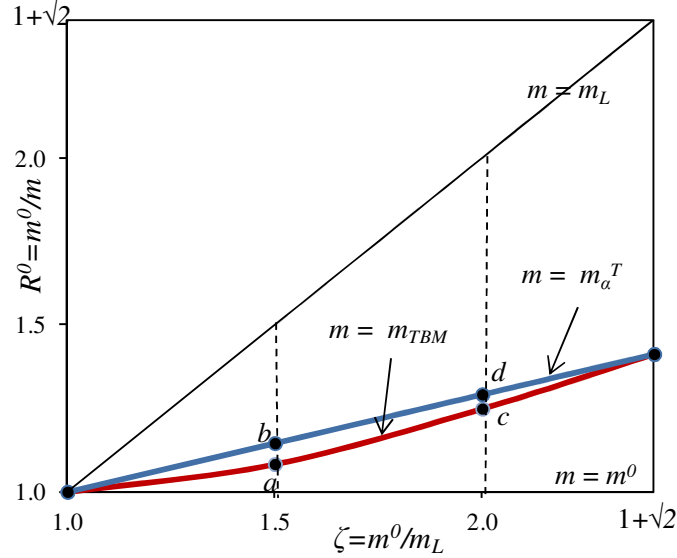


Figure 6.3 Reference TBM error estimation from constraint map

Now that the error estimation is obtained, a guideline is presented as follows in order to obtain lower bound estimate of two bar multiplier (m_{TBM}) based on linear elastic analysis. **Table 6.1** summarizes the guideline.

6.2.1 Multiplier m_{TBM} : $\zeta \leq 1 + \sqrt{2}$

Well-designed components with gentle geometric transitions under uniform load distribution are usually within this ζ range. At first the estimate of $m'\zeta$ is calculated as per Eq.(4.13). Then the estimate of $m'\zeta\left(1 - \frac{e}{100}\right)$ will provide lower bound limit load for practical components and structures. Here 'e' percent error estimate calculated based on Eq.(6.4). **Table 6.1** summarizes the guideline.

The proposed lower bound two bar multiplier estimate for the component category of $\zeta \leq 1 + \sqrt{2}$ is basically a modification of the two bar multiplier developed by Seshadri and Adibi-Asl [10].

6.2.2 Multiplier m_{TBM} : $\zeta > 1 + \sqrt{2}$

The reference two bar solution (m_{TBM}) bounds the limit load solution of other multi bar models, i.e. the multiplier m_{TBM} is a potential lower bound solution. With respect to **Figure 6.1**, the relative position of the $m=m_{TBM}$ trajectory and $m=m_\alpha^T$ line signifies that for any value of $\zeta > 1 + \sqrt{2}$, $m'\zeta < m_\alpha^T$. Therefore correction factor based on the above mentioned error estimate is not applicable. Hence $m_{TBM} = m'\zeta$ will provide lower bound estimate of limit load for this ζ range. **Table 6.1** summarizes the guideline.

Table 6.1 Guideline for lower bound limit load multiplier based on single linear elastic FEA

Component Category * ($\zeta = \frac{m^0}{m_L}$)	Description	Multiplier m_a^T	Multiplier m_{TBM}
$\zeta \leq 1 + \sqrt{2}$	Well-designed components with gentle geometric transitions	$\frac{m^0}{1 + (1 - \frac{1}{\sqrt{2}})(\zeta - 1)}$	$m' \zeta \left(1 - \frac{e}{100}\right)$
$\zeta > 1 + \sqrt{2}$	Components with stress concentrations. In the absence of stress concentrations ζ would be less than $1 + \sqrt{2}$	$\frac{m^0}{1 + (1 - \frac{1}{\sqrt{2}})(\zeta_f - 1)}$	$m' \zeta$
$\zeta > 1 + \sqrt{2}$	** Components undergoing local plastic action along with stress concentrations	$\frac{m^0(V_R)}{1 + (1 - \frac{1}{\sqrt{2}})(\zeta_f - 1)}$	$m' \zeta$
Evaluation Details			
$m^0 = \frac{\sigma_y}{\sqrt{\int_{V_T} (\sigma_{eq})^2 dV}} \sqrt{V_T}$ [Eq.(3.3)]		$m_L = \frac{\sigma_y}{(\sigma_{eq})_{\max}}$ [Eq.(3.2)]	
$m^0(V_R) = \left[\frac{1 + \left(1 - \frac{1}{\sqrt{2}}\right)(\zeta - 1)}{\frac{(1 + \zeta^2)}{2\zeta}} \right] m^0$ [Eq.(5.9)]		$\zeta_f = \left[1 + \left(1 - \frac{1}{\sqrt{2}}\right)(\zeta - 1) \right] + \sqrt{\left[1 + \left(1 - \frac{1}{\sqrt{2}}\right)(\zeta - 1) \right]^2 - 1}$ [Eq.(5.11)]	
$m' = \frac{2m^0}{1 + \zeta^2}$ [Eq.(3.18)]		$e = \frac{\left[1 + (\zeta - 1) \left(1 - \frac{1}{\sqrt{2}}\right) \right] - \left[\frac{1 + \zeta^2}{2\zeta} \right]}{\left[\frac{1 + \zeta^2}{2\zeta} \right]} \times 100$ [Eq.(6.4)]	

* m^0 and m_L is calculated from the linear elastic stress distribution of a component or structure.

** If there is ambiguity in deciding whether $V_R < V_T$ while analyzing a component, it is conservative to incorporate the reference volume correction. m^0 and $m^0(V_R)$ signify the calculation of multiplier m^0 based on total volume and reference volume respectively.

6.3 Guideline for Lower Bound m_α^T Multiplier Based on Single Linear Elastic FEA

As established in Chapter 5, for component category $\zeta \leq 1 + \sqrt{2}$, the m_α^T -multiplier estimate proposed by Seshadri and Hossain [12] is a lower bound and hence can be used without any modification.

If a defect is developed in a component during service, there will be existence of peak stress in its linear elastic stress distribution resulting $\zeta > 1 + \sqrt{2}$. Removal of the peak stress does not affect the “overall equilibrium” of the component and the corresponding stress-distribution. In other words, blunting of peak stress is assumed to occur when $\Delta m^0 \approx 0$, and the implied trajectory is horizontal (BB'' in **Figure 5.1**). Hence the reference volume is still $V_R = V_T$. Therefore no reference volume corrections (Δm^0 in **Figure 5.1**) are required due to defect although blunting of peak stress ($\Delta \zeta$ in **Figure 5.1**) is required.

On contrary, there could be local plastic action in a component along with stress concentrations (when $V_R < V_T$). In this situation, ζ is greater than $1 + \sqrt{2}$ and reference volume correction is also required. The vertical drop $B'B$ in **Figure 5.1** (when $\Delta \zeta = 0$) implies the reference volume correction.

Seshadri and Hossain [12] introduced the peak stress correction (described in Chapter 5) into the m_α^T multiplier formulation. However this solution could be an upper bound when primary load is carried by a localized region (i.e. $V_R < V_T$). Therefore it is essential to introduce the reference

volume correction (proposed in Chapter 5) into the m_α^T multiplier formulation along with the peak stress correction.

In order to achieve robust estimate of m_α^T multiplier based on single linear elastic analysis (for component category $\zeta > 1 + \sqrt{2}$), it is essential to apply reference volume and peak stress corrections judiciously on a component basis. In this section a guideline is proposed to obtain robust m_α^T multiplier based on linear elastic analysis. **Table 6.1** summarizes the guideline and a number of practical components have been analyzed in Section 6.4 and 6.5 based on the guideline. It should be noted that, if there is ambiguity in deciding whether $V_R < V_T$ while analyzing a component, it is conservative to incorporate the reference volume correction.

6.3.1 Multiplier m_α^T : $\zeta \leq 1 + \sqrt{2}$ (*well-designed components with gentle geometric transitions*)

This case refers to properly sized mechanical/pressure components with gentle geometric transitions (as discussed in Section 5.8.1). The implication is that $V_R = V_T$. The value of m^0 and

$\zeta = \frac{m^0}{m_L}$ can be determined from statically admissible distributions, obtained using a linear elastic

FEA. Hence Eq.(5.6) is directly used to evaluate the multiplier m_α^T . **Table 6.1** summarizes the guideline.

6.3.2 Multiplier m_α^T : $\zeta > 1 + \sqrt{2}$ (components with stress concentrations)

This case refers to well-designed mechanical/pressure components as described in Section 6.3.1 that develop cracks/flaws during service. In the absence of the cracks/flaws $\zeta \leq 1 + \sqrt{2}$, but the defects introduce stress concentrations. For this case,

$$m_\alpha^T = \frac{m^0}{1 + (1 - \frac{1}{\sqrt{2}})(\zeta_f - 1)} \quad (6.5)$$

where ζ_f can be calculated using Eq.(5.11). **Table 6.1** summarizes the guideline

6.3.3 Multiplier m_α^T : $\zeta > 1 + \sqrt{2}$ (local plastic action along with stress concentrations)

The large stress and strain fields are essentially introduced by cracks and flaws and kinematically inactive volume appears due to concentrated loading. In the absence of defects, there are negligible stresses. For this case Eq.(5.12) is used to obtain the m_α^T multiplier, where $m^0(V_R)$ and ζ_f can be calculated using Eq.(5.9) and Eq.(5.11) respectively. **Table 6.1** summarizes the guideline

6.4 Analytical Examples

In this section, limit load for several beam configurations subjected to an applied moment (M) has been computed based on the linear elastic stress distribution. For beams of various cross-sections, limit load calculations using the m_{TBM} and m_α^T multiplier are found to be in good agreement with the exact analytical solutions. Results are summarized in **Table 6.2**. Detailed description of calculation is provided in Appendix A for several beam configurations.

Table 6.2 Limit load multipliers for several beam configurations

Limit Load Multiplier	Rectangular beam of unit width and thickness ' t '	Solid circular beam of diameter ' d '	Circular pipe of thickness ' t ' and nominal radius ' r '
Shape factor (S)	1.50	$\frac{16}{3\pi} = 1.70$	$\frac{4}{\pi} = 1.27$
m^0	$\frac{\sigma_y t^2}{\sqrt{12}M}$	$\frac{\sigma_y \pi d^3}{16M}$	$\frac{\sqrt{2}\sigma_y \pi r^2 t}{M}$
m_L	$\frac{\sigma_y t^2}{6M}$	$\frac{\sigma_y \pi d^3}{32M}$	$\frac{\sigma_y \pi r^2 t}{M}$
ζ	$\sqrt{3}$	2	$\sqrt{2}$
m'	$\frac{\sigma_y t^2}{4\sqrt{3}M}$	$\frac{\sigma_y \pi d^3}{40M}$	$\frac{2\sqrt{2}\pi\sigma_y r^2 t}{3M}$
m	$\frac{\sigma_y t^2}{4M}$	$\frac{\sigma_y d^3}{6M}$	$\frac{4\sigma_y r^2 t}{M}$
$\frac{m'\zeta}{m}$	1	0.94	1.05
$\frac{m'\zeta}{m} \left(1 - \frac{e}{100}\right)$	0.95	0.91	0.99
$\frac{m_\alpha^T}{m}$	0.95	0.91	0.99

Note: In **Table 6.2** ' e ' is the percent error as shown in **Figure 6.2**. For a particular $\zeta = \frac{m^0}{m_L}$, this

can also be calculated based on Eq.(6.4).

6.5 Numerical Examples

In this section, limit load estimates are determined for a number of mechanical/pressure components. All the problems are modeled using the ANSYS [21] software and the Poisson's ratio is considered as $\nu=0.3$. Mesh convergence studies have been performed to verify the sensitivity of the multipliers with respect to the mesh density. For each component the m_{TBM} and m_{α}^T multiplier are calculated as per guideline provided in **Table 6.1** based on a single linear elastic analysis. Numerical examples are chosen in a way to encompass the lower bound limit load calculation methodology summarized in **Table 6.1**. Results are compared with the inelastic finite element results as well as available analytical solutions. Inelastic finite element analysis is performed as per guideline provided in Section 5.6. A relative estimate of computational time required for each method (simplified linear elastic method, EMAP and inelastic FEA) can be found in [35].

6.5.1 Thick Walled Cylinder

A cylinder under internal pressure of 50 MPa (**Figure 6.4**) is analyzed using plane strain conditions. The inner radius of the cylinder is 65 mm, and the outer radius is 90 mm. The modulus of elasticity is specified as 200 GPa and the yield strength is assumed to be 300 MPa. The geometry is modeled using eight noded isoparametric quadrilateral elements (Plane82) with symmetric consideration.

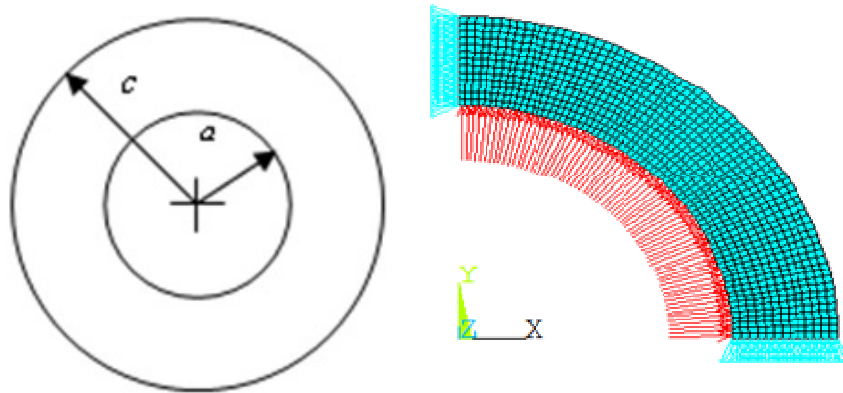


Figure 6.4 Finite element model of the thick walled cylinder

From the initial linear elastic analysis it is found that ζ is less than $1+\sqrt{2}$ (**Table 6.3**). Hence thick walled cylinder under uniform pressure is in the category of well-designed component having no stress concentrations as well as no kinematically inactive volume. The multiplier m_α^T and m_{TBM} are evaluated as per the guideline provided in **Table 6.1** and results are summarized in **Table 6.3**. Then an inelastic finite element analysis is performed, which gives a limit load multiplier of $m_{NFEA} = 2.254$. The multiplier m_{TBM} and m_α^T are lower bound when compared with the multiplier m_{NFEA} . The analytical limit load solution gives an estimate of 2.260.

Table 6.3 Limit load multipliers for thick walled cylinder

m^0 Eq.(3.3)	m_L Eq.(3.2)	$\zeta = \frac{m^0}{m_L}$	$m' = \frac{2m^0}{1+\zeta^2}$	$e\%$ Eq.(6.4)	$m_{TBM} = m' \zeta \left(1 - \frac{e}{100}\right)$	$m_\alpha^T = \frac{m^0}{1 + \left(1 - \frac{1}{\sqrt{2}}\right)(\zeta - 1)}$	m_{NFEA}
2.264	1.708	1.325	1.642	5.32	2.061	2.067	2.254

6.5.2 Torispherical head

A torispherical head (**Figure 6.5**) with average diameter $D=2000\text{ mm}$, normalized spherical cap radius $R_s / D = 0.8$, normalized knuckle radius of $R_k / D = 0.12$ and normalized thickness of $t/D=1/40$, subjected to an internal pressure of 5 MPa is examined here. The modulus of elasticity is specified as 262GPa and the yield strength is assumed to be 262 MPa. The geometry is modeled using Plane82 elements with axisymmetric consideration.

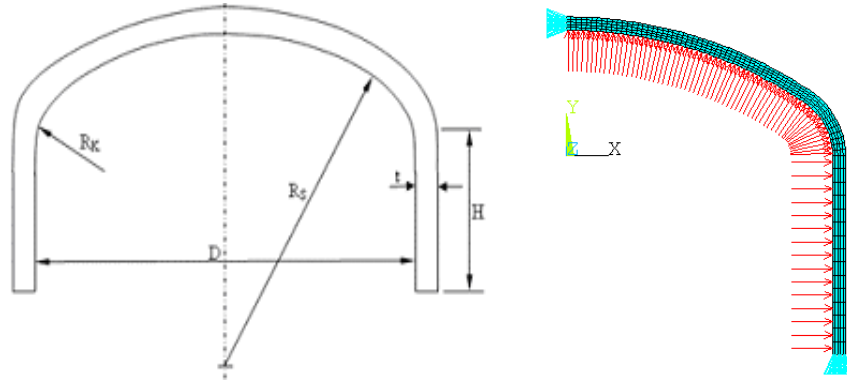


Figure 6.5 Axisymmetric finite element model of the torispherical head

Since $\zeta=2.172$ is less than $1+\sqrt{2}$, therefore the structure does not collapse locally. The multiplier m_α^T and m_{TBM} are evaluated and results are summarized in **Table 6.4** along with the inelastic FEA results. Based on the lower bound analytical approximation proposed by Drucker and Shield [22], the limit load multiplier for the torispherical head is 2.360. As shown in **Table 6.4**, the multiplier m_α^T and m_{TBM} are lower bound when compared with the inelastic FEA results.

Table 6.4 Limit load multipliers for torispherical head

m^0 Eq.(3.3)	m_L Eq.(3.2)	$\zeta = \frac{m^0}{m_L}$	$m' = \frac{2m^0}{1+\zeta^2}$	$e\%$ Eq.(6.4)	$m_{TBM} = m' \zeta \left(1 - \frac{e}{100}\right)$	$m_\alpha^T = \frac{m^0}{1 + \left(1 - \frac{1}{\sqrt{2}}\right)(\zeta - 1)}$	m_{NFEA}
2.912	1.340	2.172	1.018	2.051	<u>2.166</u>	<u>2.167</u>	<u>2.790</u>

6.5.3 Reinforced Axisymmetric Nozzle

A reinforced axisymmetric cylindrical nozzle on a hemispherical head (**Figure 6.6**), subjected to an internal pressure of 24.1 MPa is analyzed here. The inner radius of the head is $R=914.4\text{ mm}$, and the nominal wall thickness is $t=82.6\text{ mm}$. Inside radius of the nozzle is $r=136.5\text{ mm}$ and the nominal wall thickness is $t_n=25.4\text{ mm}$. The required minimum wall thickness of the head and the nozzle is $t_r=76.8\text{ mm}$ and $t_m=24.3\text{ mm}$, respectively. The geometric transitions of the reinforcement are modeled with fillet radius, $r_1=10.3\text{ mm}$, $r_2=83.3\text{ mm}$ and $r_3=115.2\text{ mm}$. Other dimensions include reinforcement thickness $T=54.6\text{ mm}$ and the angle of reinforcement, $\theta=45^\circ$. The reinforcement is bounded by the reinforcement-zone boundary, specified by circle of radius $L_n=143.5\text{ mm}$. The modulus of elasticity is specified as 262 GPa, and the yield strength is assumed to be 262 MPa. The geometry is modeled using eight-noded isoparametric quadrilateral elements (Plane82) with axisymmetric consideration.

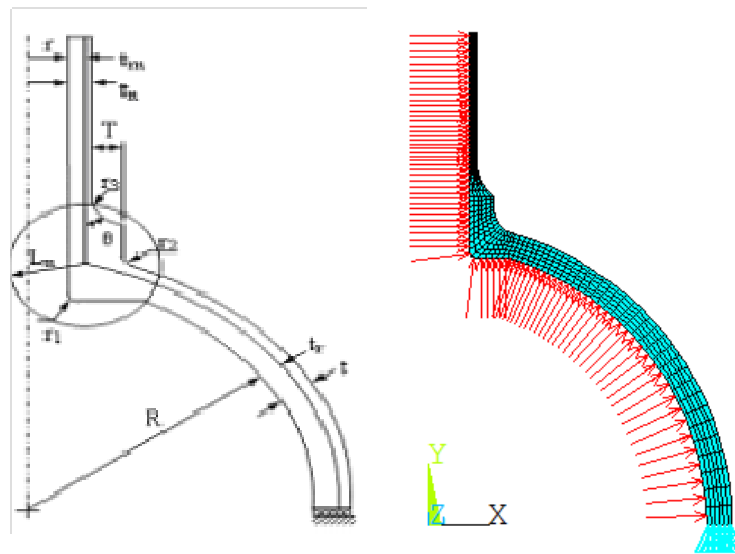


Figure 6.6 Finite element model of the reinforced axisymmetric nozzle

Similar to thick walled cylinder and torispherical head, reinforced axisymmetric nozzle is a well designed pressure component with smooth geometric transition. Therefore this should be under the category of ζ is less than $1+\sqrt{2}$. The multiplier m_α^T and m_{TBM} are evaluated as per the guideline provided in **Table 6.1** and results are summarized in **Table 6.5**. Then an inelastic finite element analysis is performed, which gives a limit load multiplier of $m_{NFEA} = 1.872$. The multiplier m_{TBM} and m_α^T are lower bound when compared with the multiplier m_{NFEA} .

Table 6.5 Limit load multipliers for reinforced axisymmetric cylindrical nozzle

m^0 Eq.(3.3)	m_L Eq.(3.2)	$\zeta = \frac{m^0}{m_L}$	$m' = \frac{2m^0}{1+\zeta^2}$	$e\%$ Eq.(6.4)	$m_{TBM} = m' \zeta \left(1 - \frac{e}{100}\right)$	$m_\alpha^T = \frac{m^0}{1 + \left(1 - \frac{1}{\sqrt{2}}\right)(\zeta - 1)}$	m_{NFEA}
1.891	1.120	1.689	0.982	5.37	<u>1.569</u>	<u>1.574</u>	<u>1.872</u>

6.5.4 Plate with a Hole

Consider a thin plate with a hole (**Figure 6.7**) with the following dimensions: plate width, $W=150\text{ mm}$; length, $L=300\text{ mm}$; and hole radius, $d=40\text{ mm}$. It is subjected to a tensile load of 100MPa. The modulus of elasticity is specified as 150 GPa and the yield strength is assumed to be 150 MPa. Due to symmetry in geometry and loading, only a quarter of the plate is modeled using eight noded isoparametric quadrilateral elements (Plane82) with plane stress consideration. Making reference to the dimensions of the plate with hole, the collapse load multiplier may be

$$\text{estimated to be } \frac{\left(\frac{W-d}{2}\right)\sigma_y}{\frac{W}{2}P} = 1.10.$$

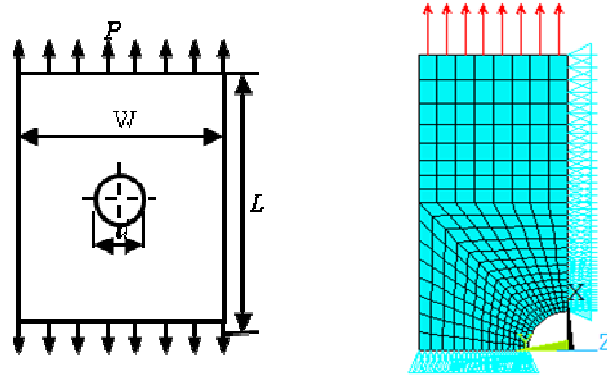


Figure 6.7 Finite element model of the plate with a hole

Plate with a hole is a uniaxial tensile problem, where stress concentration is due to the presence of the hole. From the initial linear elastic analysis it is found that ζ is greater than $1+\sqrt{2}$. Since the stress distribution is uniform at every cross-section, $\zeta > 1+\sqrt{2}$ is attributed to the existence of peak stress. Therefore this requires peak stress correction based on Eq.(6.5) for m_α^T multiplier evaluation. On the other hand for this range of ζ , no error estimate is required for m_{TBM}

evaluation. Then an inelastic finite element analysis is performed, which gives a limit load multiplier of $m_{NFEA} = 1.099$. Results are summarized in **Table 6.6**.

Table 6.6 Limit load multipliers for plate with a hole

m^0 Eq.(3.3)	m_L Eq.(3.2)	$\zeta = \frac{m^0}{m_L}$	$m' = \frac{2m^0}{1+\zeta^2}$	$m_{TBM} = m'\zeta$	ζ_f Eq.(5.11)	$m_\alpha^T = \frac{m^0}{1 + (1 - \frac{1}{\sqrt{2}})(\zeta_f - 1)}$	m_{NFEA}
1.416	0.527	2.687	0.345	0.926	2.604	0.963	1.099

6.5.5 Compact Tension (CT) Specimen

A Compact Tension Specimen (**Figure 6.8**) with a width $W=100mm$, height $H=125mm$, thickness $t=3mm$ and crack length $a=46mm$ is subjected to a tensile load of $P=5kN$. The modulus of elasticity is specified as 206.85 GPa and the yield strength is assumed to be 206.85 MPa. Due to symmetry, only a half of the plate is modeled with plane stress consideration. The compact test specimen is subjected to concentrated load and contains stress concentration ahead of crack tip.

The linear elastic stress distribution around a crack configuration can be captured by using singular elements around the crack tip. Therefore the finite element model is developed using eight noded isoparametric quadrilateral elements (Plane82), with eight singularity elements around the crack-tip. However limit load solution based on a linear elastic stress distribution requires further treatment of singularity elements, when the solution technique has explicit dependency on the maximum stress at the crack tip (i.e. classical lower bound limit load solution (m_L) is explicitly dependent on the maximum equivalent stress of the entire stress distribution). This is due to the recognition that a crack tip configuration induces very high peak stress, which is localized and gets redistributed along with the secondary stress. Proper elastic modulus modification of singular elements around the crack tip in a finite element discretization can reduce the magnitude of stress gradient to a minimum and hence the effect of peak stresses becomes small. The stress concentration at the crack tip can be blunted by modifying the elastic modulus of the singularity elements as $E_s=E/3$, while performing single linear elastic analysis. The rationale for this modulus reduction is proposed by Adibi-Asl and Seshadri [23]. A brief

description of singularity elements and their appropriate softening process is provided in Appendix B.

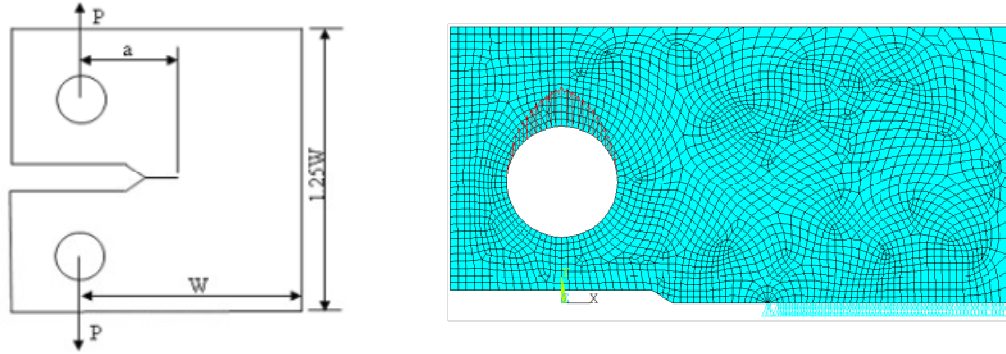


Figure 6.8 Finite element model of compact tension specimen

From the initial linear elastic analysis it is found that ζ is greater than $1+\sqrt{2}$ (**Table 6.7**). There are two possibilities which might cause $\zeta > 1+\sqrt{2}$ even after singularity element softening.

- i. There might be some peak stress left at the crack tip which requires further blunting.
- ii. Kinematically inactive volume is existing due to concentrated loading.

Hence this problem fits under the category which requires further peak stress correction as well as dead volume correction while evaluating the m_α^T multiplier. On the other hand for this range of ζ , no error estimate is required for m_{TBM} evaluation. An inelastic finite element analysis is performed, which gives a limit load multiplier of $m_{NFEA} = 1.330$. Results are summarized in **Table 6.7**.

Table 6.7 Limit load multipliers for compact tension specimen

m^0 Eq.(3.3)	m_L Eq.(3.2)	$\zeta = \frac{m^0}{m_L}$	$m' = \frac{2m^0}{1+\zeta^2}$	$m_{TBM} = m'\zeta$	$m^0(V_R)$ Eq.(5.9)	ζ_f Eq.(5.11)	$m_\alpha^T = \frac{m^0(V_R)}{1+(1-\frac{1}{\sqrt{2}})(\zeta_f-1)}$	m_{NFEA}
2.595	0.494	5.257	0.181	0.953	2.141	4.259	1.095	1.330

6.5.6 Large Grillage

A large grillage model described in Section 5.6 is analyzed here based on single linear elastic analysis. Since $\zeta=5.781$ is greater than $1+\sqrt{2}$ (Table 6.8), therefore peak stress correction and/or reference volume correction are required. This is a complex geometry and there is ambiguity in deciding whether $V_R < V_T$. Therefore conservatively it is considered that reference volume correction is appropriate along with the peak stress correction, while evaluating m_α^T multiplier. On the other hand for this range of ζ , no error estimate is required for m_{TBM} evaluation. An inelastic finite element analysis is performed, which gives the limit load multiplier $m_{NFEA} = 0.105$. Results are summarized in **Table 6.8**.

Table 6.8 Limit load multipliers for large grillage

m^0 Eq.(3.3)	m_L Eq.(3.2)	$\zeta = \frac{m^0}{m_L}$	$m' = \frac{2m^0}{1+\zeta^2}$	$m_{TBM} = m'\zeta$	$m^0(V_R)$ Eq.(5.9)	ζ_f Eq.(5.11)	$m_\alpha^T = \frac{m^0(V_R)}{1+(1-\frac{1}{\sqrt{2}})(\zeta_f-1)}$	m_{NFEA}
0.198	0.034	5.781	0.012	0.067	0.160	4.583	0.078	0.105

6.6 Discussion and Conclusion

For component category $\zeta \leq 1 + \sqrt{2}$, a correction factor is introduced into the two bar formulation in order to eliminate any possibility of its overestimation. For component category $\zeta > 1 + \sqrt{2}$, the two bar multiplier estimate proposed by Seshadri and Adibi-Asl [10] is shown to be a lower bound (in Chapter 4) and hence is used without any modification. Therefore the suggested two bar multiplier calculation guideline ensures lower bound limit load solution.

For component category $\zeta \leq 1 + \sqrt{2}$, the m_α^T -multiplier estimate proposed by Seshadri and Hossain [12] is shown to be a lower bound (in Chapter 5) and hence is used without any modification. For component category $\zeta > 1 + \sqrt{2}$, incorporation of reference volume and peak stress correction suggested in this chapter ensures lower bound m_α^T multiplier with acceptable accuracy based on single linear elastic analysis. Therefore the suggested m_α^T multiplier calculation guideline ensures lower bound limit load solution.

The multiplier m_{TBM} and m_α^T estimates lower bound limit loads based on a single linear elastic analysis as shown in Section 6.4 and 6.5. However their estimates could be conservative while analyzing structures with higher degree of indeterminacy as evident from **Figure 5.6** (e.g. a large grillage model, for which a four bar model shown in **Table 4.1** would provide more accurate estimate of limit load). In this context, the m_α^T multiplier estimates are more accurate compared to the multiplier m_{TBM} . It should be noted here that the multiplier m_{TBM} offers much better accuracy than classical lower bound solution.

Chapter 7: EMAP for Strain Hardening Material Model

7.1 Introduction

Inelastic FEA is the most frequently used approach to obtain the detail structural response and is an economic alternative to full scale experimental test. However, it is always essential to have an alternate solution tool available, in order to validate the results of a traditional elastic-plastic analysis.

Iterative elastic modulus adjustment scheme can establish inelastic-like stress and strain field by modifying the local elastic modulus of elements of an FE model in repeated linear elastic FEA. Modulus adjustment approaches are different depending on the type of stress fields anticipated. According to Adibi-Asl and Reinhardt [24], EMAP can be categorized into two classes: (i) “Full EMAP” which involves simultaneous element softening and hardening in order to obtain the limit state stress field. (ii) “Partial EMAP” in which the modification is performed only in the elements having a stress level higher than the yield strength.

In the stress-strain curve, once the yield strength is exceeded, plasticity occurs. In the initial portion of plastic region, the rise in curve is due to the presence of strain hardening feature in the material. The partial EMAP scheme previously developed for elastic-perfectly-plastic material model [24] can be extended to strain hardening material model in order to achieve inelastic-like stress and strain field under strain hardening action.

In this chapter, an elastic modulus adjustment scheme for strain hardening material model is developed. The algorithm is programmed into repeated linear elastic analysis in order to capture

the post yield behavior of a component or structure. The proposed algorithm is then applied to numerical examples and results are compared to traditional inelastic finite element results.

7.2 EMAP Categories

EMAP establishes inelastic-like stress and strain field by approximating incompressible plastic flow. Numerous sets of statically admissible and kinematically admissible distributions can be generated in this manner. However, modulus adjustment approaches are different depending on the type of stress fields anticipated. Full EMAP modifies the elastic modulus of all elements and is used to achieve the limit state. On the other hand in partial EMAP the modification is performed only for the elements having stress level higher than the yield strength. Therefore this is essentially an element softening process. Both full and partial EMAP are based on iterative linear elastic analysis, where elastic modulus and Poisson's ratio are the only material properties used for the structural analysis. In the following section, the procedure for elastic modulus adjustment to achieve limit state and elastic-plastic state are explained in parallel, to demonstrate their similarity and diversity.

7.2.1 Full EMAP

The full EMAP is used to estimate the limit load / primary stress and correspond to inelastic finite element limit load analysis considering elastic-perfectly-plastic material model. There are several approaches that employ modification of the local elastic modulus of material in successive iterations, in order to achieve inelastic-like stress distributions based on linear elastic analysis. The EMAP suggested in chapter 5 is indeed a full EMAP approach, which considers a constant value of ' q ' (known as modulus adjustment parameter). As discussed earlier, a relatively

smaller value of ‘ q ’ ensures consistent variations of limit load multipliers with iterations, (especially for those multipliers having explicit dependency on classical lower bound). Adibi-Asl *et. al.*, [25] developed a relationship between modified modulus and the initial modulus, based on Elastic Strain Energy Density (ESED) concept [20], from elastic-perfectly-plastic material model, where modulus adjustment parameter varies in element basis. By equating the area of two shaded region in **Figure 7.1**, the relationship between modified modulus and the initial modulus can be established as follows:

$$E_{i+1} = \frac{2\sigma_{ref}^2}{\sigma_{eq}^2 + \sigma_{ref}^2} E_i \quad (7.1)$$

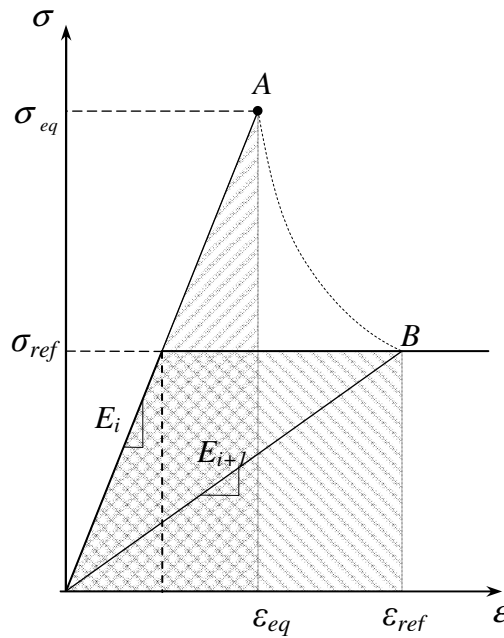


Figure 7.1 Schematic of the ESED method

As illustrated in **Figure 7.1**, when the elastic stress in each element is brought to the reference stress level in subsequent linear elastic iterations, the stress distribution in the structure will eventually reach to the stress distribution during plastic collapse and multipliers obtained from

this stress field will estimate the limit load. Eq.(7.1) can be used to modify the elastic modulus of each element in successive linear elastic iterations where σ_{ref} is the reference stress in each iteration. The only difference between the approach proposed by Adibi-Asl *et. al.*, [25] and the proposed method in Chapter 5 is that, Adibi-Asl *et. al.*, [25] considered a variable modulus adjustment parameter (q), which varies in element basis, while the proposed method in this thesis considers a fixed relatively smaller value of ‘ q ’ ($q=0.1$). A fixed small modulus adjustment parameter (q) enables smooth convergence towards the exact limit load solution with iterations, while variable ‘ q ’ [25] might cause oscillations, resulting a non-convergence (particularly for complex three dimensional FE models). This issue is specifically true for the multipliers having explicit dependency on the classical lower bound multiplier.

7.2.2 Partial EMAP

The aim of partial EMAP (partial modification) is to simulate the stress and strain distribution during inelastic action. In this method, the modification of elastic modulus only takes place in elements having equivalent stress higher than yield strength. Reference stress is considered to be equal to the yield strength of the material. Therefore reference stress term σ_{ref} in Eq.(7.1) needs to be substituted by the yield strength σ_y in order to predict inelastic stress and strain fields for elastic-perfectly-plastic material model. As mentioned in [24], peak and secondary stresses usually do not cause significant inelastic deformations. Therefore, the strains obtained from linear elastic analysis can be used to estimate the plastic strains with acceptable accuracy.

The partial EMAP scheme for elastic-perfectly-plastic material model [24] can be extended to strain hardening material model in order to achieve inelastic-like stress and strain field under the strain hardening action.

7.3 Strain Hardening Material Model

A typical form of strain hardening material model can be represented by the following equation:

$$\varepsilon = f(\sigma_y, \sigma) \quad (7.2)$$

where σ_y is the yield strength and (σ, ε) is the stress-strain state at any point on the material model.

Typical strain hardening curves are bilinear hardening and Ramberg–Osgood material models. Bilinear hardening material model can be represented by line segments with slopes related to the elastic modulus (E) and tangent modulus (E_t). This is the simplest representation of strain hardened material properties. On the other hand, Ramberg–Osgood material model is closer to actual material properties. In this model the strain hardening behavior of any ductile material is specified by a dimensionless material constant (α), and a strain hardening exponent (n) [27].

Due to strain hardening, a component or a structure can store supplementary strain energy and hence carries additional load during the inelastic deformation. The inherent strength due to strain hardening can be specified into EMAP algorithm in order to simulate the stress and strain distribution during the inelastic action.

7.4 Proposed Partial EMAP for Strain Hardening Model

In this section, the partial EMAP scheme for elastic-perfectly-plastic material model is extended to strain hardening material model in order to achieve inelastic-like stress and strain field under the strain hardening action. Mathematical model for modulus adjustment is developed for bilinear and Ramberg-Osgood strain hardening material model.

7.4.1 Partial EMAP for Bilinear Hardening Material Model

A schematic plot of a bilinear material model is shown in **Figure 7.2(a)**. With respect to **Figure 7.2(a)**, point 'a' represents the pseudo elastic stress. Therefore the element has to be softened in such a way that the stress and strain at 'a' is projected to its actual location 'a''. This can be achieved by equating the strain energy of shaded elastic region with that of shaded inelastic region as shown in **Figure 7.2(a)**.

$$\frac{1}{2} \sigma_{eq}^e \varepsilon_{eq}^e = \frac{1}{2} \sigma_y \varepsilon_y + \sigma_y (\varepsilon_{eq}^p - \varepsilon_y) + \frac{1}{2} (\varepsilon_{eq}^p - \varepsilon_y) (\sigma_{eq}^p - \sigma_y) \quad (7.3)$$

Here, σ_{eq}^e and ε_{eq}^e are stress-strain at point 'a'. σ_{eq}^p and ε_{eq}^p are stress-strain at point 'a'', respectively.

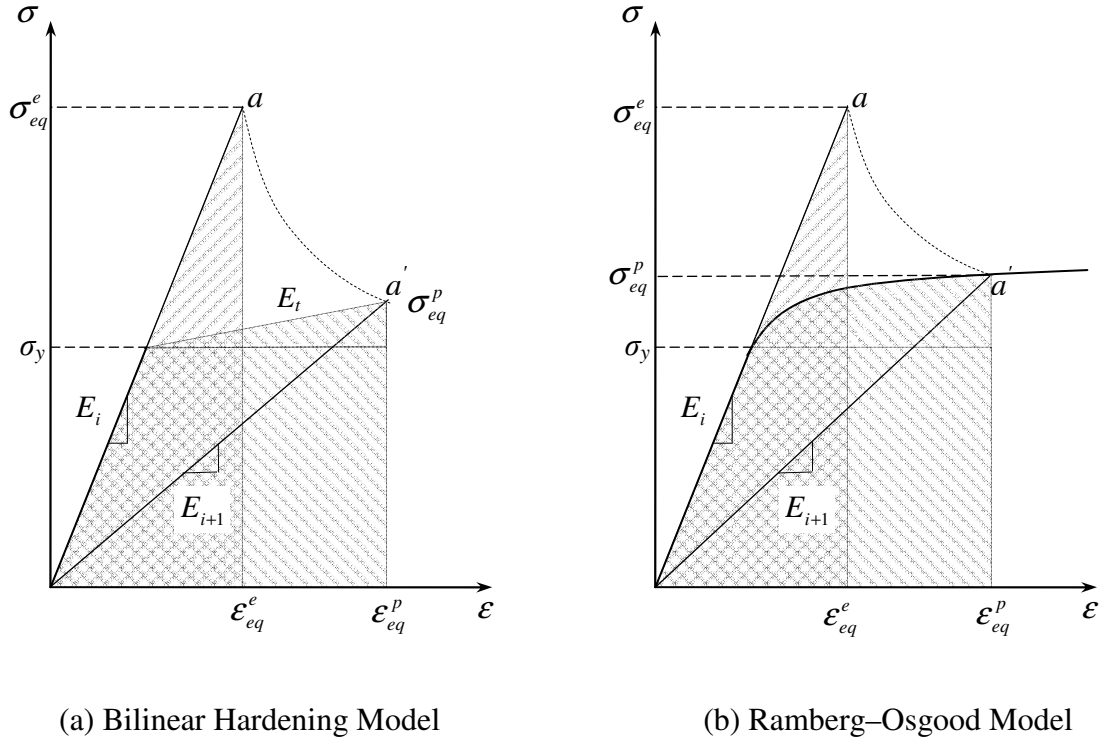


Figure 7.2 Schematic of the strain hardening material model

Let,

$$\sigma_{eq}^p = A \sigma_y \quad (7.4)$$

where ($A \geq 1$)

According to Hooke's law,

$$\epsilon_y = \frac{\sigma_y}{E_i}, \quad \epsilon_{eq}^e = \frac{\sigma_{eq}^e}{E_i}, \quad \text{and} \quad \epsilon_{eq}^p = \frac{\sigma_{eq}^p}{E_{i+1}} \quad (7.5)$$

Substituting Eq. (7.4) and Eq.(7.5) into Eq. (7.3),

$$E_{i+1} = \frac{\sigma_y^2 A(A+1)}{\sigma_{eq}^e{}^2 + A\sigma_y^2} E_i \quad (7.6)$$

In Eq.(7.6), $A=1$ indicates elastic-perfectly-plastic and $A > 1$ indicates elastic-strain-hardening material model.

From **Figure 7.2(a)**, stress-strain relationship for the strain hardening zone can be expressed as,

$$\sigma_{eq}^p = E_t \varepsilon_{eq}^p - E_t \varepsilon_y + \sigma_y \quad (7.7)$$

$$\Rightarrow \frac{\sigma_{eq}^p}{\sigma_y} = A = \frac{E_{i+1}}{E_i} \frac{E_i - E_t}{E_{i+1} - E_t} \quad (7.8)$$

Substituting A from Eq. (7.8) into Eq. (7.6),

$$E_{i+1} = \frac{\sigma_y^2 \left(\frac{E_{i+1}}{E_i} \frac{E_i - E_t}{E_{i+1} - E_t} \right) \left(\frac{E_{i+1}}{E_i} \frac{E_i - E_t}{E_{i+1} - E_t} + 1 \right)}{\sigma_{eq}^2 + \left(\frac{E_{i+1}}{E_i} \frac{E_i - E_t}{E_{i+1} - E_t} \right) \sigma_y^2} E_i \quad (7.9)$$

Eq.(7.9) has three explicit solutions for E_{i+1} and out of them one is the actual solution and the other two are trivial. Therefore the expression for modified elastic modulus can be written as:

$$E_{i+1} = \frac{\sigma_{eq}^2 E_i E_t + \sigma_y^2 E_i^2 - E_i E_t \sigma_y^2 + \sqrt{\sigma_{eq}^2 E_i^3 E_t \sigma_y^2 - 2\sigma_{eq}^2 E_i^2 E_t^2 \sigma_y^2 + E_i^4 \sigma_y^4 - 3E_i^3 \sigma_y^4 E_t + 3E_i^2 \sigma_y^4 E_t^2 + \sigma_{eq}^2 E_i^3 E_t \sigma_y^2 - E_i^3 E_t \sigma_y^4}}{\sigma_{eq}^2 E_i + E_t \sigma_y^2 - \sigma_y^2 E_t} \quad (7.10)$$

Substituting $E_t = 0$ into Eq.(7.10), it is reduced to Eq.(7.6) for $A=1$ (elastic-perfectly-plastic).

Therefore in addition to Eq.(7.7), stress and strain can also be related in terms of Hooke's law

based on $\varepsilon_{eq}^p = \frac{\sigma_{eq}^p}{E_{i+1}}$ where E_{i+1} can be calculated from Eq.(7.10).

Once the elastic stress for any element is obtained where $\sigma_{eq}^e > \sigma_y$, its modulus is reduced based on Eq.(7.10) and the next elastic analysis is performed using the new modulus (E_2 as per **Figure 7.3**). However, not all element stresses come onto the strain hardening curve with this modulus adjustment. This indicates further requirement of modulus adjustment in subsequent iterations. In

order to make subsequent modulus adjustments, σ_y of Eq.(7.10) has to be replaced by a variable term σ_y^i in subsequent iterations, which can be computed using the following equation:

$$\sigma_y^i = \frac{E_i}{E_{i-1}} \frac{E_{i-1} - E_t}{E_i - E_t} \sigma_y^{i-1} \quad (7.11)$$

(where $i \geq 2$ and $\sigma_y^{i=1} = \sigma_y$)

Therefore for $i \geq 2$, Eq.(7.10) can be re-written as,

$$E_{i+1} = \frac{\sigma_{eq}^2 E_i E_t + (\sigma_y^i)^2 E_i^2 - E_i E_t (\sigma_y^i)^2 + \sqrt{\sigma_{eq}^2 E_i^3 E_t (\sigma_y^i)^2 - 2\sigma_{eq}^2 E_i^2 E_t^2 (\sigma_y^i)^2 + E_i^4 (\sigma_y^i)^4 - 3E_i^3 (\sigma_y^i)^4 E_t + 3E_i^2 (\sigma_y^i)^4 E_t^2 + \sigma_{eq}^2 E_i^3 E_t (\sigma_y^i)^2 - E_i^3 E_t (\sigma_y^i)^4}}{\sigma_{eq}^2 E_i + E_i (\sigma_y^i)^2 - (\sigma_y^i)^2 E_t} \quad (7.12)$$

7.4.2 Partial EMAP for Ramberg–Osgood Material Model

A schematic plot of Ramberg–Osgood material model is shown in **Figure 7.2 (b)**. By equating the strain energy of elastic shaded region with that of inelastic shaded region as shown in **Figure 7.2(b)**, the following relationship can be achieved:

$$\begin{aligned} \frac{1}{2} \sigma_{eq}^e \varepsilon_{eq}^e &= \sigma_{eq}^p \varepsilon_{eq}^p - \int_0^{\sigma_{eq}^p} \varepsilon d\sigma \\ \Rightarrow \frac{(\sigma_{eq}^e)^2}{2E_i} - \frac{(\sigma_{eq}^p)^2}{E_{i+1}} + \int_0^{\sigma_{eq}^p} \varepsilon d\sigma &= 0 \end{aligned} \quad (7.13)$$

Ramberg–Osgood material model can be written as:

$$\varepsilon = \frac{\sigma}{E_i} + \frac{\alpha \sigma_y}{E_i} \left(\frac{\sigma}{\sigma_y} \right)^n \quad (7.14)$$

where α is the dimensionless material constant and n is the strain hardening exponent.

Substituting Eq. (7.13) by Eq. (7.14) and after integration it becomes,

$$\frac{(\sigma_{eq}^e)^2}{2E_i} - \frac{(\sigma_{eq}^p)^2}{E_{i+1}} + \frac{(\sigma_{eq}^p)^2}{2E_i} + \frac{\alpha(\sigma_y)^2 \left(\frac{\sigma_{eq}^p}{\sigma_y} \right)^{1+n}}{E_i(1+n)} = 0 \quad (7.15)$$

In order to calculate σ_{eq}^p , the following relationship needs to be solved:

$$\left(\sigma_{eq}^p \right)^n + \left(\frac{\sigma_y^{n-1}}{\alpha} - \frac{E_i \sigma_y^{n-1}}{\alpha E_{i+1}} \right) \sigma_{eq}^p = 0 \quad (7.16)$$

Solving Eq.(7.16) for σ_{eq}^p ,

$$\sigma_{eq}^p = \left(-\frac{\sigma_y^{n-1} (E_{i+1} - E_i)}{\alpha E_{i+1}} \right)^{\frac{1}{n-1}} \quad (7.17)$$

Substituting Eq. (7.17) into Eq. (7.15):

$$\frac{(\sigma_{eq}^e)^2}{2E_i} - \frac{\left(\left(-\frac{\sigma_y^{n-1} (E_{i+1} - E_i)}{\alpha E_{i+1}} \right)^{\frac{1}{n-1}} \right)^2}{E_{i+1}} + \frac{\left(\left(-\frac{\sigma_y^{n-1} (E_{i+1} - E_i)}{\alpha E_{i+1}} \right)^{\frac{1}{n-1}} \right)^2}{2E_i} + \frac{\alpha(\sigma_y)^2 \left(\frac{\left(-\frac{\sigma_y^{n-1} (E_{i+1} - E_i)}{\alpha E_{i+1}} \right)^{\frac{1}{n-1}}}{\sigma_y} \right)^{l+n}}{E_i(l+n)} = 0 \quad (7.18)$$

This is the implicit expression for adjusted modulus E_{i+1} . For a particular value of strain hardening exponent n , E_{i+1} can be achieved in explicit form.

7.5 Finite Element Implementation

The flow diagram for the strain hardening EMAP is shown in **Figure 7.3** which transforms σ_{eq}^e to its actual level σ_{eq}^p in successive linear elastic iterations. The flow diagram is described in terms of bilinear strain hardening material model, which can be extended for the Ramberg–Osgood material model as well. In this section the general procedure is outlined as follows:

- The first linear elastic finite element analysis is carried out for the FE model with the prescribed loading and boundary conditions. For the first linear elastic analysis, the elastic modulus is the elastic property as obtained from the material specification.
- For elements having stress level higher than the yield strength (i.e. $(\sigma_{eq}^e)_k^i > \sigma_y$), elastic modulus adjustment is made based on Eq.(7.10) and second linear elastic analysis is performed.
- For subsequent iterations, an element modulus adjustment is made if the element stress level $(\sigma_{eq}^e)_k^i$ is higher than $(\sigma_y^i)_k$, where $(\sigma_y^i)_k$ is calculated based on Eq.(7.11). The linear elastic iteration continues until the condition $(\sigma_{eq}^e)_k^i \leq (\sigma_y^i)_k$ satisfies in element basis.

It should be noted here that, for elements having stress level less than the yield strength, elastic modulus adjustment is not performed during the partial EMAP.

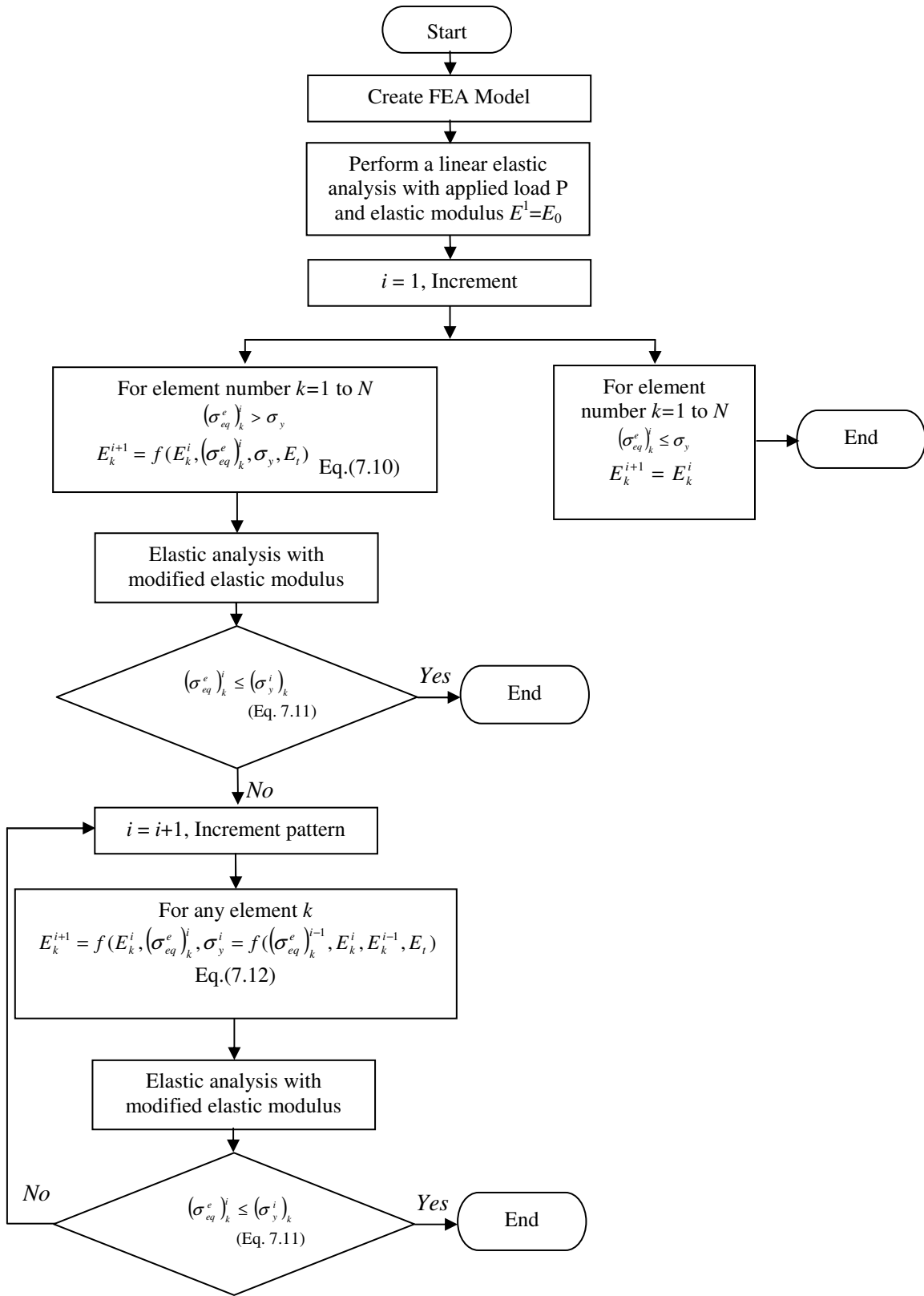


Figure 7.3 Partial EMAP flow diagram

7.6 Numerical Examples

In this section, modulus adjustment scheme for bilinear hardening material model is implemented into components: i) under axial loading, and ii) under transverse loading. Geometries are modeled using ANSYS [21]. Strain hardening effect is incorporated into linear elastic analysis on the basis of EMAP flow diagram given in **Figure 7.3**. In case of nonlinear analysis, both small and large deflection nonlinear analysis is performed considering elastic-perfectly-plastic as well as bilinear hardening material model.

7.6.1 Plate with a Hole

Consider a thin plate with a hole (**Figure 7.4**) with the following dimensions: plate width, $W=150$ mm; length, $L=300$ mm; and hole radius, $r=20$ mm. Material properties are as follows: yield strength, $\sigma_y=355$ MPa; elastic modulus, $E=207$ GPa; tangent modulus $E_t = 2$ GPa and Poisson's ratio, $\nu =0.47$. A two dimensional plane stress FEA model is developed using 8-noded plane82 element [21] with one quarter of the plate modeled due to symmetry (**Figure 7.4(b)**). Results are compared with small deflection nonlinear analysis.

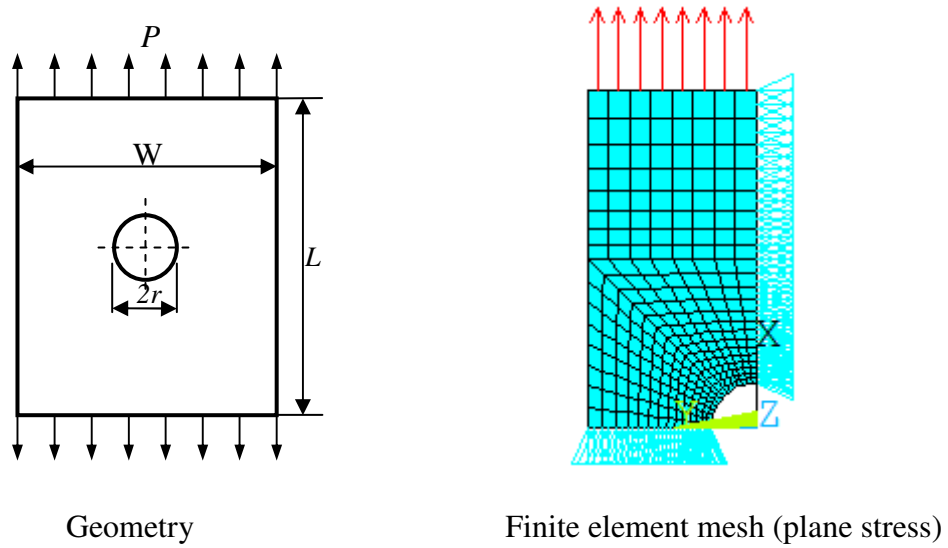


Figure 7.4 Plate with a hole

Figure 7.5 shows the load-deflection plot for the plate using elastic-perfectly-plastic as well as elastic-strain-hardening material model, obtained from nonlinear elastic-plastic analysis. It is evident from the figure that, in case of elastic-perfectly-plastic material model, the component does not exhibit any reserved capacity and limit load obtained from full EMAP (shown in **Figure 7.5**) is essentially the maximum load up to which load-deflection curve progresses. In the case of a strain hardening model, load-deflection curve exhibits the reserved capacity as evident from **Figure 7.5**.

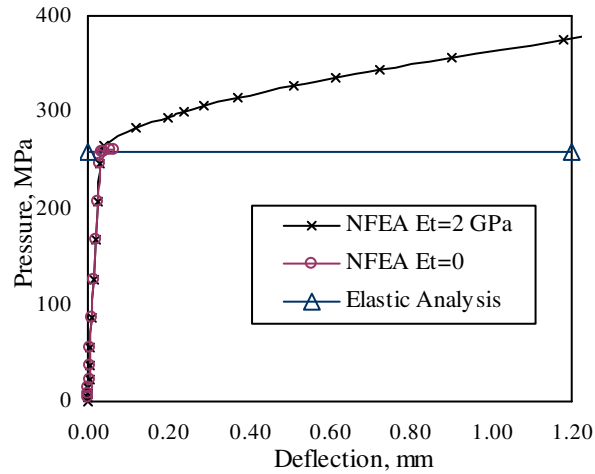


Figure 7.5 Load-deflection curve for plate with a hole

In order to investigate how the stress and strain reaches to its intended convergence, the element of maximum stress is studied. **Figure 7.6** and **Figure 7.7** shows the convergence of elastic stress and strain to their actual value in subsequent linear elastic analysis. In this case the applied load ($P = 283$ MPa) is higher than the limit load. This loading causes a very high peak stress in the maximum stress element. From **Figure 7.6** it is evident that, for a particular element, the computed σ_y^i and elastic stress σ_{eq}^i eventually reaches to the actual σ_{eq}^p stress level and becomes constant. Similarly, elastic strain also converges towards the actual plastic strain as shown in **Figure 7.7**.

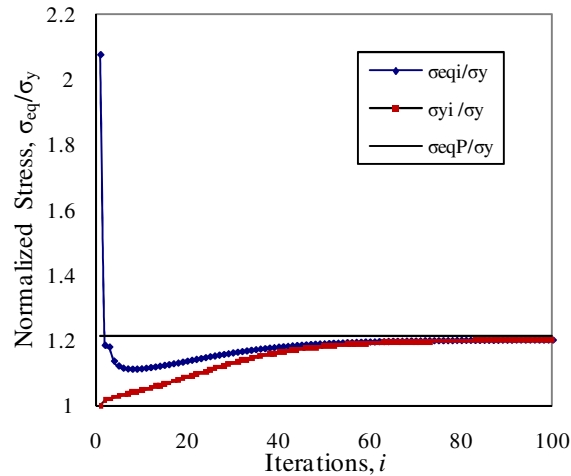


Figure 7.6 Variation of stress with iterations

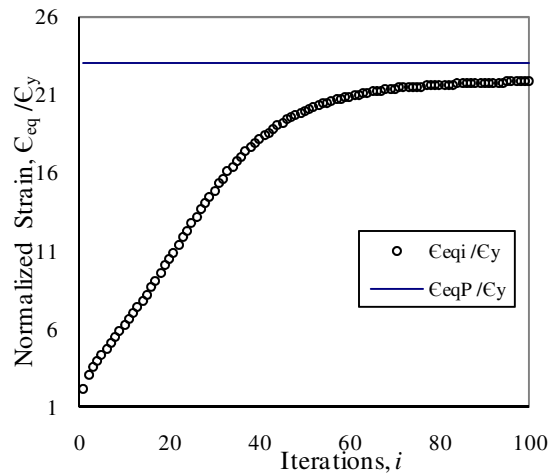


Figure 7.7 Variation of strain with iterations

Figure 7.8 shows the comparison of stress-strain plot obtained from two different analyses. In the case of elastic analysis, the flow chart given in **Figure 7.3** is iterated for different load increments and for each load step; normalized stress and strain are plotted in **Figure 7.8**. It is evident that results obtained from proposed method are in well agreement with the small deflection nonlinear FEA results. **Figure 7.9** is basically the extension of load-deflection plot

shown in **Figure 7.5**. It is evident from the figure that for a particular load step, calculated deflections from the proposed technique are in good agreement with the deflections obtained from nonlinear FEA.

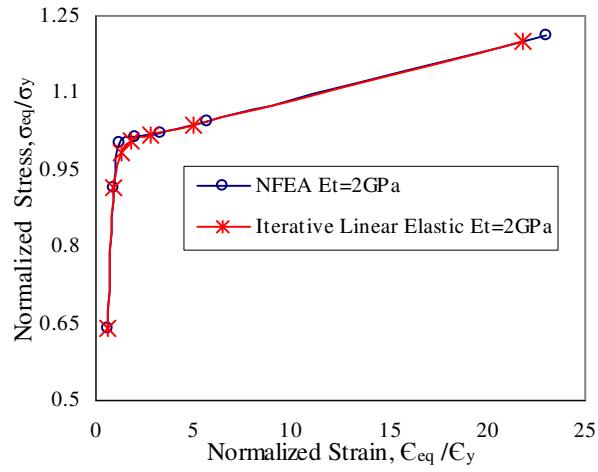


Figure 7.8 Normalized stress-strain plot

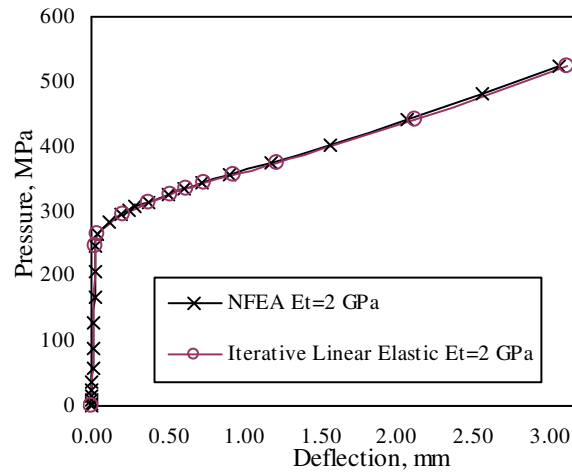


Figure 7.9 Comparison of load-deflection behavior

7.6.2 Stiffened Plate Subjected to Transverse Loading

A stiffened plate model considers a stiffener with the attached shell plate as a representative of the entire structure. Length of the model is taken 2.5 m and other dimensions are shown in **Figure 7.10**. Symmetric boundary conditions are applied along the length of the plate to simulate the support provided by the neighboring structure. Shorter ends are fixed to simulate the support provided by the continuing frame and transverse members. Elastic modulus of the material is 207 GPa, tangent modulus is 2 GPa and yield strength is 355 MPa. A three dimensional FEA model is developed using 4-noded shell181 element. Results are compared with small deflection as well as large deflection nonlinear analysis results.

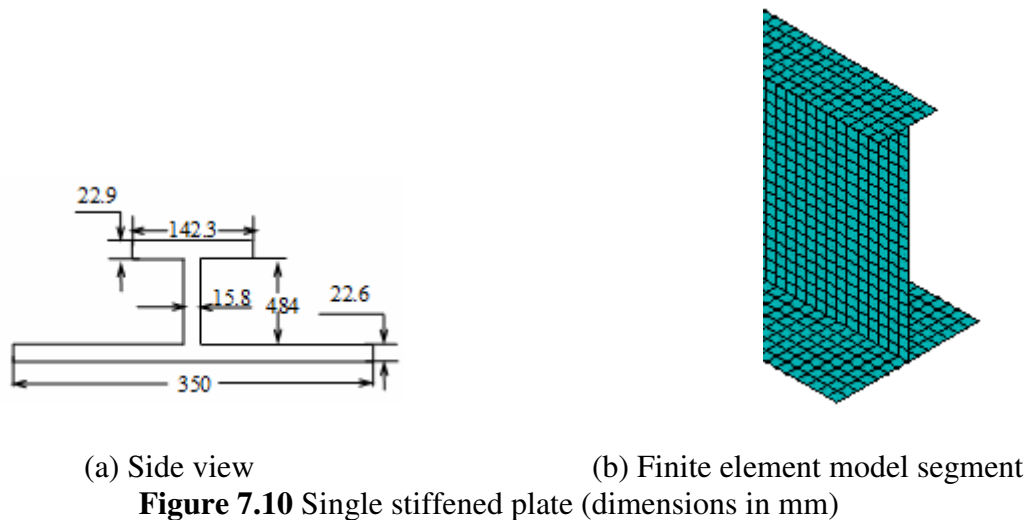


Figure 7.11 shows the comparison of load-deflection behavior obtained from different analyses. An arbitrary node is chosen from the node set connecting the web with the plate and nodal deflection is plotted against the corresponding load increment. Results obtained from the proposed methodology are in good agreement with the small deflection nonlinear FEA results as shown in **Figure 7.11**. It should be mentioned here that geometric nonlinearity effect increases the post yield reserved capacity of the structure. As the geometric nonlinearity effect is not

considered into the suggested method, it yields conservative load-deflection curve (follows the small deflection nonlinear FEA result) compared to that obtained from large deflection nonlinear analysis as shown in **Figure 7.11**.

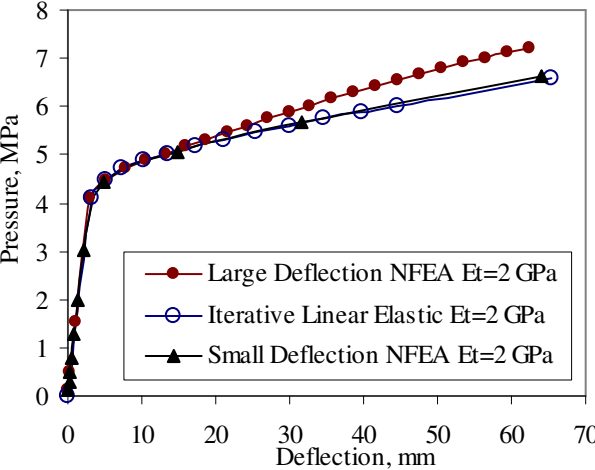


Figure 7.11 Comparison of load-deflection behavior

7.7 Applications

The proposed technique can be implemented for the estimation of stress-strain at the notch root of a component having strain hardening feature, which is useful for FCI (fatigue crack initiation) prediction and can be utilized as an independent verification tool for the available techniques. Similar investigation was carried out previously by Adibi-Asl and Seshadri [15] for elastic-perfectly-plastic material model. The proposed method can be utilized to obtain the plastic response of a structure beyond its yield point, which provides an idea about the reserved capacity of the structure against environmental/accidental loads. The method can also be implemented to identify the boundary between shakedown and ratcheting when the structure experiences strain hardening effect (similar solution was reported by Adibi-Asl and Reinhardt [24] for elastic-perfectly-plastic material model). This is a non-cyclic approach and hence can offer as an alternative to cyclic elastic-plastic analysis. Pressure vessel components described in the literature (for example: cylinders, pressure vessel support skirts, nozzles, frames etc), and other steel structures (for example: plates, beams, shells, stiffeners, grillages etc) can be suitably analyzed by the proposed method. As the degrees of freedom of FE model increases, the method offers better economic value compared to nonlinear FEA, in terms of computational time, effort and computer storage space.

7.8 Discussion and Conclusion

In this chapter, mathematical formulation for elastic modulus adjustment procedure has been developed for strain hardening material model. These formulations are then integrated to the linear elastic analysis and an algorithm has been proposed to capture the post yield behavior.

In order to obtain the load deflection behavior on the basis of proposed method, applied load has to be incremented and strain hardening EMAP algorithm (**Figure 7.3**) has to be iterated for each load increment. The proposed method achieves inelastic stress and strain convergence by systematic modulus adjustment in subsequent iterations while the inelastic FEA achieves convergence through the achievement of equilibrium and compatibility condition at a particular load increment. Therefore, although the proposed methodology approximates the inelastic distribution with sufficient accuracy, there are slight deviations in results due to the difference in underlying algorithm.

The method has shown good agreement with small deflection nonlinear FEA results and thus can be used as a suitable tool for structural analyses, when large deflection is not an occurrence. The proposed method can be extended further to incorporate the in-plane membrane effect and geometric nonlinearity effect into the mathematical formulation.

Chapter 8: Conclusions and Future Research

8.1 Summary and Conclusions

This thesis is dedicated to the examination of the bounds of several limit load approximations, and subsequently suggests procedures and guidelines for robust limit load approximations. These methods can be employed for estimating primary stress and limit loads and hence can be utilized as an analysis tool for design as well as integrity assessment of practical components and structures. Simplified approximations are also attractive for Level 2 Fitness-for-service (FFS) evaluations. Level 2 is intended for use by facilities or plant engineers in an engineering plant environment with the availability of limited analysis capabilities. The following section summarizes the key conclusions drawn from this thesis:

The lower bound estimate of the multiplier m''_{μ} relies on the exact distribution of plastic flow parameter. It is found that for an approximate distribution of flow parameter, m''_{μ} is either upper bound or its bounds are not obvious. Since the exact distribution of plastic flow parameter is only available from the limit state stress distribution, the multiplier m''_{μ} could not be established as a lower bound based on a single linear elastic analysis.

Simha and Adibi-Asl [14] proposed an inequality relation ($m'' < m''_{\mu}$) for lower bound m'' . It is concluded that the inequality ($m'' < m''_{\mu}$) cannot guarantee a lower bound m'' , when m''_{μ} is estimated from an approximate distribution of plastic flow parameter.

The reference two bar model introduces a transformation parameter, which scales up the overly conservative estimate of Mura's lower bound multiplier to a better accuracy. The reference two

bar multiplier bounds the limit load solution of multi bar models. A general mechanical component can be represented by a suitable multi bar model in terms of limit load estimation. Furthermore, the correction factor introduced to the reference two bar solution eliminates any possibility of overestimation of limit loads using the reference two bar multiplier. Hence the proposed estimate of reference two bar solution provides lower bound limit load. However, reference two bar multiplier at times provides conservative results, although its accuracy is far better compared to classical lower bound.

The m_α^T multiplier which offers better accuracy than the two bar multiplier is also established as a lower bound by investigating exact solution trajectory, utilizing the constraint map construction. Furthermore, the m_α^T multiplier bounds the limit load solution of multi bar models. The suggested m_α^T multiplier estimate thus gives more accurate lower bound limit loads (compared to the two bar solution) using single linear elastic analysis.

The proposed estimate of reference two bar multiplier and the m_α^T multiplier can be used (i) to obtain lower bound limit load / primary stress of mechanical components and structures, (ii) to assess the integrity of components with and without defects, and (iii) to assess the Level 2 FFS evaluations of an in-service component. These methods are simple, reliable, cost efficient as well as easy to implement based on a single linear elastic analysis.

An elastic modulus adjustment scheme for elastic-perfectly-plastic material model has been developed, which reduces the convergence difficulties usually encountered in EMAP for complex component configurations. The m_α -tangent multiplier is used in conjunction with the

elastic modulus adjustment procedure for limit load determination. The lower boundedness of the m_α -tangent multiplier for any iteration is ensured by incorporating reference volume and peak stress corrections. By the virtue of the faster convergence feature, the m_α^T -multiplier permits gentler modulus adjustments, and at the same time estimates sufficiently accurate lower bound limit load within a relatively small number of elastic iterations.

Single linear elastic analysis based techniques are attractive when a quick and inexpensive calculation is required (e.g. Level 2 FFS type assessment). If the limit load/primary stress can be estimated from a linear elastic stress analysis in order to meet the ASME design qualification requirement ([1] [11]), then it will save the expense to set-up and perform a detailed inelastic analysis. However when the analyst cannot afford any kind of conservatism, EMAP can be utilized to achieve better accuracy. Basically the first EMAP iteration is nothing but the single linear elastic analysis.

An elastic modulus adjustment scheme for strain hardening material model has been developed and the algorithm is programmed into repeated linear elastic analysis in order to capture the post yield behavior of a component or structure. The modulus adjustment scheme results for bilinear hardening material model have shown good agreement with small deflection nonlinear FEA results. Hence it can be used as a suitable and an alternative technique for elastic-plastic analysis.

The simplified methodologies developed in this thesis are limited to components subjected to small deformation.

8.2 Original Contributions

The following are the original contributions of this thesis:

(1-a) NSSC rules [15] are introduced into the expression of plastic flow parameter distribution proposed by Pan and Seshadri [7]. A general expression of plastic flow parameter distribution is proposed in a form which enables parametric examination of the possible approximations of the plastic flow parameter based on a linear elastic analysis.

(1-b) An extended expression for the multiplier m''_{μ} [13] is proposed in a form which enables parametric examination of its estimate based on the possible approximations of the plastic flow parameter distribution. It is concluded that the limit load bounds of the multiplier m''_{μ} is not obvious for an approximate distribution of flow parameter.

(1-c) Since the limit load bounds of the multiplier m''_{μ} is not obvious for an approximate distribution of flow parameter, the inequality ($m'' < m''_{\mu}$) cannot guarantee a lower bound m'' [14], if m''_{μ} is estimated based on an approximate distribution of plastic flow parameter.

(2-a) The reference two bar model is developed on the basis of the generalized two-bar analysis. The generalized two-bar analysis eliminates the equal two bar area assumption previously considered in the literature [10].

(2-b) A transformation parameter has been obtained from the reference two bar model which scales up Mura's overly conservative lower bound multiplier to a multiplier with improved accuracy.

(2-c) Since a mechanical component or structure can be represented by a suitable multi bar model, a general expression of the multi bar model has been developed. It is found that the reference two bar multiplier bounds the limit load solution of multi bar models.

(2-d) A correction factor is introduced to the reference two bar multiplier in order to eliminate any possibility of overestimation of limit loads using the reference two bar multiplier. Therefore a lower bound reference two bar multiplier has been achieved.

(2-e) A guideline is proposed to obtain sufficiently accurate lower bound limit load using the two bar multiplier, based on a single linear elastic analysis.

(3-a) The m_α -tangent multiplier [12] is established as a lower bound on the basis of the constraint trajectory map. Moreover it is shown that the m_α -tangent multiplier bounds the limit load solution of multi bar models.

(3-b) Reference volume correction is proposed in order to ensure lower bound m_α -tangent solution for practical components and structures. This multiplier is found to be the most robust simplified approximation available in the literature.

(3-c) The m_α -tangent method [12] is used in conjunction with the elastic modulus adjustment procedure for determining accurate lower bound limit loads. The lower boundedness of the m_α -tangent multiplier for any iteration is ensured by incorporating reference volume and peak stress corrections. By the virtue of the faster convergence feature, the m_α^T -multiplier permits gentler modulus adjustments, and at the same time estimates sufficiently accurate lower bound limit load within a relatively small number of elastic iterations. The convergence difficulties usually encountered in EMAP for limit load estimation have been significantly minimized.

(3-d) A guideline is proposed to obtain sufficiently accurate lower bound limit load (using the m_α^T -multiplier) based on a single linear elastic analysis, which involves judicious incorporation of reference volume and peak stress correction.

(4-a) Mathematical model of elastic modulus adjustment scheme has been derived for bilinear hardening and Ramberg–Osgood material model, utilizing the “strain energy density” theory, in order to capture the post yield behavior of a component or structure.

(4-b) The proposed algorithm of iterative elastic modulus adjustment scheme developed for strain hardening material model is programmed into repeated linear elastic FEA.

(5) A number of analytical and numerical examples of varying complexity have been worked out and the results are compared with conventional analyses techniques. It is found that the simplified limit load approximation techniques can be used for analyzing complex problems with minimum effort and resources.

8.3 Recommendations for Future Research

Recommendations for future work are as follows:

1. The proposed guideline for the m_α -tangent and reference two bar multiplier evaluation method can be implemented for the limit load analysis of complex three dimensional finite element models (which might include inhomogeneous and anisotropic behavior). A similar implementation was carried out by Jain [32] for the design of a pressure vessel manway cover as per the ASME Boiler and Pressure Vessel Code guidelines.
2. Implementation of the m_α -tangent and reference two bar method as a design tool per API 579 Fitness-for-Service (Level 2), ASME Section III and Section VIII design-by-analysis guideline.
3. Simplified methods in its current form are only suitable for the integrity assessment of two dimensional crack-like flaw models. Application of these methods to the three dimensional flaw models would be useful.
4. Fracture parameter like J-integral and ductile fracture stability can be evaluated based on the proposed simplified methods.
5. The proposed strain hardening model can be implemented for the estimation of stress-strain at the notch root of a component having strain hardening feature, which is useful for FCI (fatigue crack initiation) prediction and can be utilized as an independent verification tool for the

available techniques. Similar investigation was carried out previously by Adibi-Asl and Seshadri [15] for elastic-perfectly-plastic material model.

6. The proposed strain hardening model can be utilized to obtain the plastic response of a structure beyond its yield point, which provides an idea about the reserved capacity of the structure against environmental/accidental loads.

7. The strain hardening model can also be implemented to identify the boundary between shakedown and ratcheting when the structure experiences strain hardening effect (similar solution was reported by Adibi-Asl and Reinhardt [24] for elastic-perfectly-plastic material model). This is a non-cyclic approach and can be utilized as an alternative to cyclic elastic-plastic analysis.

8. Simplified methods have already been employed in the Level 2 fitness-for-service (FFS) assessments of several tank and vessel geometries. There is a scope of implementing the simplified FFS assessment technique to the annular tanks. Recently annular tanks are considered as the emergency heat sinks for the high temperature pressure vessel containments. These tanks are usually susceptible to environmental corrosion.

References

- [1] ASME Boiler and Pressure Vessel Code, 2010, Section VIII, Division 2.
- [2] Ainsworth, R. A., Dean, D. W., and Budden, P. J. 2000. Development in Creep Fracture Assessments within the R5 Procedure, IUTAM Symposium on Creep in Structures, Nagoya, Japan, 321–330.
- [3] Calladine, C. R., 1969, *Engineering Plasticity*, Pergamon Press, Oxford, UK.
- [4] Lubliner, J., 1990, *Plasticity Theory*, Macmillan, London, UK.
- [5] Mura, T., Rimawi, W. H., and Lee, S. L., 1965, “Extended Theorems of Limit Analysis,” *Q. Appl. Math.*, **23(2)**, pp. 171–179.
- [6] Seshadri, R., and Mangalaramanan, S.P., 1997, “Lower Bound Limit Loads using Variational Concepts: the m_α –method,” *Int. J. Pressure Vessels & Piping*, **71**, pp. 93-106.
- [7] Pan, L., and Seshadri, R., 2002, “Limit Load Estimation using Plastic Flow Parameter in Repeated Elastic Finite Element Analyses,” *J. Pressure Vessel Technology*, **124**, pp. 433-439.
- [8] Reinhardt, W. D., and Seshadri, R., 2003, “Limit Load Bounds for the m_α Multiplier”, *J. Pressure Vessel Technology*, **125(1)**, pp. 11-18.
- [9] Adibi-Asl, R., Hossain, M. M., Mahmood, S.L., Reddy, P.S., and Seshadri, R., 2011, “Reference Volume Consideration in the m_α -Tangent Method Based on Linear Elastic Analysis”. Proceedings of the ASME 2011 Pressure Vessels & Piping Division, PVP2011-57822, July 17-21, 2011, Baltimore, Maryland, USA.
- [10] Seshadri, R., and Adibi-Asl, R., 2007, “Limit Loads of Pressure Components Using the Reference Two-Bar Structure,” *ASME J. Pressure Vessel Technology*, **129**, pp. 280–286.
- [11] ASME Boiler and Pressure Vessel Code, 2010. Section III Division 1.

- [12] Seshadri, R., and Hossain, M. M., 2009, “Simplified Limit Load Determination using the m_{α} -tangent method,” *J. Pressure Vessel Technology*, **131**(2), pp.287-294.
- [13] Seshadri, R., and Indermohan, H., 2004, “Lower Bound Limit Load Determination: The $m(\beta)$ -multiplier Method,” *ASME J. Pressure Vessel Technol.*, **126**(2), pp. 237–240.
- [14] Simha, C. H. M., and Adibi-Asl, R., 2012. “Lower Bound Limit Load Estimation Using a Linear Elastic Analysis”. *Journal of Pressure Vessel Technology*. **134**(2), pp. 021207(1-10).
- [15] Adibi-Asl, R., and Seshadri, R., 2010, “Improved Prediction Method for Estimating Notch Elastic Plastic Strain,” *Int. J. Pressure Vessels Technology*, **132**(1), pp. 011401(1-8).
- [16] Neuber, H., 1961, “Theory of Stress Concentration for Shear-Strained Prismatical Bodies with Arbitrary Non-Linear Stress-Strain Law,” *ASME J. Appl. Mech.*, **28**, pp. 544–550.
- [17] Gowhari-Anaraki, A. R., and Hardy, S. J., 1991, “Low Cycle Fatigue Life Predictions for Hollow Tubes With Axially Loaded Axisymmetric Internal Projections,” *J. Strain Anal.*, **26**, pp. 133–146.
- [18] Leis, B. N., Gowda, C. V. B., and Topper, T. H., 1973, “Some Studies of the Influence of Localized and Gross Plasticity on the Monotonic and Cyclic Concentration Factors,” *J. Test. Eval.*, **1**, pp. 341–348.
- [19] Conle, A., and Nowack, H., 1977, “Verification of a Neuber-Based Notch Analysis by the Companion-Specimen Method,” *Exp. Mech.*, **17**, pp. 57–63.
- [20] Molski, K., Glinka, G., 1981, “A Method of Elastic-Plastic Stress and Strain Calculation at a Notch Root,” *Materials Science and Engineering*, **50**, No. 2, pp. 93-100.
- [21] ANSYS, *University Research Version*, Release 12.0.

- [22] Drucker, D. C , and Shield, R. T., 1959, "Limit Analysis of Symmetrically Loaded Thin Shells of Revolution," *ASME Journal of Applied Mechanics*, **26**, pp. 61-68.
- [23] Adibi-Asl, R. and Seshadri, R., 2007, "Simplified Limit Load Estimation of Components with Cracks Using the Reference Two-Bar Structure", *ASME J. Pressure Vessel Technol.* **131(1)**, 011204 (8 pages).
- [24] Adibi-Asl, R., and Reinhardt, W. D., 2009, "Shakedown/Ratcheting Boundary Determination using Iterative Linear Elastic Schemes," *ASME Pressure Vessels and Piping Division Conference*, Paper no. PVP2009-77863, pp. 109-119.
- [25] Adibi-Asl, R., Fanous, I. F. Z., and Seshadri, R., 2006, "Elastic Modulus Adjustment Procedures-Improved Convergence Schemes," *Int. J. Pressure Vessels and Piping*, Vol. 83, pp. 154-160.
- [26] Molski, K., Glinka, G., 1981, "A Method of Elastic-Plastic Stress and Strain Calculation at a Notch Root," *Materials Science and Engineering*, Vol. 50, No. 2, pp. 93-100.
- [27] Hosford, W. F., 2005, '*Mechanical Behavior of Materials*,' Cambridge University Press, New York.
- [28] Calladine, C. R., and Drucker, D. C., 1962, "A Bound Method for Creep Analysis of Structures: Direct use of Solutions in Elasticity and Plasticity," *Journal of Mechanical Engineering Science*, Vol. 4, No. 1. pp. 1-11.
- [29] Calladine, C. R. and Drucker, D. C., 1962, "Nesting Surfaces for Constant rate of Energy Dissipation in Creep," *Quarterly of Applied Mathematics*, Vol. 20, pp. 79-84.
- [30] Mura, T., and Lee, S. L., 1963, "Application of Variational Principles to Limit Analysis," *Quarterly of Applied Mathematics*, Vol. 21, pp. 243-248.

- [31] Y. Yamada, Y. Ezawa, I. Nishiguchi and M. Okabe, Reconsiderations on singularity or crack tip elements. *Int. J. Numer. Meth. Engng.* 14, 152&1544 (1979).
- [32] Jain, R., 2012. "Use of limit load analysis for design of pressure vessel cover". Proceedings of the ASME 2012 Pressure Vessels & Piping Conference. PVP2012-78111.
- [33] R5, Assessment Procedure for High Temperature Response of Structures, Nuclear Electric, Berkeley, U.K., 1995.
- [34] R6, Assessing the Integrity of Structures Containing Defects, Nuclear Electric, Berkeley, U.K., 1995.
- [35] Mahmood, S.L., Haddara, M.R., and Seshadri, R., 2010. "Limit Loads of Ship Structure Components Using the Elastic Modulus Adjustment Procedure (EMAP)", *Journal of Ocean Engineering*. Vol. 37 (2010), pp. 1452-1463.

APPENDICES

Appendix A: Derivation of Limit Load Solution for Several Beam Configurations

Beams of various cross-sections have different limit load capacity, as governed by their section modulus and shape factor. Limit loads of various beam configurations have been analytically obtained and expressed in terms of the reference two bar solution.

A.1 Rectangular Beam

Regarding the beam in Figure A.1, consider the elastic stress field under bending moment, and the axial stress as a function of height from the neutral axis, y .

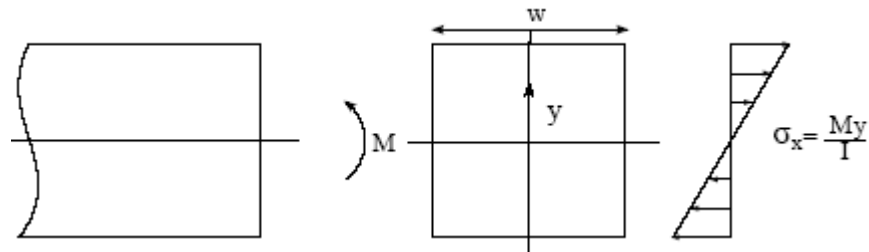


Figure A.1 Elastic stress fields for beam under moment loads

Lower bound limit moment for beam is the yield strength times the beam section modulus,

i.e.
$$M_y = \sigma_y Z \quad (\text{A.1})$$

Here Z = Section modulus and σ_y = Yield strength and M_y = Moment at first yield.

Lower bound multiplier can be obtained by normalizing Eq.(A.1) with the applied moment M ,

$$m_L = \frac{M_y}{M} = \frac{\sigma_y Z}{M} \quad (\text{A.2})$$

Similarly, exact limit load multiplier for a beam is the normalized form of plastic moment,

$$\text{i.e.} \quad m_{beam} = \frac{M_p}{M} = \frac{SM_y}{M} \quad (\text{A.3})$$

Here S = Shape factor and M_p = Plastic moment.

Now the upper bound multiplier for a rectangular beam section can be expressed as:

$$m^0 = \frac{\sigma_y}{\sigma_{ref}} = \frac{\sigma_y}{\sqrt{\frac{\int_V (\sigma_x(y))^2 dV}{\int_V dV}}} \quad (\text{A.4})$$

For a rectangular section of unit width, the section properties are:

$$I = \frac{t^3}{12}; \quad Z = \frac{t^2}{6}; \quad S = \frac{3}{2}$$

where t is the thickness of the rectangular beam and I is the moment of inertia. Therefore for a rectangular beam the expressions for the above multipliers can be re-written as:

$$m_L = \frac{\sigma_y t^2}{6M}$$

$$m^0 = \frac{\left(\frac{I\sigma_y}{M}\right) \sqrt{\int_{-\frac{t}{2}}^{\frac{t}{2}} dy}}{\sqrt{\int_{-\frac{t}{2}}^{\frac{t}{2}} y^2 dy}} = \frac{\sigma_y t^2}{\sqrt{12}M}$$

$$m_{Rect_beam} = \frac{\sigma_y t^2}{4M}$$

Now $\zeta = \frac{m^o}{m_L}$ for the rectangular beam will stipulate the length ratio of the equivalent reference

two bar structure.

i.e.
$$\zeta = \frac{m^o}{m_L} = \sqrt{3} \quad (\text{A.5})$$

Now the expression for Mura's lower bound multiplier can be expressed as,

$$m' = \frac{\sigma_y t^2}{4\sqrt{3}M} \quad (\text{A.6})$$

The ratio of Mura's lower bound multiplier and exact multiplier for a rectangular beam can be obtained as follows:

$$\frac{m'}{m_{\text{Rect_beam}}} = \frac{1}{\sqrt{3}} = \frac{1}{\zeta} \quad (\text{A.7})$$

$$\Rightarrow m_{\text{Rect_beam}} = m' \zeta$$

This clearly shows that once $\zeta = \frac{m^o}{m_L}$ and m^o for a rectangular beam are obtained and substituted

into the reference two bar multiplier formulation (Eq.(A.7)), it will provide the exact solution for the rectangular beam. The expressions of the limit load multipliers for a rectangular beam are tabulated below:

Table A.1 Limit load multipliers for a rectangular beam

Shape factor, S	m^o	m_L	$\zeta = \frac{m^o}{m_L}$	m'	m_α^T	$m = m_{\text{Rect_beam}}$	$\frac{m' \zeta}{m}$
$\frac{3}{2}$	$\frac{\sigma_y t^2}{\sqrt{12}M}$	$\frac{\sigma_y t^2}{6M}$	$\sqrt{3}$	$\frac{\sigma_y t^2}{4\sqrt{3}M}$	$\frac{\frac{\sigma_y t^2}{\sqrt{12}M}}{1 + \left(1 - \frac{1}{\sqrt{2}}\right)(\sqrt{3} - 1)}$	$\frac{\sigma_y t^2}{4M}$	1

The multiplier m_α^T , m'' and m''_μ are also presented below for the rectangular beam in a normalized form:

$$\Rightarrow \frac{m_\alpha^T}{m} = \frac{4}{\sqrt{6}(1 + \sqrt{6} - \sqrt{3})} = 0.95$$

$$\frac{m''}{m} = \frac{\left(\frac{\sigma_y \cdot l^2}{\sqrt{12} \cdot M} \right)}{\left(\frac{\sigma_y \cdot l^2}{4 \cdot M} \right)} \cdot \left[1 + \frac{1}{4t} \int_{-\frac{t}{2}}^{\frac{t}{2}} \left(\left(\left(\frac{\sigma_y \cdot l^2}{\sqrt{12} \cdot M} \right) \cdot \left(\frac{M \cdot y}{l^2} \right)^2 - 1 \right) \Phi \right)^2 \right]$$

$$\frac{m''_\mu}{m} = \frac{\left(\frac{\sigma_y \cdot l^2}{\sqrt{12} \cdot M} \right)}{\left(\frac{\sigma_y \cdot l^2}{4 \cdot M} \right)} \cdot \left[1 + \frac{1}{2} \cdot \frac{\int_{-\frac{t}{2}}^{\frac{t}{2}} \left(\left(\frac{3}{2} \cdot \frac{1}{\left(\frac{\sigma_y}{\left(\frac{M \cdot y}{l^2} \right)^q} \right)^q} \cdot E \right) \cdot \left(\left(\frac{\sigma_y \cdot l^2}{\sqrt{12} \cdot M} \right) \cdot \left(\frac{M \cdot y}{l^2} \right)^2 - 1 \right) \Phi \right)}{\int_{-\frac{t}{2}}^{\frac{t}{2}} \left(\frac{3}{2} \cdot \frac{1}{\left(\frac{\sigma_y}{\left(\frac{M \cdot y}{l^2} \right)^q} \right)^q} \cdot E \right) \Phi} \right]$$

A.2 Solid Circular Beam

For a solid circular beam of diameter d , the axial stress can be represented as:

$$\sigma_x = \frac{M \frac{d}{2} \sin \theta}{I} \quad (\text{A.8})$$

Now for a solid circular beam section, the general section properties are:

$$I = \frac{\pi d^4}{64}; Z = \frac{\pi d^3}{32}; Z_p = \frac{d^3}{6} \quad S = \frac{Z_p}{Z} = \frac{16}{3\pi}$$

The upper bound multiplier for a circular beam section,

$$m^0 = \frac{\sigma_y}{\sigma_{ref}} = \frac{\sigma_y}{\sqrt{\frac{\int_V (\sigma_x(\theta))^2 dV}{\int_V dV}}} = \frac{\left(\frac{I \sigma_y}{M}\right) \sqrt{\int_0^{\frac{d}{2}} r dr \int_0^\pi d\theta}}{\sqrt{\int_0^{\frac{d}{2}} r^3 dr \int_0^\pi (\sin \theta)^2 d\theta}} \quad (\text{A.9})$$

The expressions of the limit load multipliers for a solid circular beam are tabulated below:

Table A.2 Limit load multipliers for a solid circular beam

Shape factor, S	m^0	m_L	$\zeta = \frac{m^0}{m_L}$	m'	m_α^T	$m = m_{Solid_Circ_beam}$	$\frac{m' \zeta}{m}$
$\frac{16}{3\pi}$	$\frac{\sigma_y \pi d^3}{16M}$	$\frac{\sigma_y \pi d^3}{32M}$	2	$\frac{\sigma_y \pi d^3}{40M}$	$\frac{\sigma_y \pi d^3}{16M} \frac{1}{1 + \left(1 - \frac{1}{\sqrt{2}}\right)(2-1)}$	$\frac{\sigma_y d^3}{6M}$	0.94

A.3 Thin Circular Pipe

Regarding the circular pipe in Figure A.2, consider the elastic stress field under bending moment.

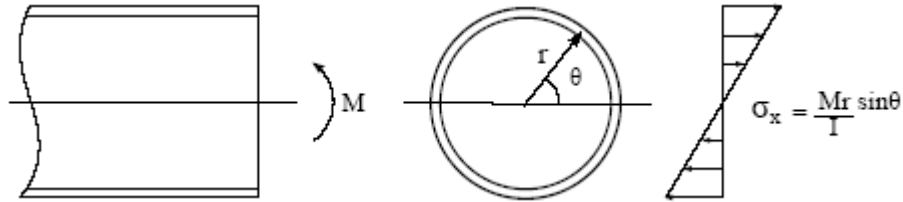


Figure A.2 Elastic stress fields for circular pipe under moment loads

Here r is the nominal tube radius and t is the tube thickness. Now for a pipe section, the general section properties:

Area Moment of Inertia:

$$I = \frac{\pi}{64} \left((2r+t)^4 - (2r-t)^4 \right)$$

$$\Rightarrow I = \pi r^3 t \left(1 + \frac{t^2}{4r^2} \right)$$

Elastic Section Modulus:

$$Z = \frac{\pi \left((2r+t)^4 - (2r-t)^4 \right)}{32 (2r+t)}$$

$$\Rightarrow Z = \frac{1}{2} \frac{\pi r t (4r^2 + t^2)}{(2r+t)}$$

Plastic Section Modulus:

$$Z_p = \frac{\left((2r+t)^3 - (2r-t)^3 \right)}{6}$$

Shape Factor:

$$S = \frac{Z_p}{Z} = \frac{48r^3 + 24r^2t + 4rt^2 + 2t^3}{12\pi r^3 \left(1 + \frac{t^2}{4r^2} \right)}$$

Therefore the limit load multipliers are:

Classical Lower Bound:

$$m_L = \frac{\sigma_y \pi r^2 t}{M} \left(\frac{4r + \frac{t^2}{r}}{4r + 2t} \right) \quad (\text{A.10})$$

Upper Bound:

$$m^0 = \frac{\left(\frac{I \sigma_y}{Mr} \right) \sqrt{\int_0^\pi d\theta}}{\sqrt{\int_0^\pi (\sin \theta)^2 d\theta}} = \frac{\sqrt{2} \sigma_y \pi r^2 t}{M} \left(1 + \frac{t^2}{4r^2} \right) \quad (\text{A.11})$$

Exact Solution:

$$m_{\text{Circ-pipe}} = \frac{4 \sigma_y r^2 t}{M} \left(1 + \frac{t^2}{12r^2} \right) \quad (\text{A.12})$$

Hence $\zeta = \frac{m^0}{m_L}$ will stipulate the length ratio of the equivalent reference two bar structure.

i.e.

$$\zeta = \frac{m^0}{m_L} = \sqrt{2} \frac{\left(1 + \frac{t^2}{4r^2} \right)}{\left(\frac{4r + \frac{t^2}{r}}{4r + 2t} \right)} \quad (\text{A.13})$$

The expression for Mura's lower bound multiplier can be expressed as:

$$m' = \frac{2 \frac{\sqrt{2} \sigma_y \pi r^2 t}{M} \left(1 + \frac{t^2}{4r^2} \right)}{\left(1 + \sqrt{2} \frac{\left(1 + \frac{t^2}{4r^2} \right)}{\left(\frac{4r + \frac{t^2}{r}}{4r + 2t} \right)} \right)^2} \quad (\text{A.14})$$

For a thin circular pipe ($t \ll r$), neglecting the higher order terms, the expressions for the limit load multipliers are tabulated below:

Table A.3 Limit load multipliers for a thin circular pipe

Shape factor, S	m^0	m_L	$\zeta = \frac{m^0}{m_L}$	m'	m_α^T	$m = m_{Thin_Circ_pipe}$	$\frac{m'\zeta}{m}$
$\frac{4}{\pi}$	$\frac{\sqrt{2}\sigma_y \pi r^2 t}{M}$	$\frac{\sigma_y \pi r^2 t}{M}$	$\sqrt{2}$	$\frac{2\sqrt{2}\pi\sigma_y r^2 t}{3M}$	$\frac{\sqrt{2}\sigma_y \pi r^2 t}{M}$ $1 + \left(1 - \frac{1}{\sqrt{2}}\right)(\sqrt{2} - 1)$	$\frac{4\sigma_y r^2 t}{M}$	1.05

Appendix B: Detail Derivation of the m_α -Method

In this section, Mura's variational formulation is extended to obtain the m_α -multiplier [6]. The derivation of the m_α -multiplier requires some unique algebraic manipulations which haven't been documented in any previous works. In the following section the step-by-step derivation of the m_α -multiplier is provided, showing all the algebraic operations, in order to reach the final expression.

The expression for Mura's lower bound multiplier m' can be expressed as:

$$m' = \frac{2m^0}{1 + \left(\frac{m^0}{m_L}\right)^2} \quad (\text{B.1})$$

From a differentiation of the above equation with respect to $\zeta = \frac{m^0}{m_L}$, follows the expression:

$$\frac{dm'}{d\zeta} = \left(\frac{\partial m'}{\partial m^0}\right) \frac{dm^0}{d\zeta} + \left(\frac{\partial m'}{\partial \frac{1}{m_L}}\right) \frac{\partial \frac{1}{m_L}}{d\zeta} \quad (\text{B.2})$$

In terms of finite differences, the equation becomes,

$$\Delta m' = \left(\frac{\partial m'}{\partial m^0}\right) \Delta m^0 + \left(\frac{\partial m'}{\partial \frac{1}{m_L}}\right) \Delta \left(\frac{1}{m_L}\right) \quad (\text{B.3})$$

where

$$\Delta m' = m' - m_\alpha$$

$$\Delta m^0 = m^0 - m_\alpha$$

$$\Delta \left(\frac{1}{m_L}\right) = \frac{1}{m_L} - \frac{1}{m_\alpha}$$

Now differentiating Eq.(B.1) with respect to m^0 and m_L separately:

$$\left(\frac{\partial m'}{\partial m^0}\right) = \frac{2}{1 + \left(\frac{m^0}{m_L}\right)^2} - \frac{4\left(\frac{m^0}{m_L}\right)^2}{\left(1 + \left(\frac{m^0}{m_L}\right)^2\right)^2} \quad (\text{B.4})$$

$$\left(\frac{\partial m'}{\partial \frac{1}{m_L}}\right) = -\frac{4(m^0)^2\left(\frac{m^0}{m_L}\right)}{\left(1 + \left(\frac{m^0}{m_L}\right)^2\right)^2} \quad (\text{B.5})$$

Substituting Eq.(B.3) by Eq.(B.1),(B.4) and (B.5):

$$\frac{2m^0}{1 + \left(\frac{m^0}{m_L}\right)^2} - m_\alpha = 2 \frac{1 - \left(\frac{m^0}{m_L}\right)^2}{\left(1 + \left(\frac{m^0}{m_L}\right)^2\right)^2} (m^0 - m_\alpha) - 4 \frac{(m^0)^2 \left(\frac{m^0}{m_L}\right)}{\left(1 + \left(\frac{m^0}{m_L}\right)^2\right)^2} \left(\frac{1}{m_L} - \frac{1}{m_\alpha}\right) \quad (\text{B.6})$$

Eq.(B.6) is a second order polynomial of m_α and thus it has two roots. Solving the roots,

$$m_\alpha = \frac{2m^0 m_L \left[2(m^0)^2 m_L + \sqrt{4(m^0)^4 (m_L)^2 + m^0 (m_L)^5 - 4(m^0)^3 (m_L)^3 - (m^0)^5 (m_L)} \right]}{-(m_L)^4 + 4(m^0)^2 (m_L)^2 + (m^0)^4} \quad (\text{B.7})$$

$$m_\alpha = \frac{2m^0 m_L \left[2(m^0)^2 m_L - \sqrt{4(m^0)^4 (m_L)^2 + m^0 (m_L)^5 - 4(m^0)^3 (m_L)^3 - (m^0)^5 (m_L)} \right]}{-(m_L)^4 + 4(m^0)^2 (m_L)^2 + (m^0)^4} \quad (\text{B.8})$$

Assuming positive root as the desired solution, multiply Eq.(B.7) by $\left(\frac{1}{m_L}\right)^4$ in both numerator and denominator. Then the final expression for the m_α -multiplier (as shown in Eq.(B.9)) is achieved through the following steps:

$$m_\alpha = 2m^0 \frac{\left[2\left(\frac{m^0}{m_L}\right)^2 + \left(\frac{1}{m_L}\right)^3 \sqrt{4(m^0)^4(m_L)^2 + m^0(m_L)^5 - 4(m^0)^3(m_L)^3 - (m^0)^5(m_L)} \right]}{-\frac{(m_L)^4 + 4(m^0)^2(m_L)^2 + (m^0)^4}{(m_L)^4}}$$

$$\Rightarrow m_\alpha = 2m^0 \frac{\left[2\left(\frac{m^0}{m_L}\right)^2 + \sqrt{4\left(\frac{m^0}{m_L}\right)^4 + \left(\frac{m^0}{m_L}\right) - 4\left(\frac{m^0}{m_L}\right)^3 - \left(\frac{m^0}{m_L}\right)^5} \right]}{\left(\frac{m^0}{m_L}\right)^4 + 4\left(\frac{m^0}{m_L}\right)^2 - 1}$$

$$\Rightarrow m_\alpha = 2m^0 \frac{\left[2\left(\frac{m^0}{m_L}\right)^2 + \sqrt{\left(\frac{m^0}{m_L}\right) \left[4\left(\frac{m^0}{m_L}\right)^3 + 1 - 4\left(\frac{m^0}{m_L}\right)^2 - \left(\frac{m^0}{m_L}\right)^4 \right]} \right]}{\left(\frac{m^0}{m_L}\right)^4 + 4\left(\frac{m^0}{m_L}\right)^2 + 2^2 - (\sqrt{5})^2}$$

$$\Rightarrow m_\alpha = 2m^0 \frac{\left[2\left(\frac{m^0}{m_L}\right)^2 + \sqrt{\left(\frac{m^0}{m_L}\right) \left[4\left(\frac{m^0}{m_L}\right)^3 + 1 - 4\left(\frac{m^0}{m_L}\right)^2 - \left(\frac{m^0}{m_L}\right)^4 \right]} \right]}{\left[\left(\frac{m^0}{m_L}\right)^2 + 2 \right]^2 - (\sqrt{5})^2}$$

$$\Rightarrow m_\alpha = 2m^0 \frac{\left[2\left(\frac{m^0}{m_L}\right)^2 + \sqrt{\left(\frac{m^0}{m_L}\right) \left[4\left(\frac{m^0}{m_L}\right)^3 + 1 - 4\left(\frac{m^0}{m_L}\right)^2 - \left(\frac{m^0}{m_L}\right)^4 \right]} \right]}{\left(\left(\frac{m^0}{m_L}\right)^2 + 2 - \sqrt{5} \right) \left(\left(\frac{m^0}{m_L}\right)^2 + 2 + \sqrt{5} \right)}$$

$$\begin{aligned}
\Rightarrow m_\alpha &= 2m^0 \frac{\left[2\left(\frac{m^0}{m_L}\right)^2 + \sqrt{\left(\frac{m^0}{m_L}\right)\left[\left(\frac{m^0}{m_L}-1\right)\left[-\left(\frac{m^0}{m_L}\right)^3 + 3\left(\frac{m^0}{m_L}\right)^2 - \left(\frac{m^0}{m_L}\right) - 1\right]\right]}{\left(\left(\frac{m^0}{m_L}\right)^2 + 2 - \sqrt{5}\right)\left(\left(\frac{m^0}{m_L}\right)^2 + 2 + \sqrt{5}\right)} \\
\Rightarrow m_\alpha &= 2m^0 \frac{\left[2\left(\frac{m^0}{m_L}\right)^2 + \sqrt{\left(\frac{m^0}{m_L}\right)\left[\left(\frac{m^0}{m_L}-1\right)\left[-\left(\frac{m^0}{m_L}-1\right)\left(\left(\frac{m^0}{m_L}\right)^2 - 2\left(\frac{m^0}{m_L}\right) - 1\right)\right]\right]}{\left(\left(\frac{m^0}{m_L}\right)^2 + 2 - \sqrt{5}\right)\left(\left(\frac{m^0}{m_L}\right)^2 + 2 + \sqrt{5}\right)} \\
\Rightarrow m_\alpha &= 2m^0 \frac{\left[2\left(\frac{m^0}{m_L}\right)^2 + \sqrt{\left(\frac{m^0}{m_L}\right)\left[\left(\frac{m^0}{m_L}-1\right)^2\left[-\left(\left(\frac{m^0}{m_L}\right)^2 - 2\left(\frac{m^0}{m_L}\right) + 1 - (\sqrt{2})^2\right)\right]\right]}{\left(\left(\frac{m^0}{m_L}\right)^2 + 2 - \sqrt{5}\right)\left(\left(\frac{m^0}{m_L}\right)^2 + 2 + \sqrt{5}\right)} \\
\Rightarrow m_\alpha &= 2m^0 \frac{\left[2\left(\frac{m^0}{m_L}\right)^2 + \sqrt{\left(\frac{m^0}{m_L}\right)\left[\left(\frac{m^0}{m_L}-1\right)^2\left[(\sqrt{2})^2 - \left(\left(\frac{m^0}{m_L}\right) - 1\right)^2\right]\right]}{\left(\left(\frac{m^0}{m_L}\right)^2 + 2 - \sqrt{5}\right)\left(\left(\frac{m^0}{m_L}\right)^2 + 2 + \sqrt{5}\right)} \\
\Rightarrow m_\alpha &= 2m^0 \frac{2\left(\frac{m^0}{m_L}\right)^2 + \sqrt{\frac{m^0}{m_L}\left(\frac{m^0}{m_L}-1\right)^2\left(1 + \sqrt{2} - \frac{m^0}{m_L}\right)\left(\frac{m^0}{m_L}-1 + \sqrt{2}\right)}{\left(\left(\frac{m^0}{m_L}\right)^2 + 2 - \sqrt{5}\right)\left(\left(\frac{m^0}{m_L}\right)^2 + 2 + \sqrt{5}\right)} \tag{B.9}
\end{aligned}$$

The above expression (Eq.(B.9)) is used in the literature to represent the multiplier m_α .

Appendix C: Modeling of Components with Cracks for Simplified Limit Load Analysis

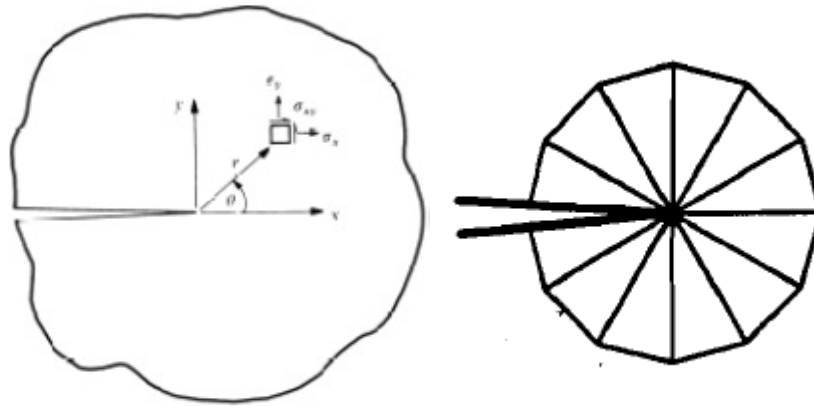
This section discusses the modeling of components with cracks, for the purpose of limit load estimation based on a linear elastic analysis. The linear elastic stress distribution around a crack configuration can be captured by using singular elements around crack tip. However limit load solution based on a linear elastic stress distribution requires further treatment of singularity elements; if the solution technique has explicit dependency on the maximum stress at the crack tip (e.g. classical lower bound limit load solution is explicitly dependent on the maximum equivalent stress of the entire stress distribution). This is due to the recognition that a crack tip configuration induces very high peak stress which is localized and gets redistributed along with the secondary stress. Modifying the elastic modulus of singular elements around the crack tip in a finite element discretization can reduce the magnitude of stress gradient to a minimum and hence the effect of peak stresses becomes small. Therefore use of singularity elements and their proper softening are important modeling considerations during the limit load analysis of cracked components, on the basis of linear elastic analysis.

C.1. Elastic Stresses Around the Crack Tip

Consider a crack configuration shown in Figure C.1 for which the stresses at the crack tip can be expressed as:

$$\sigma_x = \sigma_y = \sigma_{\max} = \frac{K_I}{\sqrt{2\pi r}} \quad (C.1)$$

$$\sigma_z = \begin{cases} 0 \rightarrow \text{Plane Stress} \\ 2\nu\sigma_{\max} \rightarrow \text{Plane Strain} \end{cases}$$



(a) Stress ahead of crack tip

(b) Distribution of singularity elements around crack tip

Figure C.1 Crack tip representation

Here K_I is the opening mode of fracture. Eq.(C.1) reveals that the cracked structure possess a singular stress field that is proportional to $\frac{1}{\sqrt{r}}$. Here r is the distance from the crack tip along the

crack length. The stress gradient in the vicinity of the crack tip is extremely high. The singularity element facilitates the variation of stress and strain as a function of $\frac{1}{\sqrt{r}}$, and hence can represent

the elastic stress distribution around the crack tip.

C.2. The Singular Element

The singular element is an element where stresses and strains are singular at the crack tip varying proportional to $\frac{1}{\sqrt{r}}$, shown in Eq.(C.1). Here r is the distance from the crack tip along the crack length. Proper crack-tip displacement, stress and strain fields can be modeled by standard quadratic order isoparametric finite elements by moving the element's mid-side node to the position one quarter of the way from the crack tip to the far end of the element. Such an element introduces a singularity into the mapping between the element's parametric coordinate space and Cartesian space, therefore is called singular element. For example, three nodes of a quadratic element are joined (Node 1, 7, and 8) and the mid-side nodes are moved to the quarter point adjacent to the crack tip node as shown in Figure C.2.

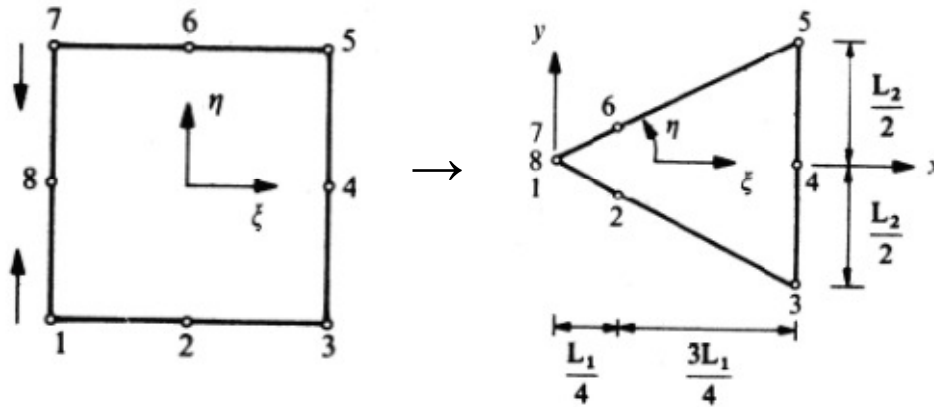
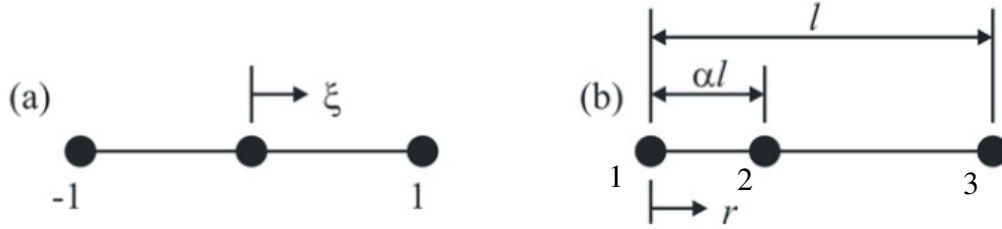


Figure C.2 The singular element.

The effect of moving the side node of a quadratic element to the quarter-point position can be best illustrated by a one-dimensional element. A 1-D quadratic order element is shown in Figure C.3, where the location of the center node is controlled by the parameter ' α ', and the crack tip is located at $r=0$ [31].



(a) Natural Coordinate System of the element (b) The Cartesian space of the element
Figure C.3 A 1-D quadratic element

Recalling the isoparametric formulation of a 1D quadratic element:

$$\begin{aligned}
 N_1 &= -\frac{1}{2}\xi(1-\xi) \\
 N_2 &= (1-\xi^2) \\
 N_3 &= \frac{1}{2}\xi(1+\xi)
 \end{aligned}
 \tag{C.2}$$

For an isoparametric element, the same approximation is used for the geometry as well as for the displacements field variable. Therefore the geometry of the 1-3 edge may be expressed as:

$$r = \sum_{i=1}^3 N_i r_i = -\frac{1}{2}\xi(1-\xi)r_1 + (1-\xi^2)r_2 + \frac{1}{2}\xi(1+\xi)r_3
 \tag{C.3}$$

By locating the mid-node (node#2) at $r_2 = \alpha l = \frac{l}{4}$ and substituting the nodal coordinates with respect to Figure C.3:

$$r = (1-\xi^2)\frac{l}{4} + \frac{1}{2}\xi(1+\xi)l
 \tag{C.4}$$

Now solving for ξ :

$$\xi = 2\sqrt{\frac{r}{l}} - 1
 \tag{C.5}$$

For the isoparametric element the displacement field variable can be expressed as:

$$\begin{aligned}
 u &= \sum_{i=1}^8 N_i u_i = -\frac{1}{2} \xi(1-\xi)u_1 + (1-\xi^2)u_2 + \frac{1}{2} \xi(1+\xi)u_3 \\
 &\Rightarrow u = u_2 + \frac{1}{2}(u_3 - u_1)\xi + \left[\frac{1}{2}(u_1 + u_3) - u_2 \right] \xi^2
 \end{aligned} \tag{C.6}$$

where u_1 , u_2 and u_3 are the displacements at nodes 1, 2 and 3. Using Eq.(C.5) in Eq.(C.6),

$$\begin{aligned}
 u &= u_2 + \frac{1}{2}(u_3 - u_1) \left(2\sqrt{\frac{r}{l}} - 1 \right) + \left[\frac{1}{2}(u_1 + u_3) - u_2 \right] \left(2\sqrt{\frac{r}{l}} - 1 \right)^2 \\
 &\Rightarrow u = u_1 + [-3u_1 + 4u_2 - u_3] \sqrt{\frac{r}{l}} + [2u_1 - 4u_2 + 2u_3] \frac{r}{l}
 \end{aligned} \tag{C.7}$$

Differentiating yields the following expression for strains in the element:

$$\varepsilon = \frac{du}{dr} = \frac{1}{2} [-3u_1 + 4u_2 - u_3] \frac{1}{\sqrt{rl}} + [2u_1 - 4u_2 + 2u_3] \frac{1}{l} \tag{C.8}$$

The three terms in the displacement expression (Eq.(C.7)) consists of a constant value, a linear variation in r , and the square root variation of r . This corresponds to the leading terms in the expressions for the near crack-tip displacement. Similarly, the expression for the strains (Eq.(C.8)) contains a constant term and a singular term that varies as a function of $\frac{1}{\sqrt{r}}$, the form

of expression given in Eq.(C.1).

C.3. Quarter Mid-Side Nodes at Crack Tip with ANSYS

As discussed in the former sections, it is useful to use a singularity element with quarter mid-side nodes in order to capture the stress singularities. In terms of finite element modeling, the first row of elements around the crack tip should be singular, as illustrated in Figure C.1 and it is convenient to model only one half of the crack region, with symmetry boundary conditions. For reasonable results, the first row of elements around the crack tip should have a radius of approximately $r/8$ or smaller, where r is the distance from the crack tip along the crack length. In the circumferential direction, roughly one element every 30 or 40 degrees is recommended and the crack tip elements must not be distorted.

C.4. Singularity Element Softening for Blunting Peak Stresses

By softening the elastic modulus of regions around the crack tip (singular elements that surround the crack tip in a finite element discretization), the magnitude of stress gradient reaches a minimum (shown in Figure C.4) and the effect of peak stresses becomes small. Adibi-Asl and Seshadri [23] proposed the following procedure for the relaxation of peak stresses around the crack tip, utilizing the singularity element softening approach.

Considering the principal stress components from Eq.(C.1), von-Mises equivalent stress can be computed as:

$$\sigma_{eq} = A \frac{K_I}{\sqrt{2\pi r}} \quad (C.9)$$

where $A=1$ represents plane stress and $A = (1 - 2\nu)$ represents plane strain

The average stress along the crack orientation in the singularity domain can be calculated as:

$$\bar{\sigma}_{eq} = \frac{\int_0^{r_s} \sigma_{eq}}{r_s} = 2A \frac{K_I}{\sqrt{2\pi r_s}} \quad (C.10)$$

With respect to Figure C.4, at $r=r_s$ the equivalent stress is equal to the reference stress; thus

$$\sigma_{ref} = A \frac{K_I}{\sqrt{2\pi r_s}} \quad (C.11)$$

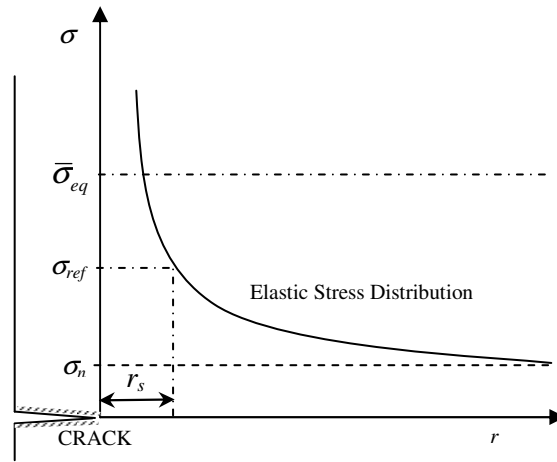


Figure C.4 Elastic stress distribution ahead of the crack tip

Therefore the relationship between the modified elastic modulus (E_s) and initial elastic modulus (E_0) can be written as:

$$\begin{aligned} \frac{E_s}{E_0} &= \left(\frac{\sigma_{ref}}{\bar{\sigma}_{eq}} \right)^q \\ \Rightarrow \frac{E_s}{E_0} &= \left(\frac{1}{2} \right)^q \end{aligned} \quad (C.12)$$

The value of parameter ' q ' can be within the range of $1 \leq q \leq 2$. Applying the values of $q=1$ and

$q=2$, the $\frac{E_s}{E_0}$ ratio will vary between 0.5 and 0.25 respectively. Based on extensive numerical

investigation on different crack configurations, Adibi-Asl and Seshadri [23] proposed $E_s = \frac{E_0}{3}$ for modifying singular elements around a crack tip.

Therefore in order to obtain sufficiently accurate estimate of lower bound limit loads for components with cracks (based on single linear elastic analysis), the singular elements around the crack tip are softened as $E_s = \frac{E_0}{3}$, while all other elements having an elastic modulus of E_0 .